ISSN: 2408-2384 (Online)
ISSN: 1686-5456 (Print)

Environment and Natural Resources Journal

Volume 19, Number 5, September - October 2021

Environment and Natural Resources Journal (EnNRJ)

Volume 19, Number 5, September - October 2021 ISSN: 1686-5456 (Print)
ISSN: 2408-2384 (Online)

AIMS AND SCOPE

The Environment and Natural Resources Journal is a peer-reviewed journal, which provides insight scientific knowledge into the diverse dimensions of integrated environmental and natural resource management. The journal aims to provide a platform for exchange and distribution of the knowledge and cutting-edge research in the fields of environmental science and natural resource management to academicians, scientists and researchers. The journal accepts a varied array of manuscripts on all aspects of environmental science and natural resource management. The journal scope covers the integration of multidisciplinary sciences for prevention, control, treatment, environmental clean-up and restoration. The study of the existing or emerging problems of environment and natural resources in the region of Southeast Asia and the creation of novel knowledge and/or recommendations of mitigation measures for sustainable development policies are emphasized.

The subject areas are diverse, but specific topics of interest include:

- Biodiversity
- Climate change
- Detection and monitoring of polluted sources e.g., industry, mining
- Disaster e.g., forest fire, flooding, earthquake, tsunami, or tidal wave
- Ecological/Environmental modelling
- Emerging contaminants/hazardous wastes investigation and remediation
- Environmental dynamics e.g., coastal erosion, sea level rise
- Environmental assessment tools, policy and management e.g., GIS, remote sensing, Environmental Management System (EMS)
- Environmental pollution and other novel solutions to pollution
- Remediation technology of contaminated environments
- Transboundary pollution
- Waste and wastewater treatments and disposal technology

Schedule

Environment and Natural Resources Journal (EnNRJ) is published 6 issues per year in January-February, March-April, May-June, July-August, September-October, and November-December.

Publication Fees

There is no cost of the article-processing and publication.

Ethics in publishing

EnNRJ follows closely a set of guidelines and recommendations published by Committee on Publication Ethics (COPE).

Environment and Natural Resources Journal (EnNRJ)

Volume 19, Number 5, September - October 2021 ISSN: 1686-5456 (Print)
ISSN: 2408-2384 (Online)

Editorial Office Address
Research Management and Administration Section,
Faculty of Environment and Resource Studies, Mahidol University
999, Phutthamonthon Sai 4 Road, Salaya, Phutthamonthon, Nakhon Pathom, Thailand, 73170
Phone +662 441 5000 ext. 2108 Fax. +662 441 9509-10
Website: https://ph02.tci-thaijo.org/index.php/ennrj/index
E-mail: ennrjournal@gmail.com

Environment and Natural Resources Journal (EnNRJ)

Volume 19, Number 5, September - October 2021 ISSN: 1686-5456 (Print)
ISSN: 2408-2384 (Online)

CONTENT

Radiological Impact Assessment of Class 3 Landfill of TENORM Waste from Tin Industry in Bangka Island

Zeni Anggraini*, Budi Setiawan, Nazhira Shadrina, and Dadong Iskandar

Center for Radioactive Waste Technology, National Nuclear Energy Agency, South Tangerang-Banten 15314, Indonesia

ARTICLE INFO

Received: 22 Feb 2021
Received in revised: 20 May 2021
Accepted: 27 May 2021
Published online: 29 Jun 2021
DOI: 10.32526/ennrj/19/2021020

Keywords:
Tin slag/ Doses/ Cancer risk/ Landfill/ Bangka Island

*** Corresponding author:**
E-mail: zeni.anggraini@batan.go.id

ABSTRACT

This study assessed the potential radiological impact of a class 3 landfill as a disposal facility of the final tin slag from the tin industry in Bangka Island. Tin slag that contains TENORM (Technically Enhanced Naturally Occurring Radioactive Material) with activity concentrations above exemption level limits should be stored safely and securely. The radiological impact analysis of storing TENORM waste was carried out before and after the construction of a landfill facility. RESRAD OFFSITE version 3.2 software was used to simulate dose and cancer risk, and analyze the contribution of exposure pathways. Radionuclide concentration, landfill facility specifications, hydrogeological data, climatological data, and food and water consumption data were used as input parameters of RESRAD. The receptor was a resident farmer who lives 100 meters from the facility, grows his own food, and consumes water from his land. The total dose before and after the construction of the landfill were 3.13 mSv/year and 1.84×10^{-2} mSv/year while cancer risks were 5.69×10^{-3} and 6.50×10^{-5}, respectively. The exposure pathways from inhalation of radon become a major contributor to dose acceptance and cancer risk. Based on these results, the landfill facility is effective in reducing the potential impact of radiological hazards from dose acceptance and cancer risk.

1. INTRODUCTION

Bangka Island is a province in Indonesia which is famous for its tin industry (Sari, 2019). In 2010-2014 Indonesia was ranked the second-largest tin producer in the world with an average production of 89,900 tons (Brown et al., 2016). The activities of tin industry in Bangka Island have led to an increase in the concentration of radionuclides in the environment in the form of Technically Enhanced Naturally Occurring Radioactive Material (TENORM) which is found in tailings, slags, by-products, and by-product industry waste (Husain and Sakhnini, 2017). These wastes contain NORM, i.e., Ra-226 (Uranium series), Th-232 (Thorium series), and K-40 (Hamzah et al., 2018; Ibeanu et al., 2013). Based on the secondary data from Nuclear Energy Regulatory Agency of Indonesia (BAPETEN), the amount of tin slag that contains TENORM from tin industry in Bangka Island is approximately 43,800,000 kg (Iskandar et al., 2019). From the results of field observations, it was found that many people, including workers, store tailings and slag in their homes where the tailing and slag materials have potential radiological impacts on workers and residents, which can pose radiation exposure to them and contaminate the environment (Attallah et al., 2020).

RESRAD ONSITE version 6.5 has been used to estimate the potential radiological impact on workers in the fertilizer industry from phosphogypsum deposits containing TENORM (dos Reis and da Costa Lauria, 2014). The simulation results showed that the radionuclide Ra-226 and environmental exposure pathways from the ingestion of fish contributed to the high dose received by workers. Received doses that exceed the safe dose limit can increase a person's carcinogenic risk. In the provisions of the International Atomic Energy Agency (IAEA), when the concentration of a radioactive substance in TENORM is ≥1000 Bq/kg, then TENORM must be controlled as radioactive waste because it can contaminate the environment (International Atomic Energy Agency, 2003). In Nigeria, by-products from tin mining are dumped around the mining site. The waste

Citation: Anggraini Z, Setiawan B, Shadrina N, Iskandar D. Radiological impact assessment of class 3 landfill of TENORM waste from tin industry in Bangka Island. Environ. Nat. Resour. J. 2021;19(5):337-347. (https://doi.org/10.32526/ennrj/19/2021020)

contaminated the surrounding environment and caused exposure to the biosphere through the leaching process. Regulation regarding tailings waste management is needed to protect humans and the environment (Aliyu et al., 2015).

The safety assessment simulation of disposal for TENORM waste is very effective to reduce the radiological impacts on the residents and the environment (ALNabhani et al., 2016; Pontedeiro et al., 2007). In addition, the disposal which is engineered from soil materials can minimize costs and maintain waste integrity in the long term. The landfill method of TENORM waste from tin industry in Indonesia could be a disposal option. Based on The Regulation of Ministry of Environment and Forestry of The Republic of Indonesia, landfill facilities are divided into three classes, namely class 1, 2, and 3 (Ministry of Environment and Forestry, 2016). The difference between the three classes of landfill is the existence of the geomembrane. Class 1 consists of HDPE geomembrane double liners, class 2 consists of a single liner of HDPE geomembrane, and class 3 does not use HDPE geomembrane. The requirements and procedures for the landfill are contained in Regulation of The Ministry of Environment and Forestry of The Republic of Indonesia (Ministry of Environment and Forestry, 2016).

Bangka Regency was chosen as the research location because it is the main location for the tin industry in Indonesia. The safety assessment was conducted on the lowest class (class 3 landfill) to know whether this class provides enough safety at more affordable cost. So far, there has been no research discussing the use of class 3 landfills for TENORM waste from tin industry and its radiological impact on residents and the environment. Radiological impact estimation was assessed by using RESRAD OFFSITE version 3.2 software. The objective of the research is to assess the potential radiological impact to residents and the environment from the construction of a class 3 landfill facility for TENORM waste from tin industry in Bangka Island. The results of this study are expected as recommendation for tin stakeholders, for them to realize and eventually minimize the potential radiological impact.

2. METHODOLOGY

2.1 Study area

Most of the geological stratigraphy of Bangka Island consists of the Tanjung Genting Formation which consists of clay (Sari, 2019). Clay naturally has a good ability to prevent fluid flow which is very suitable to be used as a natural barrier to minimize the occurrence of radionuclide leakage (Carcione et al., 2019; Zhang, 2018). Therefore, the area with the Tanjung Genting Formation can be a potential area choice for the landfill facility. Based on previous studies, Bangka Regency was selected as a potential area for landfill which is marked with the red box (Figure 1) (Septiadi et al., 2018; Sucipta et al., 2020). The location that is close to the center of the tin industry makes transportation easier and saves time.

2.2 Concentration of radionuclides

Tin ore produced from the exploitation process is increased in tin content to 70% by the shaking table method or jig installation (Handini, 2020; Hutahaean and Yudoko, 2013). From this process, by-products will be produced such as monazite, ilmenite, and zircon which have high concentrations of radionuclides and are of economic value (Hamzah et al., 2018). In addition, the final tin slag which has a high concentration of radionuclides containing Ra-226, Th-232, and K-40 will also be produced but is no longer economically valuable. For this study, the final tin slag (as waste) was used as a source to be disposed in a landfill facility. The final tin slag contains Ra-226=6 Bq/g; Th-232=10.14 Bq/g; K-40=0.60 Bq/g (Iskandar et al., 2019).

2.3 Exposure scenario

In this study to estimate the dose and cancer risk of residents who spend time near the contamination zone, two exposure scenarios were used for the simulation, they are before and after the construction of a class 3 landfill facility. Class 3 landfill is the lowest class for contaminated solid waste. Class 3 consists of a compacted clay layer, primary leachate collection system (SPPL I), barrier soil, secondary leachate collection system (SPPL II), and protective layer. The requirements for each layer are contained in the Regulation of Ministry of Environment and Forestry of The Republic of Indonesia (Ministry of Environment and Forestry, 2016). Landfill facility has an exclusion zone with a radius of 100 meters, where within this distance is a limited activity. The exposure scenario assumes that primary contamination is transported to agricultural areas, wells, dwellings, and the groundwater flows from the NORM waste stack toward fishponds and livestock. Since they produce all their own food and consume water from the well near

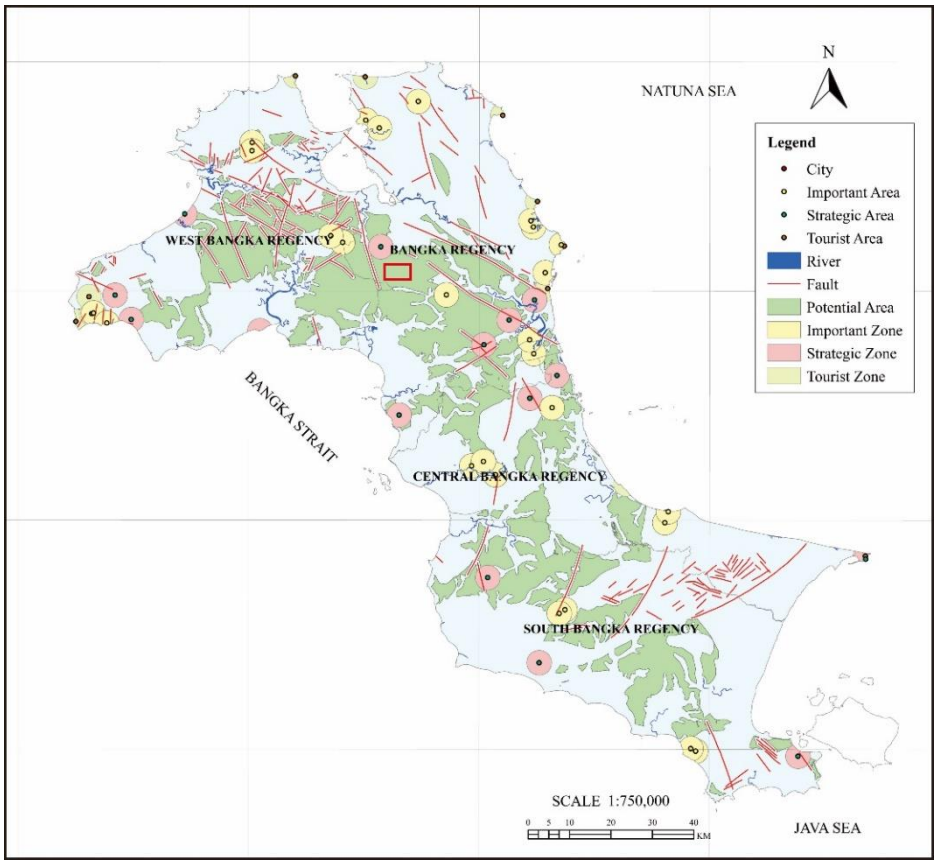

Figure 1. Map of potential site for class 3 landfill facility in Bangka Island (Sucipta et al., 2020)

their homes, the release of radionuclides to the environment can pose internal and external radiation exposure. The considered exposure pathways are radon, inhalation, ingestion (vegetable, milk, meat, and fish), drinking water, and ingestion of soil.

Figure 2 shows an illustration of the layers used in a class 3 landfill facility that must be had for the placement of TENORM waste, according to the Regulation of The Ministry of Environment and Forestry of The Republic of Indonesia No. P.63/Menlhk/Setjen/KUM.1/7/2016 (Ministry of Environment and Forestry, 2016). The use of local natural materials such as bentonite as compacted clay or a protective layer can be applied in this activity (Setiawan and Sriwahyuni, 2018; Sriwahyuni and Setiawan, 2019). This is intended to make the landfill facility to be built more economical and also to increase the local content of the facility.

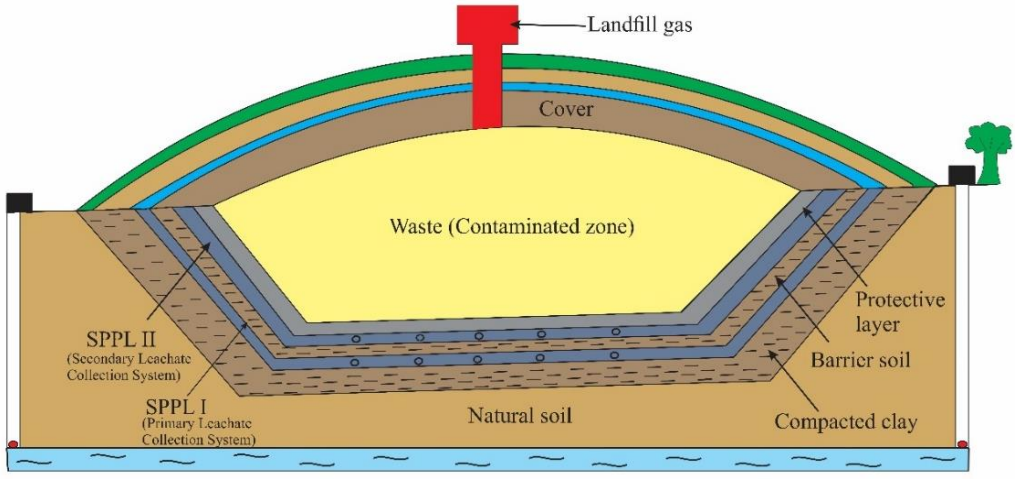

Figure 2. Design of class 3 landfill facility (Ministry of Environment and Forestry, 2016)

2.3 RESRAD OFFSITE version 3.2

RESRAD OFFSITE version 3.2 is a software developed by Argonne National Laboratory which is used to estimate the dose and cancer risk of individuals who are living outside the contaminated zone (dos Reis and da Costa Lauria, 2014). The dose and cancer risk can be estimated using Equation (1) and (2) as follows (Cheng and Yu, 1993):

$$(\text{Dose})_{j,p}(t) = \text{DCF}_{j,p}(t) \times \text{ETF}_{j,p}(t) \times \text{SF}_{i,j}(t) \times \text{S}_i(0) \quad (1)$$

Where; $(\text{Dose})_{j,p}(t)$=effective dose (mrem/year), $\text{DCF}_{j,p}(t)$=dose conversion factor (mrem/pCi), $\text{ETF}_{j,p}(t)$=the environmental transport factor (g/year), $\text{SF}_{i,j}(t)$=source factor, and $\text{S}_i(0)$=soil concentration of radionuclide.

$$(\text{Cancer})_{j,p}(t) = (\text{Intake})_{j,p}(t) \times \text{Sf}_{j,p} \times \text{ED} = \sum_{t=1}^{M} \text{ETF}_{j,p}(t) \times \text{SF}_{i,j}(t) \times \text{S}_i(0) \times \text{Sf}_{j,p} \times \text{ED} \quad (2)$$

Where; $(\text{Intake})_{j,p}$=inhalation and ingestion pathways, M=number of initially existent radio-nuclides, $\text{SF}_{i,j}(t)$=slope factor for radionuclide, and ED=exposure duration (year).

In this study, a conservative approach was estimated using the type of soil, due to the unavailability of site-specific data. According to the authors, these default values in RESRAD code have been carefully and realistically selected from various sources (Yu et al., 2015). To estimate the dose more accurately, site-specific parameter values should be used whenever possible. Therefore, some of the default parameter values were changed according to the site-specific data in Bangka Island (Table 1).

Table 1. Parameters input for the scenario

Parameter	Value	References
Soil concentration		
Ra-226	6.00 Bq/g	Iskandar et al. (2019)
Th-232	10.14 Bq/g	Iskandar et al. (2019)
K-40	0.66 Bq/g	Iskandar et al. (2019)
Contaminated zone		
Area	4,200 m^2	Scenario assumption
Thickness	4 m	Scenario assumption
Length parallel to aquifer flow	100 m	Scenario assumption
Dry bulk/density	2.65 g/cm^3	Iskandar et al. (2019)
Erosion rate	0.20 m/year	RESRAD Default
Total porosity	0.39	Yu et al. (2015)
Effective porosity	0.30	Yu et al. (2015)
Hydraulic conductivity	10^{-2} -10^{1} m/year	Yu et al. (2015)
b parameter	4.05	Yu et al. (2015)
Field capacity	0.25	Yu et al. (2015)
Runoff coefficient	0.37	Yu et al. (2015)
Evapotranspiration coefficient	0.42	Mahfiz et al. (2019)
Precipitation	2.07 m/year	BPS-Statics of Bangka Regency (2020)
Number of unsaturated zone strata	5	Ministry of Environment and Forestry (2016)
Unsaturated zone 1 (Compacted clay)		
Thickness	1 m	Ministry of Environment and Forestry (2016)
Dry bulk/density	1.20 g/cm^3	Yu et al. (2015)
Total porosity	0.42	Yu et al. (2015)
Effective porosity	0.20	Yu et al. (2015)
b parameter	11.4	Yu et al. (2015)
Field capacity	0.45	Yu et al. (2015)
Hydraulic conductivity	40.50 m/year	Yu et al. (2015)
Unsaturated zone 2 (SPPL I)		
Thickness	0.30 m	Ministry of Environment and Forestry (2016)

Table 1. Parameters input for the scenario (cont.)

Parameter	Value	References
Dry bulk/density	3 g/cm^3	Yu et al. (2015)
Total porosity	0.34	Yu et al. (2015)
Effective porosity	0.28	Yu et al. (2015)
b parameter	4.05	Yu et al. (2015)
Field capacity	0.89	Yu et al. (2015)
Hydraulic conductivity	10^4 m/year	Yu et al. (2015)
Unsaturated zone 3 (Barrier soil)		
Thickness	0.30 m	Ministry of Environment and Forestry (2016)
Dry bulk/density	1.20 g/cm^3	Yu et al. (2015)
Total porosity	0.42	Yu et al. (2015)
Effective porosity	0.20	Yu et al. (2015)
b parameter	11.40	Yu et al. (2015)
Field capacity	0.45	Yu et al. (2015)
Hydraulic conductivity	40.50 m/year	Yu et al. (2015)
Unsaturated zone 4 (SPPL II)		
Thickness	0.30 m	Ministry of Environment and Forestry (2016)
Dry bulk/density	3 g/cm^3	Yu et al. (2015)
Total porosity	0.34	Yu et al. (2015)
Effective porosity	0.28	Yu et al. (2015)
b parameter	4.05	Yu et al. (2015)
Field capacity	0.89	Yu et al. (2015)
Hydraulic conductivity	10,000 m/year	Yu et al. (2015)
Unsaturated zone 5 (Protective layer)		
Thickness	0.30 m	Ministry of Environment and Forestry (2016)
Dry bulk/density	1.44 g/cm^3	Yu et al. (2015)
Total porosity	0.45	Yu et al. (2015)
Effective porosity	0.20	Yu et al. (2015)
b parameter	4.38	Yu et al. (2015)
Field capacity	0.35	Yu et al. (2015)
Hydraulic conductivity	4,930 m/year	Yu et al. (2015)
Saturated zone		
Thickness	10 m	Scenario assumption
Dry bulk/density	1.20 g/cm^3	Yu et al. (2015)
Total porosity	0.42	Yu et al. (2015)
Effective porosity	0.20	Yu et al. (2015)
Hydraulic conductivity	100 m/year	Yu et al. (2015)
Cover zone		
Thickness	5 m	Scenario assumption
Drybulk density	1.20 g/cm^3	Yu et al. (2015)
Total porosity	0.42	Yu et al. (2015)
Inhalation rate	8,400 m^3/year	RESRAD Default
Mass loading for inhalation	10^4 g/m^3	RESRAD Default
Soil ingestion rate	36.50 g/year	RESRAD Default
Drinking water intake	510 L/year	RESRAD Default
Irrigation	0.20 m/year	RESRAD Default
Well pumping rate	5,100 m^3/year	RESRAD Default
Leafy vegetable consumption	33 kg/year	BPS-Statics of Bangka Regency (2020)

Table 1. Parameters input for the scenario (cont.)

Parameter	Value	References
Milk consumption	92 L/year	RESRAD Default
Meat consumption	43 kg/year	BPS-Statics of Bangka Regency (2020)
Fish consumption	63 kg/year	BPS-Statics of Bangka Regency (2020)

3. RESULTS AND DISCUSSION

RESRAD OFFSITE 3.2 analysis results were used to determine the effectiveness of class 3 landfill as disposal of TENORM waste from the tin industry in Bangka Island. Table 2 shows that the dose value received by residents at a distance of 100 meters from the contaminated zone before the construction of a landfill facility is 3.13 mSv/year at t=75 years. The main contributor to the high total dose came from Ra-226 radionuclide in the first year to year 6 and the dose decreased to 0.51 mSv/year in year 970. In contrast, Th-232 showed an increasing trend during 970 years with the maximum dose value of 2.18 mSv/year in year 75 to 970. The increasing trend of this graph is caused by the progenies of Th-232 with a half-life from the order of seconds to thousands of years which will show an increasing trend until it reaches secular equilibrium conditions. The half-life of Th-232 as a parent (1.4×10^{10} years) is longer than the half-life of the progenies. Equilibrium conditions are shown by a horizontal graph. When conditions were at equilibrium, the concentration of the progenies was the same or close to the concentration of the parent (Th-232) (Senftle et al., 1956; Rasito et al., 2007). The total dose will decrease when the parent concentration (Th-232) decreases. The concentration will affect the dose calculation. Potassium-40 (K-40) radionuclide does not contribute to the total dose because K-40 had low activity concentrations in the soil sample compared to Ra-226 and Th-232.

Table 2. Dose before the construction of a landfill facility

RN	Dose (mSv/year)									
	t=0	t=1	t=3	t=6	t=12	t=30	t=75	t=175	t=420	t=970
Ra-226	0.92	0.92	0.92	0.92	0.93	0.95	0.95	0.89	0.75	0.51
Th-232	0.08	0.08	0.34	0.78	1.49	2.10	2.18	2.18	2.19	2.21
K-40	0	0	0	0	0	0	0	0	0	0
∑	1.00	1.00	1.26	1.70	2.42	3.05	3.13	3.07	2.94	2.72

By using the class 3 landfill and considering the scenarios established for all exposure pathways after the post-closure, an estimated maximum total dose obtained was 1.84×10^{-2} mSv/year at the first year as presented in Table 3. This dose was below the dose limit for the public of 1 mSv/year by the regulatory body (BAPETEN) (BAPETEN Chairman, 2013). The main contributor to this dose is Ra-226 which is responsible for 100% of the total dose with a downward trend during 970 years, from 1.84×10^{-2} mSv/year to 0.95×10^{-2} mSv/year. In addition, the ionizing radiation dose for radon has a recommended annual effective dose threshold of 10 mSv/year, so the measured total dose from radon remains at a safe level (Harrison and Marsh, 2020). Even though the measured dose is relatively low, radiation exposure should always be monitored carefully. The results of the total dose before and after the construction of a landfill facility are illustrated in Figure 3.

Table 3. Dose after the construction of a landfill facility

RN	Dose ($\times10^{-2}$ mSv/year)									
	t=0	t=1	t=3	t=6	t=12	t=30	t=75	t=175	t=420	t=970
Ra-226	1.84	1.84	1.84	1.83	1.82	1.80	1.75	1.63	1.38	0.95
Th-232	0	0	0	0	0	0	0	0	0	0
K-40	0	0	0	0	0	0	0	0	0	0
∑	1.84	1.84	1.84	1.83	1.82	1.80	1.75	1.63	1.38	0.95

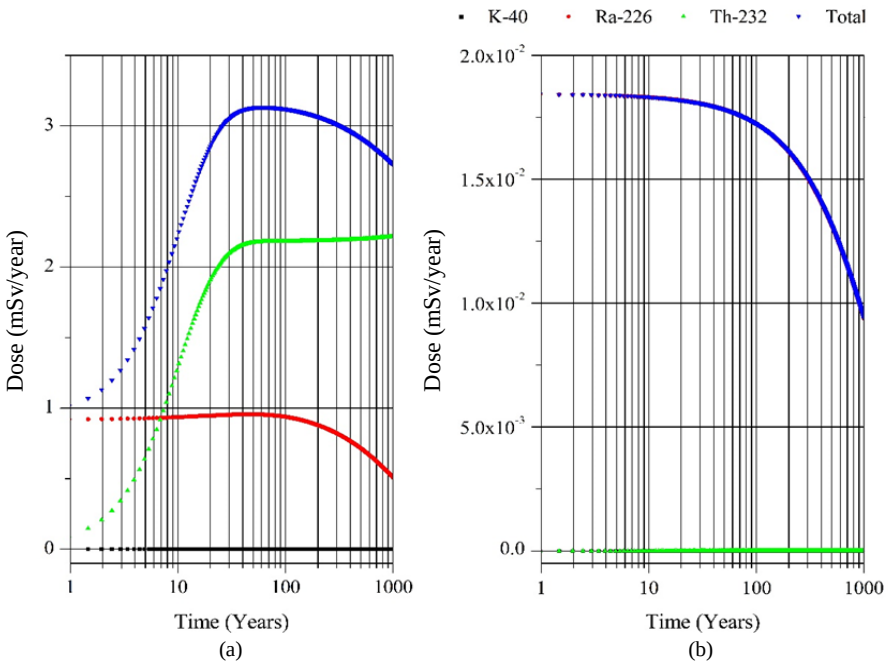

Figure 3. Total dose before (a), and after (b) the construction of a landfill facility

The component exposure pathway contribution to the total dose for each individual radionuclide Ra-226, Th-232, and K-40 during 970 years is shown in Table 4. Ra-226 became the major contributor in the first year through the radon gas (Rn-222) exposure pathways as the first progeny in Ra-226 decay chain with a half-life of 3.8 days (Szabo et al., 2005). Rn-222 will be released into the atmosphere and the dose decreases when the concentration of Ra-226 decreases. Meanwhile, radon gas (Rn-220) which comes from Ra-224 as a progeny of Th-232 tends to contribute only 2% of the total dose in the first year. This is expected due to radionuclide Th-232 taking a longer decay time to produce radon gas, so the dose will be low in the first year and begin to predominate from year 12 to year 970 (Sujo et al., 2004; Tölgyessy and Harangozó, 2005). In general, the total dose derived from the radon gas exposure pathway Th-232 was greater than Ra-226 and K-40, due to the higher activity concentration of Th-232 in tin slag sample.

Table 4. The component exposure pathways before the construction of a landfill facility

RN	Dose (mSv/year)											
	t=0				t=75				t=970			
	Radon		Fish		Radon		Fish		Radon		Fish	
	Dose	%	Dose	%	Dose	%	Dose	%	Dose	%	Dose	%
Ra-226	0.91	96	0	0	0.87	27	0.08	3	0.47	17	0.05	2
Th-232	0.02	2	0	0	2.15	67	0.04	1	2.15	76	0.19	4
K-40	0	0	0	0	0	0	0	0	0	0	0	0

The result of the calculation of RESRAD code shows that the radionuclide concentrations of Ra-226 and Th-232 in the surface water (fish pond) are 12.15×10^{-7} Bq/L in year 75. The result is less than 1% of the total initial concentrations of Ra-226 and Th-232 before being released into the environment. The contributor to the total dose also came from ingestion of fish, which is responsible for 3% from Ra-226 and followed 1% by Th-232. It is estimated that there has been a release of Ra-226 from TENORM waste dump into water bodies. Therefore, the biota in the water becomes contaminated. This can occur because Ra-226 is absorbed into the soil through the leaching process and dissolves into the liquid phase of the contamination zone. Ra-226 will flow with water into the water body (Rajaretnam and Spitz, 2000). Otherwise, Th-232 is difficult to dissolve in the material. Th-232 takes time to decay to be Ra-228 and Ra-224 with respective half-life of 5.75 years and 3.66 days, as ingrowth progenies in the total dose and

excess cancer risk for Th-232. Ra-228 and Ra-224 will dissolve and are responsible for water and biota pollution through the leaching process. The ingestion of fish from Th-232 will contribute 4% of the dose and only 2% comes from Ra-226 in year 970. In general, the other pathways were responsible for less than 2% of the total dose during 970 years.

Ra-226 became a major contributor to the total dose after the construction of a landfill facility (Table 5). The simulation shows that the radon gas Rn-222, a progeny of Ra-226, is responsible for 100% of the total dose, which is due to cover erosion. Rn-220, a progeny of Th-232, is estimated to be strongly absorbed and confined by the fine clay mineral fraction in the cover and soil layer of landfill (Ames and Rai, 1978; Melson, 2011). It is suspected that Rn-220 decays before it reaches the surface because the half-life of Rn-220 is only 55 s (Madansky and Rasetti, 1956; Dziurowicz et al., 2017). The construction of a landfill facility acts as a barrier to radionuclide contamination through ingestion of fish and radon gas exposure pathways, as seen in Figure 4.

Table 5. The component exposure pathways after the construction of a landfill facility

RN	Dose ($\times 10^{-2}$ mSv/year)											
	t=0				t=75				t=970			
	Radon		Fish		Radon		Fish		Radon		Fish	
	Dose	%	Dose	%	Dose	%	Dose	%	Dose	%	Dose	%
Ra-226	1.84	100	0	0	1.75	100	0	0	0.95	100	0	0
Th-232	0	0	0	0	0	0	0	0	0	0	0	0
K-40	0	0	0	0	0	0	0	0	0	0	0	0

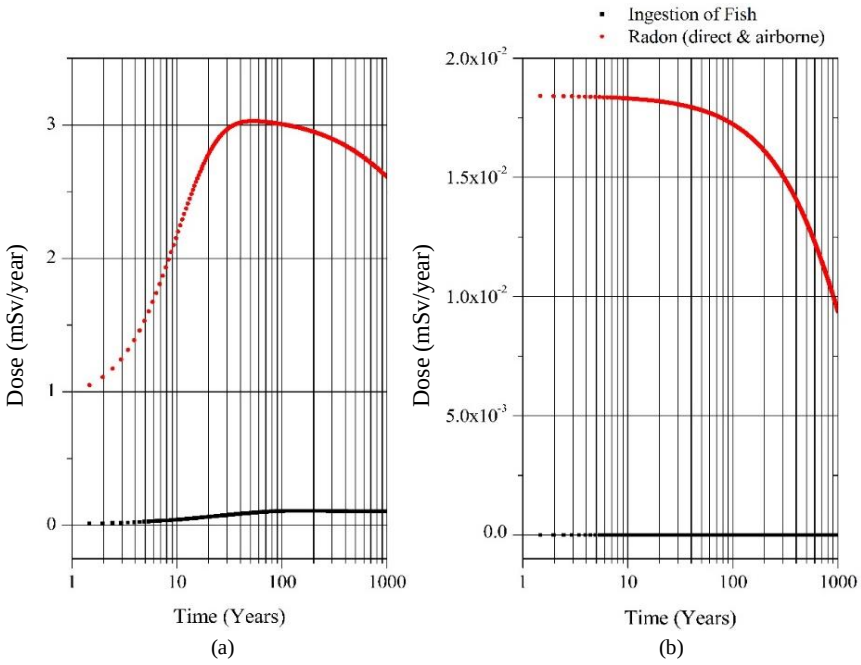

Figure 4. The component exposure pathways before (a), and after (b) the construction of a landfill facility

In addition to the estimate dose absorbed by the body, the simulation results using RESRAD were also used to estimate the excess cancer risk for 970 years. The excess cancer risk for each individual radionuclide Ra-226, Th-232, and K-40 are illustrated in Table 6 and Table 7. The results showed the highest excess cancer risk before and after the construction of a class 3 landfill facility is mainly due to the release of radon gas from tin slag stack, followed by its inhalation. Radon through the diffusion process in the environment will migrate and appear predominantly in locations around the tin slag stack. Radon will stick to dust and small particles in the air that can be inhaled and contribute to internal exposure (Singh et al., 2019).

Several cases have shown that radon can increase the risk of cancer during long-term inhalation due to the release of alpha particles from the decay of

radon gas that stays and damages the cells lining the respiratory channel in the lungs. Therefore, preventive action is needed (Lecomte et al., 2014; Vogiannis and Nikolopoulos, 2015). Figure 5 shows the excess cancer risk received by residents was decreased significantly if a class 3 landfill facility was constructed from 5.69×10^{-3} to 6.50×10^{-5}, so the value is close to the recommendation by IAEA (International Atomic Energy Agency, 2011). This indicates that the mitigation strategy in the safety assessment of the construction of a landfill facility is quite effective to prevent the release of TENORM waste to the residents and the environment. Based on the scenario simulation of TENORM waste release by considering the possibility of transporting radionuclide contamination through geological media to the environment, radionuclide contamination can contribute significantly to the acceptance of dose and cancer risk to the residents and the environment. The safety assessment will be useful in the policymaking processes related to the planning development phase and the post-closure of the landfill facility.

Table 6. Excess cancer risk before the construction of a landfill facility

RN	Excess cancer risk ($\times10^{-3}$)					
	t=0		t=75		t=970	
	Radon	Fish	Radon	Fish	Radon	Fish
Ra-226	3.32	0.03	3.15	0.08	1.70	0.04
Th-232	1.68	0.08	2.54	0.03	2.54	0.08
K-40	0	0	0	0	0	0
∑	5.00	0.11	5.69	0.11	4.24	0.12

Table 7. Excess cancer risk after the construction of a landfill facility

RN	Excess cancer risk ($\times10^{-5}$)					
	t=0		t=75		t=970	
	Radon	Fish	Radon	Fish	Radon	Fish
Ra-226	6.50	0	6.35	0	3.46	0
Th-232	0	0	0	0	0	0
K-40	0	0	0	0	0	0
∑	6.50	0	6.35	0	3.46	0

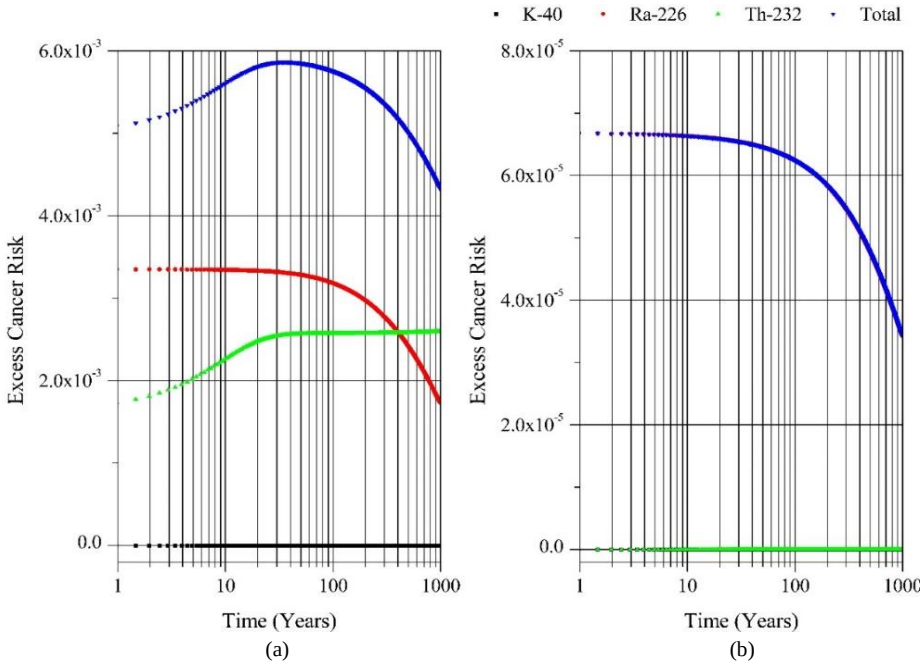

Figure 5. Excess cancer risk before (a), and after (b) the construction of a landfill facility

4. CONCLUSION

The total dose value generated from the two scenarios for the preparation of a landfill facility shows that a class 3 landfill facility is quite effective in reducing the total dose and cancer risk, especially for inhalation of radon gas and ingestion of fish. The main contributors before the construction of a landfill facility came from radon gas exposure and ingestion of fish. The total dose and cancer risk after the construction of a landfill facility was 1.84×10^{-2} mSv/year and 6.50×10^{-5} at the first year, with the primary contributor to the exposure pathway from the release of radon gas. However, regarding the limitation of this study and to decrease the uncertainties in the results, it would be helpful to input more detailed site-specific parameters. This can be explored in future research. Nevertheless, the results obtained from this study can be used by stakeholders in policymaking during the planning and post-closure phases of a landfill facility to protect workers, residents, and the environment from the impact of radiological hazards.

ACKNOWLEDGEMENTS

A part of the experiment was supported by a grant from the Ministry of Research and Technology-Republic of Indonesia under the INSINAS Project of 2019 FY. Thanks are due to the Managements of the Center for Radioactive Waste Technology-National Nuclear Energy Agency for their supports and opportunity.

REFERENCES

Aliyu AS, Mousseau TA, Ramli AT, Bununu YA. Radioecological impacts of tin mining. Ambio 2015;44:778-87.

ALNabhani K, Khan F, Yang M. Scenario-based risk assessment of TENORM waste disposal options in oil and gas industry. Journal of Loss Prevention in the Process Industries 2016;40:55-66.

Ames LL, Rai D. Radionuclide Interactions with Soil and Rock Media: Volume 1. Washington, USA: Battelle Pacific Northwest Labs., Richland; 1978.

Attallah MF, Abdelbary HM, Elsofany EA, Mohamed YT, Abo-Aly MM. Radiation safety and environmental impact assessment of sludge TENORM waste produced from petroleum industry in Egypt. Process Safety and Environmental Protection 2020;142:308-16.

BPS-Statics of Bangka Regency. Bangka Regency in Figures 2020. Bangka, Indonesia: BPS-Statics of Bangka Regency; 2020.

BAPETEN Chairman R. Radiation Protection and Safety in the Utilization of Nuclear Power. Jakarta, Indonesia: Nuclear Energy Regulatory Agency; 2013.

Brown TJ, Wrighton CE, Idoine NE, Raycraft ER, Shaw RA, Deady EA, et al. World Mineral Production 2010-14. Nottingham, United Kingdom: British Geological Survey; 2016.

Carcione JM, Gei D, Yu T, Ba J. Effect of clay and mineralogy on permeability. Pure and Applied Geophysics 2019;176:2581-94.

Cheng J-J, Yu C. Using the RESRAD computer code to evaluate human health risks from radionuclides and hazardous chemicals. Journal of Hazardous Materielas 1993;35:353-67.

Dziurowicz M, Malczewski D, Żaba J. 222Rn and 220Rn concentrations in selected soils developed on the igneous rocks of the Kaczawa Mountains (Sudetes, Poland). Journal of Environmental Radioactivity 2017;92:144-64.

Hamzah Y, Mardhiansyah M, Firdaus LN. Characterization of rare earth elements in tailing of ex-tin mining sands from Singkep Island, Indonesia. Aceh International Journal of Science and Technology 2018;7:131-7.

Handini T. Separation the zircon mineral from tailing Tin mining using shaking table. Proceedings International Conference on Nuclear Capaciy Building, Education, Research and Applications (I-Concern); 2019 Sep 6-7; Royal Ambarrukmo Hotel, Yogyakarta: Indonesia; 2020.

Harrison JD, Marsh JW. ICRP recommendations on radon. Annals of the International Commission on Radiological Protection (ICRP) 2020;49:68-76.

Husain H, Sakhnini L. Radiological impact of NORM generated by oil and gas industries in the kingdom of Bahrain. Journal of Environmental Radioactivity 2017;167:127-33.

Hutahaean BP, Yudoko G. Analysis and proposed changes of TIN ORE processing system on cutter suction dredges into low grade to improve added value for the company. Indonesian Journal of Business Administration 2013;2:67813.

International Atomic Energy Agency (IAEA). Disposal of Radioactive Waste: Specific Safety Requirements: No. SSR-5. Vienna, Austria: International Atomic Energy Agency (IAEA); 2011.

International Atomic Energy Agency (IAEA). Radiation Protection and the Management of Radioactive Waste in the Oil and Gas Industry: No.34. Vienna, Austria: International Atomic Energy Agency (IAEA); 2003.

Ibeanu IGE, Zakari IY, Akpa TC. Validity of tin mine stream sediments in the construction of residential homes. Research Journal of Environmental and Earth Sciences 2013;5:751-5.

Iskandar D, Sucipta S, Sutoto S, Nurliati G, Subiarto S, Setyawan A. Inventory and Study of TENORM Waste Management Technology in Bangka Belitung Islands. South of Tangerang, Indonesia: National Nuclear Energy Agency of Indonesia; 2019.

Lecomte J-F, Solomon S, Takala J, Jung T, Strand P, Murith C, et al. ICRP publication 126: Radiological protection against radon exposure. Annals of the International Commission on Radiological Protection (ICRP) 2014;43:5-73.

Madansky L, Rasetti F. Decay of Rn 220 and Rn 222. Physical Review 1956;102(2):464

Mahfiz RE, Risdiyanto I, Mahfud MA, Rahman AH, Primadi VB. Evapotranspiration estimation using vegetation index and surface reflectance SWIR Landsat-8 combination on various land cover. Proceedings of Sixth International Symposium on LAPAN-IPB Satellite; 2019 Sep 17; Pusteksat, Bogor: Indonesia; 2019.

Melson NH. Sorption of Thorium onto Subsurface Geomedia [dissertation]. Alabama, Faculty of Auburn University; 2011.

Ministry of Environment and Forestry R. Requirements and Procedures for Disposed Hazardous and Toxic Waste (B3) at the Final Landfill Facility. Jakarta, Indonesia: Ministry of Environment and Forestry R; 2016.

Pontedeiro EM, Heilbron PFL, Cotta RM. Assessment of the mineral industry NORM/TENORM disposal in hazardous landfills. Journal of Hazardous Material 2007;139:563-8.

Rajaretnam G, Spitz HB. Effect of leachability on environmental risk assessment for naturally occurring radioactive materials in petroleum oil fields. Health Physics 2000;78:191-8.

Rasito R, Sofywan S, Desita T. Radon concentration in air PTNBR-BATAN Bandung. Proceedings of the National Seminar on Nuclear Science and Technology; 2007 Jul 17-18; Center for Applied Nuclear Science and Technology, Bandung: Indonesia; 2007.

dos Reis RG, da Costa Lauria D. The potential radiological impact from a Brazilian phosphate facility. Journal of Environmental Radioactivity 2014;136:188-94.

Sari TP. Determination of primary tin zone use gravity method in tanjung gunung village central bangka regency. Proceedings of the International Conference on Maritime and Archipelago (ICoMA 2018); 2018 Sep 13-15; Universitas Bangka Belitung, Bangka: Indonesia; 2019.

Senftle FE, Farley TA, Lazar N. Half-life of Th^{232} and the branching ratio of Bi^{212}. Physical Review 1956;104(6):1629.

Septiadi D, Sugeng Y, Anzhar K, Suntoko H. An Extreme meteorological events analysis for nuclear power plant (NPP) siting project at Bangka Island, Indonesia. Proceedings of 41st HAGI Annual Convention and Exhibition; 2016 Sep 26-29; The 7th Hotel, Lampung: Indonesia; 2018.

Setiawan B, Sriwahyuni H. Determination of 137Cs elimination from solution by tasikmalaya bentonite and belitung quartz sand as barrier material candidate on the near surface disposal facility. Journal of Valence Chemistry 2018;4:14-21.

Singh B, Kant K, Garg M, Singh A, Sahoo BK, Sapra BK. Radiological impact of radon and thoron levels in dwellings measured using solid state nuclear track detectors. Proceedings of International Conference on Advances in Basic Science (ICABS 2019); 2019 Feb 7-9; GDC Memorial College, Bahal: India; 2019.

Sriwahyuni H, Setiawan B. Sorption ability of bentonite rocks from yogyakarta to eliminate the radiocesium elements in solution. Journal of Science Chemistry and Applications 2019;22:17-22.

Sucipta S, Hendra AP, Dadong I. Site selection for landfill disposal of NORM waste from tin industry in Bangka Island. Proceedings of International Conference on the Management of Radioactive Material (NORM) in Industry; 2020 Oct 19-30; IAEA Headquarters, Vienna: Austria; 2020.

Sujo LC, Cabrera MEM, Villalba L, Villalobos MR, Moye ET, Leon MG, et al. Uranium-238 and thorium-232 series concentrations in soil, radon-222 indoor and drinking water concentrations and dose assessment in the city of Aldama, Chihuahua, Mexico. Journal of Environmental Radioactivity 2004;77:205-19.

Szabo Z, DePaul VT, Kraemer TF, Parsa B. Occurrence of Radium-224, Radium-226, and Radium-228 in Water of the Unconfined Kirkwood-Cohansey Aquifer System, Southern New Jersey: 2004-5224. Virginia, USA: U. S. Geological Survey; 2005.

Tölgyessy J, Harangozó M. Radiochemical Methods Radionuclide Monitoring. Bratislava, Slovak Republic: Elsevier; 2005.

Vogiannis EG, Nikolopoulos D. Radon sources and associated risk in terms of exposure and dose. Frontiers in Public Health 2015;2:207.

Yu C, Kamboj S, Wang C, Cheng J-J. Data Collection Handbook to Support Modeling Impacts of Radioactive Material in Soil and Building Structures: No. ANL/EVS/TM-14/4. Illinois, USA: Argonne National Lab.(ANL); 2015.

Zhang C-L. Thermo-hydro-mechanical behavior of clay rock for deep geological disposal of high-level radioactive waste. Journal of Rock Mechanics and Geotechnical Engineering 2018;10:992-1008.

Treatment of Flue Gas from an Infectious Waste Incinerator using the Ozone System

Wenich Vattanapuripakorn[1], Khomson Khannam[1], Sathapon Sonsupap[1], Umakorn Tongsantia[2], Jiradanai Sarasamkan[3], and Bopit Bubphachot[4*]

[1]Department of Mechanical Engineering, Faculty of Engineering, Mahasarakam University, Mahasarakam 44150, Thailand
[2]Department of Public Health Administration, Faculty of Public Health, Khon Kaen University, Khon Kaen 40002, Thailand
[3]Department of Radiology, Faculty of Medicine, Khon Kaen University, Khon Kaen 40002, Thailand
[4]Heat Pipe and Thermal Tools Design Research Unit (HTDR), Faculty of Engineering, Mahasarakam University, Mahasarakam 44150, Thailand

ARTICLE INFO

Received: 31 Dec 2020
Received in revised: 29 Apr 2021
Accepted: 8 Jun 2021
Published online: 20 Jul 2021
DOI: 10.32526/ennrj/19/2020282

Keywords:
Infectious waste/ Ozone/ Treatment/ Air pollution /Rotary kiln/ Atmosphere/ Oxidation

*** Corresponding author:**
E-mail: bopit.b@msu.ac.th

ABSTRACT

Recently, levels of air pollution caused by exhaust gases from infectious waste combustion have been rising at a startling rate. Pollutant gases such as carbon monoxide (CO) and nitrogen dioxide (NO_2) have numerous health implications when unsafe amounts are released into the atmosphere. Thus, Pollution Control Systems (PCS) and Gas Cleaner Systems (GCS) play an important role in industries and the monitoring of incinerators. This research evaluated the GCS of rotary kilns in medical facilities located in the Northeast of Thailand. Data was collected from various sites, analyzed, and examined. Furthermore, Ozone (O_3) technology was applied to the rotary kiln allowing for the collection of new information on the pollution treatment systems. O_3 technology was installed along with the Wet Scrubber System (WSS) catalyzing the oxidation of O_3 and pollutant gases. In addition, a chiller was added to control and stabilize the temperature of the water. After the water temperature was controlled, the concentration of O_3 increased resulting in an efficient pollution treatment system. Levels of pollutant gas emission were found to be beneath control standards of both Thailand and those of the U.S. EPA. TSP content was reduced significantly from 22.0 mg/m³ to 3.4 mg/m³ (97%), CO content from 13.6 mg/m³ to 1.7 mg/m³ (96%), and NO_2 content fell from 16.3 (mg/m³) to 2.0 mg/m³ (99%). It is clear that the rotary kiln and Ozone technology should be used together in order to create a new and far more effective method of pollution treatment in small and mid-sized cities of Thailand.

1. INTRODUCTION

At present, solid waste management in Thailand is already considered a serious problem and continues to grow. According to the data in a 2018 report on solid waste and hazardous waste, the amount of solid waste was about 27.8 million tons, an increase of 1.64% compared to 2017. Due to the rapid expansion of urban communities, the shift from an agricultural society to an urban society, population increase, a significant rise in tourism, and increased consumption, the country is generating solid waste at levels never seen before. Municipal waste of roughly 9.58 million tons (34.0%) was separated at the source and reused, an increase of 13.0% from the previous year. Most of it was utilized as recyclable waste and organic waste. Disposal methods also play an important role as a total of 10.88 million tons (39.0%) was disposed of properly, whereas the remainder totaling approximately 7.36 million tons of waste (27.0%) was disposed of incorrectly (PCD, 2018). According to the Thailand state of pollution report 2012-2016, the amount of infectious waste is more than likely set to increase continuously. According to the report, a steady upward trend in the amount of infectious waste produced can clearly be seen with 43,800 50,481 52,147 53,868 and 55,656 tons per year, respectively. Infectious waste is classified by its source of origin, namely, public hospitals (56.79%), private hospitals

Citation: Vattanapuripakorn W, Khannam K, Sonsupap S, Tongsantia U, Sarasamkan J, Bubphachot B. Treatment of flue gas from an infectious waste incinerator using the ozone system. Environ. Nat. Resour. J. 2021;19(5):348-357. (https://doi.org/10.32526/ennrj/19/2020282)

(17.0%), clinics (19.2%), sub-district health promotion hospitals (6.375%), animal hospitals (0.6%), and hazardous laboratories (0.01%) (PCD, 2017). The staggering amount of waste produced requires a number of different management methods such as landfills, incineration, recycling, sustainability practices, biological reprocessing, energy recovery, avoidance and reduction, waste handling and transport, technologies, etc. (Bacinschi et al., 2010). The incineration method is the most popular because it requires the least amount of space and it can eliminate large amounts of waste which can be processed into energy. However, a major drawback is the high air pollution it generates (Innocent et al., 2013). The combustion of fossil fuels, solid wastes, and biomass emits large amounts of pollutants, including sulfur dioxide (SO_2), nitrogen dioxide (NO_2), organic pollutants, heavy metals, and particulate matter (PM). Substance emissions released from incineration include carbon monoxide (CO), hydrogen chloride (HCl), nitrogen dioxide (NO_2), sulfur dioxide (SO_2), and metal vapor (National Research Council, 2000). Smoke, dust, noxious fumes, and acid rain are all byproducts of the incineration method as well. This can pose a serious risk to quality and length of life as well as environmental ecology (Ma et al., 2012; Perera, 2017). The greatest risk air pollution poses is on breathing and the increased likelihood of respiratory problems. NO_2 inflames the lining of the lungs and reduces immunity to lung infections. This can cause health effects such as wheezing, coughing, colds, flu, and bronchitis with complications leading inevitably to more severe cases of diseases such as pneumonia and cancer. Children with asthma and older people with heart disease are most at risk.

This review focuses on the work in fuel pollutant treatments through low temperature ozone oxidation, especially CO, NO_2, organic pollutants, and industrial applications for the simultaneous removal of SO_2 and NO_2 with ozone. To date, most industrial research publications continue to contribute to the simultaneous elimination of SO_2 and NO_x, which has been written about extensively. This work is primarily concerned with more serious applications of ozone gas generators with wet scrubbing technology in industries. (Wang and Zhong, 2016), such as carbon black drying kiln furnaces (Ma et al., 2016), marine emissions (Xi et al., 2019; Zhou et al., 2016), glass melting furnaces (Yamamoto et al., 2016), and pulverized coal boilers (Si et al., 2019).

According to the analysis of the amount of pollutants emitted from the chimney of the infectious waste incineration system after the addition of the O_3 system, the addition of one additional oxygen atom resulted in new molecules with conditions which were stable to high energy and hard to damage due to factors such as temperature, heat, pressure, and reaction with substances with lower energy leading to rapid oxidation. O_3 has been found to have an oxidation potential of up to 2.07 electron Volts (eV). According to the principles of electrical energy, the corona discharge phenomena (CD ozone) is a method for allowing pure and dry oxygen gas to pass through thousands of volts of an electrical field (50-100 Hz), at medium frequency (100-1,000 Hz) and high frequency (1,000 Hz or more) at the discharge gap caused by the production of electricity at the dielectric surface that is a factor causing the ozone concentration (Hartmann et al., 2009). This electric field causes the oxygen in the air to split into oxygen atoms (O^-) that are stable and combine with other oxygen molecules. O_3 is released in a high concentration, from 1-10% by weight, which can be used to treat water and air effectively. The machine sizes range from small to large (milligrams to kilograms per hour level); machines have very low operating and maintenance costs, and they can be used forever. It is not necessary to replace old machines like those which use other deodorizing chemicals, which is a distinctive feature of ozone. (except for storage under low temperatures or ice) (U.S. EPA, 1999a). The decay of ozone depends on temperature and humidity, it has a high concentration and a pungent smell, is comparable to a gas, has the potential to perform bactericidal disinfection in both water and air, and it is a very potent oxidizing agent. Therefore, it can react with organic and inorganic substances. The mechanisms of pollutant treatment from the O_3 generator that causes oxygen to react with pollutants in the system before being released into the environment are quite highly effective. (U.S. EPA, 2011), Knowledge of rotary kiln technology and the application of O_3 technology for flue gas treatment is essential for design, construction, and optimization of flue gas treatment systems on an industrial scale. (Wang et al., 2010). Another important element is the residence time that ozone can be treated in. It is suggested that the optimum residence time of 1.25 seconds for NO_2 production should be extended to 8 seconds for N_2O_5 generation. In previous studies it has been stated that NO oxidation to NO_2 can be achieved within 0.1 seconds, while

N_2O_5 generation requires 3-5 seconds at optimum temperature, using a plasma system catalytic method. (Wei et al., 2007; Lin et al., 2016). As mentioned above, NO can be converted to NO_2 and N_2O_5, with O_3 and ozone catalysis promoting efficiency and oxidation rate. It is an important step in the conversion of NO_x to nitrates, (Ding et al., 2016a; Ding et al., 2016b; Zhao et al., 2016; Guo et al., 2016; Han et al., 2018; Liu et al., 2019). Ozone oxidation and absorption in a water-filled scrubber recorded concurrent elimination efficiency levels of 90%, 93%, and 100%, respectively, with a molar O_3/NO ratio of 0.6 and (NH_2), CO/NaOH adsorption. N_2O_5 has a much higher solubility which allows it to be absorbed without any need for additives. At the same time, oxidation in treatment areas for wet pollution can also be the best choice for industries (Lin et al., 2020). The positive effects of ozone input and the promotion effect of ozone additive control on the catalytic efficiency were significant. Several changes were found in the conversion process of ozone-induced organic pollutants with the PCDD/Fs destruction efficiency of 45% compared to V-Mn/Ti-CNT at 150°C while this value increased to 91% with low concentrations (50 ppm) for the optimal use of ozone concentrations for pollution treatment (Wang et al., 2018). The SO_2 and NO_x removal efficiencies of ozone attained levels ranging from 85% to 90%, in particular, the removal of NO_2 due to the reaction with O_3 (Shao et al., 2019; U.S. EPA, 1999b). The dissolution of NO_x and mercury will increase with suspension status and organic pollutants can be decomposed into non-toxic small molecules by oxidation. O_3 is a strong oxidizing agent of gases and can cause early oxidation reactions at low temperatures and uses adsorption to eliminate NO_2 by complete oxidation. In addition, O_3 takes part in an oxidation reaction with CO_2 gas by decomposing carbon monoxide, according to $O_3 + CO \rightarrow CO_2 + O_2$ and eliminates carbon monoxide poisoning. (Young and Jordan, 1995). In summary, there are countless advantages of employing this technique though it is hardly necessary to completely abandon or overhaul the current pollution treatment systems. Only a heat exchanger and low temperature oxidation chiller are needed to assist in the control of the temperature allowing for ozone gas emissions at 20-25°C, a feature that increases the safety and flexibility of the system. Most importantly, it can be combined with other technologies to achieve lower emissions and near-zero emissions. This can be achieved by adjusting the ozone injection mixed with cold water to reach the highest ozone concentration possible. Including the use of oxygen gas to help create ozone concentrations, voltage adjustments are also required to determine the most effective ozone concentration of the ozone generator and flow field optimization, the strictest NO_x, emission standards for these approaches still face challenges to meet stringent requirements to reduce environmental pollution in both air and water treatment systems. This ozone oxidation technique can be a good alternative, either as a supplement or a standalone arrangement for the treatment of different exhaust gases or adaptation of technology to incinerators for hospitals. Overall, this approach has the following advantages: high efficiency at low temperatures; Simple regeneration of the process without affecting the front operation, and is suitable for all varieties of complex exhaust gas environments. (Lin et al., 2020; U.S. EPA, 2019; Sung et al., 2013; Yuan et al., 2016).

In this paper, the researcher studied the effects of the modified treatment of flue gas from infectious waste incinerators using an ozone system. The waste incinerator was modified by applying Ozone technology in order to be both more efficient and effective. The incinerator was designed in accordance with the U.S. EPA standards. A three step combustion function was added to the incinerator and LP gas was used as fuel in the combustion of the waste while the temperature was controlled so as to not fall below 800°C (chamber 1), 1,200°C (chamber 2), and 1,400°C (chamber 3). This temperature was high enough to combust metal waste and destroy the structure of dioxins/furans (PCDDs/PCDFs). The O_3 system was installed at the WSS where O_3 and water were mixed. This mixture injected pollutants before being released into the atmosphere. Also, the setting of the voltage system played an important role in this process since highly concentrated O_3, which was used to treat pollutant gases, was generated here. The oxygen generator was added to stabilize the concentrated O_3 generation. The efficiency of O_3 on the treatment depended on the concentration of O_3 and the temperature. Furthermore, time is another key factor that must be controlled as it allows O_3 to oxidize pollutant gases to the fullest extent. Temperature inside the scrubber room had to be maintained at the correct temperature range while the chiller kept the water temperature at 20-25°C to allow O_3 to treat pollutant gases most effectively. A chemical study of O_3 was analyzed to generate the O_3 treatment that affected the efficiency of pollutant gases which were NO_2 and CO. It was revealed that the oxidation

between O_3 and low temperature exhaust gas significantly diluted the concentration of NO_2 and CO. The result suggested that the rotary kiln with O_3 application was more efficient than the one with no O_3 technology installed. Furthermore, the level of pollutant gas emissions decreased significantly when measured by the U.S. EPA and Thailand standards. The treatment method resulted in nearly zero pollutants being released. Therefore, the application of O_3 treatment methods of infectious waste incinerators needs further study as it is not only practical for industries, but also carries wide ranging implications for the global environment and human health.

2. METHODOLOGY

2.1 Infectious waste resources

The study utilized a total of 178 kg of infectious waste which came from hospitals, clinics, and medical establishments and was produced by medical services from a variety of treatments, dentistry, pharmaceuticals, laboratory diagnosis, and immunization as well as research studies conducted on humans in which there was contamination through contact with pathogens from patients or patient products. There was a clear collection process with general waste in which physical and chemical properties data were analyzed before waste was put into the incinerator. The samples of infectious waste analyzed in this research were of considerable importance because each kind of waste affected the burn and emitted different pollutants. The composition of the waste needed to be analyzed physically and chemically. Data such as weight, moisture, and density were collected. After that, each kind of waste was packed into 25×30×60 cm containers and the weight of each type of waste was recorded. The bags were completely sealed when burned and all that remained was ash after the combustion process was completed.

2.2 The infectious waste incinerator system

There are various air pollution control technologies related to maintaining safe levels of SO_2, NO_x, CO, organic pollutants, and mercury. Treatment site location and type of pollution are the two biggest factors when designing technology according to the flue behavior. A rotary kiln is designed in accordance with U.S. EPA standards. It combusts hazardous waste at least 850°C. Inside the kiln, there is a long tube placed in a horizontal line. This tube rotates while the machine is operating and is coated in fire-proof material so the machine can perform a long run combustion so that the hazardous waste is completely combusted. The function of a discharge breaching is to isolate the bottom ash caused by the combustion before the remaining ash is imported into the secondary combustion chamber. The secondary combustion chamber combusts the exhaust gases, which were left from the first combustion chamber, at a temperature not below 1,200-1,400°C (Jiang et al., 2019). At this high temperature, various types of steel, glass splinters and stainless steel are burned. A three-step kiln is designed to improve the combustion as it provides a more complete process leaving nothing remaining. The rotary kiln incinerator used in this experiment was developed using combustion furnace technology in Japan. An analysis of research advances for rotary incinerators found that the basic research for rotary incinerators tends to be mature. The latest research in rotary kilns is interdisciplinary and focused on technology integration with ozone generators. From a new perspective, this research further focuses on the comparative analysis of air emissions before and after ozone treatment of gas emissions, (Jiang et al., 2019) and was designed to achieve the highest possible efficiency for incineration systems used to dispose of infectious waste. Several recent improvements to the incinerator system in this study included improvements to the front gate of the primary chamber, where the combustion temperature is 800-1,200-1,400°C. Air-filling waste is heated and volatilized in the primary chamber. An aeration fan is used to inject and move air into the combustion chamber, which was designed to have an air flow through the front and back pipes, equalizing the air flow from both sides. The secondary chamber is used for the second round of exhaust gas combustion to eliminate gas pollution (dioxins and furans). Generally, the element mercury accounts for 20-50% in coal-burning fuel gas and 10-20% from conventional incinerators (Carpi, 1997). The cyclone separator functions as a dust collector; it typically employs centrifugal force, a form of inertia, to force the air containing dirt and dust through a vertical cylinder with a cone-shaped bottom. The aeration fan uses a high-pressure 0.5 horsepower pump to increase the pressure of the remaining gases after combustion and thus move them from the cyclone separator toward the wet scraper. The oxidized mercury is highly soluble in water and is reactive and can be absorbed in a wet scrubber. Therefore, an efficient pre-oxidation method can convert insoluble NO and Hg to highly soluble NO_2, N_2O_5, and Hg^{+2}, then simultaneous elimination

can occur in the post-absorption apparatus together with SO_2 (Zhao et al., 2015). Gas scrubbing involves dust and small particles that pass through the cyclone separator. The gas treatment chamber hosts a high oxidation reaction. The cool water tank stores the cool water required for injection from a nozzle during gas scrubbing. A small portion of the warm water is subsequently released into the warm water tank. The warm water tank stores warm water heated by the absorbed pollutants from the exhaust gases produced via combustion. The debris is dropped to the bottom of the tank and subsequently disposed of. Thereafter, clean water is fed into a chilling machine. The chilling machine produces cold water that is stored in the coolant tank before it is sprayed into the scrubbing tank. Once the water absorbs the heat, leading to an increase in its temperature, it is circulated back to the chiller to be cooled again (Figure 1).

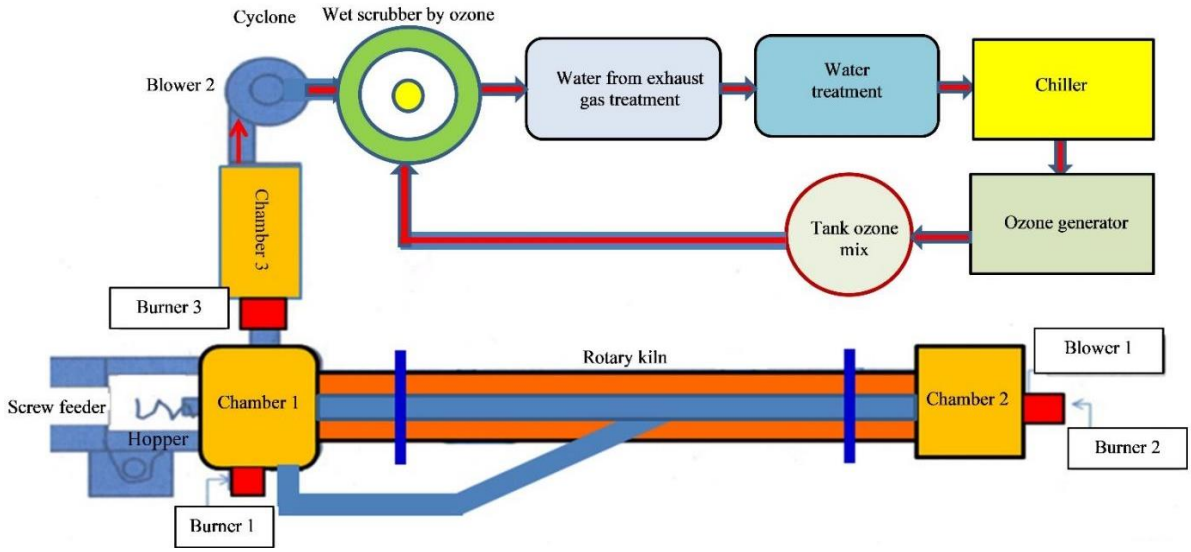

Figure 1. Infectious waste incinerator and ozone generator system

2.3 Air pollutants sampling and measurement

Sampling of the released exhaust gases at the end of the incinerator vent was performed at 2.2 m above the top end of the chimney. This process was based on the Air Quality of U.S. EPA (1999b) standard of gas emission sampling which recommends the collection of samples at a height equal to ten times the diameter of the chimney (0.22 m). The principle of emission suction from stationary sources was used to collect and analyze air quality samples for particulates.

For the sample collection in this study, the isokinetic (dry basis) sampling method was adopted; this method employs a filter cured at 105°C at the same wind velocity present during measuring, to prevent the refraction of moving particles and maintain an acceptable isometric kinetic range of ±10%. The methods used for air sampling and analyses are listed in Table 1. The results of fuel gas analysis were compared with the Thailand regulatory system and the U.S. EPA (1999b) standard.

Table 1. Methods of air pollution sampling and analysis

Parameters	Analysis method	Standard Value U.S. EPA (1999b)
Mercury (Hg)	Isokinetic, Cold Vapor - ASS	0.05 mg/m^3
Lead (Pb)	Isokinetic, ICP-AES	1.50 mg/m^3
Cadmium	Isokinetic, ICP-AES	0.50 mg/m^3
Hydrogen fluoride (HF)	Ion Chromatography	16.40 mg/m^3
Particulate (TSP)	Isokinetic, Gravimetric	320.00 mg/m^3
Sulfur dioxide (SO_2)	Barium Thorin Titrimetric	79.00 mg/m^3
Oxides of nitrogen (NO_x as NO_2)	Chemical Absorption, Colorimetric	470.00 mg/m^3
Carbon monoxide (CO)	Bag, Non-Dispersive Infrared	45.80 mg/m^3
Hydrogen chloride (HCl)	Ion Chromatography	119.00 mg/m^3

2.4 Ozone generator for fuel gas treatment

The O_3 generator (Figure 2) used in this experiment was developed and designed to achieve the highest possible efficiency for treatment systems used to dispose of infectious waste. The several recent improvements to the treatment system in this study are described below (Table 2).

Table 2. Infectious waste treatment system by ozone generator

Parameters	Value
Temperature chamber wet scrubber	20-25°C
Oxygen consumption rate	10 L/min
Ozone concentration	100-160 g/Nm^3
Effect of residence time	3-8 sec
Flow rate mixing	65 L/min
AC voltage	5-10 kV
Oxidation duration time	0.5-5 min

(a) The O_3 generator tube corona discharge is responsible for producing O_3. There were many sizes depending on the needs of use. Its sizes range from small to large (milligrams to kilograms per hour). It uses high voltage electricity to supply power to the ozone tube. A transformer was applied to increase the voltage to achieve high efficiency and low loss of power. This was achieved by switching the power supply and by changing the voltage from 220 V, 50 Hz to 1-10 kV, 1-10 kHz.

(b) The O_3 machine was responsible for producing O_3 (Zumozone brand, model: OZ100G/H, serial number: OZ 160726616, max capacity: 100 g/h, O_3 concentration: 100-160 g/Nm^3, type of O_3 cell cooling: water 220 V, 50 Hz).

(c) The oxygen generator is responsible for producing more than 90% oxygen to be supplied to the ozone machine (oxygen concentration: 90±3%; power consumption: 550-Watt Max; oxygen flow rate: 10 L/min; Built-in oil-free air compressor: 220 V/50 Hz).

(d) The O_3 mixing unit is responsible for mixing O_3 with water (flow rate mixing: 65 L/min; mixing unit two-tube pump, centrifugal pump 1 HP: 220 V, 50 Hz).

(e) Venturi injectors are a highly efficient means of mixing liquids or gasses into a stream of water. They work on the principle of differential pressure. Water enters the venturi at a higher pressure rate than it exits with. The difference in the entry and exit pressures creates a vacuum at the suction port on the side of the venturi. The bigger the difference in pressure, the greater the force of the vacuum, and therefore the efficiency of the mixing.

(f) Wet scrubbing traps dust and small particles that pass through the cyclone separator. The gas then flows through from a side of the tank above water into the cooling pad in the opposite direction. Water is kept at a temperature of 20-25°C and sprayed from the top towards the steering wheel that directs the flow to the activated charcoal which absorbs toxic gases and odors such as methyl sulfide.

(g) The gas treatment chamber with a high oxidation reaction eliminates most types of microbes, especially the most dangerous. Bacteria, odors, chemical compounds, and toxic gases are also eliminated using the treatment in this chamber before the gases are released to the atmosphere.

(h) The cool water tank stores the cool water required for injection from a nozzle during gas scrubbing. The water gate adjusts and mixes water containing heat and toxic gas before this water enters the cool water pump. A small portion of the warm water is subsequently released into the warm water tank.

(i) The water tank stores warm water that is heated by the absorbed pollutants from the exhaust gases produced via combustion. The debris is dropped to the bottom of the tank and subsequently disposed of clean water is fed into a chilling machine.

(j) The chilling machine has a capacity of 60,000 BTU/HR (condensing unit "CARRIER" R410; Water tank 550 L; SUS304 supply). The water pump circulates water through the system. The water pump (temperature control Dixell; water temperature inlet was 12°C; water temperature outlet was 7°C) produces cold water that is stored in the coolant tank before it is sprayed into the scrubbing tank. Once the water absorbs the heat leading to an increase in its temperature, it is circulated back to the chiller to be cooled again.

2.4.1 The method of ozone generator system

Oxygen generator generates pure oxygen and Ozone generator generates pure ozone. After pure ozone and pure oxygen are mixed, the injector pump suctions these gases through the pipe and water is injected into the pump. Then, the gases and water are mixed by the Venturi injector system. The mixing unit is compressed by the injector pump to the storage tank before it is used at the wet scrubber room as shown in Figure 2.

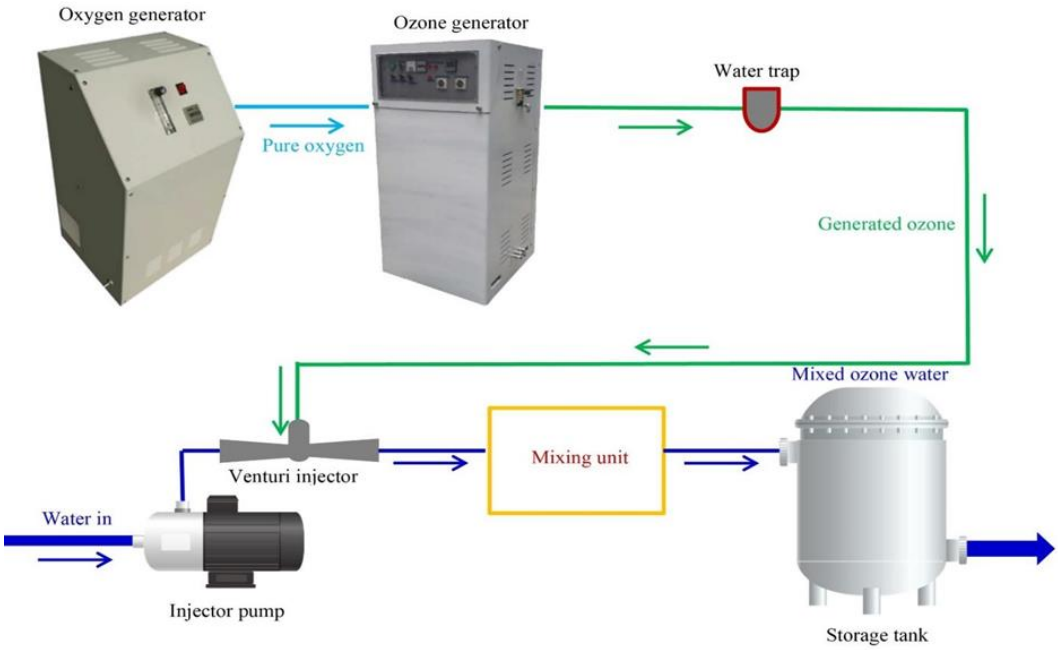

Figure 2. Ozone generator systems

3. RESULTS AND DISCUSSION

3.1 Physical and chemical properties of waste

The components were analyzed by drying and weighing after drying. The highest level of plastic waste was 58.64%, followed by other various types of metal and textiles waste (21.38%), and rubber and glass splinter waste (11.45%). In addition, it was found that plastic waste pollution is one fifth of all infectious waste. (Olanrewaju, 2019). The proximate analysis of infectious waste showed that the moisture content was 42.69%, volatile matter content was 39.75%, ash content was 11.70%, and this infectious waste had a density equal to 173.45%. The most common chemical composition found was carbon (59.48%), followed by oxygen (31.30%), hydrogen (8.75%), and the remaining gas was nitrogen. This is consistent with the ratio of elements that can be found in both general waste and infectious waste. The chemical composition in the hospital waste was studied, and it was found that the highest carbon content was 34% and the oxygen content was 14%. The elemental composition analysis of hospital infectious waste revealed that the compositions of infectious waste were carbon content (34%) and oxygen content (15%) (Li and Jenq, 1993). Solid municipal waste was analyzed as well, and it was reported that the elemental compositions of the waste were carbon content (60%), hydrogen content (7.2%), oxygen content (22%), and nitrogen content (4.6%).

3.2 Comparative results of air pollution gases before and after using the ozone system in a rotary waste incinerator

The results of the gas values obtained from the comparison of the emission of air pollutants before and after using the ozone system in a rotary waste incinerator can be seen in the following list in descending order of amounts: dust, sulfur dioxide gas, carbon monoxide, nitrogen dioxide, hydrogen chloride gas, and opacity. The results revealed that air pollution gases before using the ozone system were as follows: TSP content was 22.0 (mg/m³), CO content was 13.6 (mg/m³), and NO_2 content was 16.3 (mg/m³). After the O_3 system had been applied to the Wet Scrubber System of the rotary kiln, it was obvious that pollutant gas levels decreased significantly as follows; the level of TSP content was 3.4 (mg/m³) (84%), the level of CO content was 1.7 (mg/m³) (87%), and the level of NO_2 content was 2.0 (mg/m³) (87%). It was found to be more efficient than those which had not applied O_3 technology as shown in Figure 3.

3.3 Comparison of air pollutant levels in the ozone system with U.S. EPA standards

The incineration process taking place inside the incinerator has been specially designed to match the characteristics of the waste, namely the high humidity rate and to be considerate of the variable heat value. Combustion has to be well controlled to prevent the

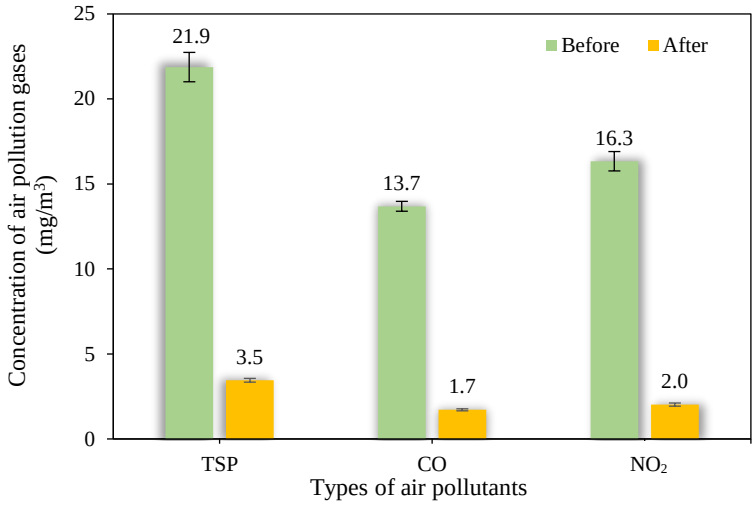

Remark: 15% Oxygen Content

Figure 3. The comparison of air pollution gases before and after using the ozone system in a rotary waste incinerator

release of harmful pollution into the environment in the form of s toxic gases, soot, and odors. The gases generated by combustion must be free of soot and particles as regulated by law before they are released into the atmosphere. O_3 technology was applied to the rotary kiln greatly improving its efficiency as highly concentrated O_3 worked optimally at the appropriate temperature (Lin et al., 2020). Additionally, O_3 treated and reduced SO_2 and NO_2 as well (Wang et al., 2018; Shao et al., 2019). Table 3 demonstrates the comparison of pollutant gas levels before and after using the ozone system in a rotary waste incinerator. It was found that the level of TSP content was 3.40 (mg/m³), the level of CO content was 1.7 (mg/m³), and the level of NO_2 content was 2.0 (mg/m³). Even though pollutant gases were still detected, they were far below the U.S. EPA standards. The Pollution Control Department of Thailand follows U.S. EPA standards set as the guideline for Thailand's own set of standards. The established standard is that the TPS content level is 120 (mg/m³), CO content level is 46 (mg/m³), and NO_2 content level is 339 (mg/m³). The comparison of pollutant gases after using the O_3 system under the U.S. EPA standard system demonstrated a significant reduction in pollutant gases as follows: TSP content was 3.4 (mg/m³) (97%), CO content was 1.7 (mg/m³) (96%), and NO_2 content was 2.0 (mg/m³) (99%). According to pollutant gas emission controls and of the U.S. EPA standards, the regulations for the amount of solid waste combustion is between 1 to 50 tons per day as shown in Table 3.

Table 3. Fuel gas concentration

Parameters	Concentrations			Unit
	15% O_2	7% O_2	U.S. EPA[(1)]	
TSP	3.4	7.4	120	mg/m^3
SO_2	1.3	1.3	30	ppm
NO_x as NO_2	1.0	1.0	180	ppm
CO	1.5	3.3	40	ppm
Hg	0.001	0.001	0.050	mg/m^3
Cd	ND[(2)]	ND[(3)]	0.05	mg/m^3
Pb	ND[(2)]	ND[(3)]	0.50	mg/m^3
HF	0.013	0.034	20	ppm
HCl	<0.015	<0.015	25	ppm
Opacity	5.0	5.0	10.0	%

[(1)] The standards for controlling the emissions of pollutants released from an infectious waste incinerator in accordance with the methods prescribed by the United States Environmental Protection Agency (U.S. EPA), burning less than 50 tons/day

[(2)] MDL=Method Detection Limit (MDL of Lead=0.19 mg/m^3), (MDL of Cadmium=0.02 mg/m^3)/N=Not Detected

[(3)] Results of actual % O_2

3.4 Effect of ozone system addition on NO_2 and CO reduction in infectious waste incineration

The results clearly presented the stark contrast in numbers when employing the system before using the ozone system, NO_2 content was 16.300 (mg/m³) and CO content was 13.600 (mg/m³), and after using the ozone system, NO_2 content was 2.0 (mg/m³) and CO content was 1.7 (mg/m³). Similar results were obtained by Ding et al. (2016a) and Ding et al. (2016b) which stated that a chemical study of O_3 was carried out to reveal how the O_3 treatment affects the concentration of pollutant gases such as NO_2 and CO. It showed that the oxidation between O_3 and low temperature exhaust gas, NO_2 and CO, significantly diluted the concentration of NO_2 and CO. Furthermore, the results suggested that O_3 application for the treatment of pollutant gases in the wet scrubber room is practical for industries (Wang and Zhong, 2016).

4. CONCLUSION

The study found that levels of pollutant gases such as TSP, NO_2, and CO emitted from infectious waste incinerator chimneys were significantly reduced after O_3 technology was installed. The results revealed that air pollution gases before using an ozone system were as follows; TSP content was 22.0 (mg/m³), CO content was 13.6 (mg/m³), and NO_2 content was 16.3 (mg/m³). Then, after an O_3 system had been applied to the Wet Scrubber System of the rotary kiln, it was immediately apparent that the process caused air pollution gas levels to drop significantly as follows; the level of TSP content was 3.4 (mg/m³) (84%), the level of CO content was 1.7 (mg/m³) (87%), and the level of NO_2 content was 2.0 (mg/m³) (87%). Results obtained from the study show levels which are far below the U.S. EPA standards. The established standard states that the acceptable TPS content level is 120 mg/m³, CO content level is 46 mg/m³, and NO_2 content level is 339 mg/m³. The study showed the result of air pollution gases after using the O_3 system as follows; TSP content was 3.4 mg/m³ (97%), CO content was 1.7 mg/m³ (96%), and NO_2 content was 2.0 mg/m³ (99%). The results suggest that the rotary kiln with O_3 application was more efficient than the one without O_3 technology installed. Therefore, the application of an O_3 system on infectious waste incinerators warrants further study as it is practical for a wide variety of industries, will have a considerable impact on the global environment, and the health and quality of life for people everywhere.

Further study of flue gas pollutants removal by O_3 oxidation and studies on the quality of water used for ozone-reactive blending for the injection of flue gas treatment of pollution in the wet scrubber room is strongly urged in the race to find a solution to treat the wastewater with the ratio of consumption. The water quality can be further utilized before being released from the treatment system for future use in industrial, agricultural, and various other fields.

ACKNOWLEDGEMENTS

This research was provided with financial support and technical support by Energy Experts Thailand Co., Ltd.

REFERENCES

Bacinschi Z, Rizescu CZ, Stoian EV, Necula C. Waste management practices used in the attempt to protect the environment. Proceedings of the 3rd WSEAS International Conference on Engineering Mechanics, Structures, Engineering Geology; 2010 Oct 24-26; Wisconsin: USA; 2010.

Carpi A. Mercury from combustion sources: A review of the chemical species emitted and their transport in the atmosphere. Water, Air, and Soil Pollution 1997;983(4):241-54.

Ding J, Lin J, Xiao J, Zhang Y, Zhong Q, Zhang S, et al. Effect of fluoride doping for catalytic ozonation of low-temperature denitrification over cerium-titanium catalysts. Journal of Alloys and Compounds 2016a;665:411-7.

Ding J, Zhong Q, Cai H, Zhang S. Structural characterizations of fluoride doped CeTi nanoparticles and its differently promotional mechanisms on ozonation for low-temperature removal of NO_x (x=1, 2). Chemical Engineering Journal 2016b;286:549-59.

Guo L, Zhong Q, Ding J, Ou M, Lv Z, Song F. Low-temperature NO_X (x=1, 2) removal with OH radicals from catalytic ozonation over α-FeOOH. Ozone: Science and Engineering 2016;385:382-94.

Han C, Zhang S, Guo L, Zeng Y, Li X, Shi Z, et al. Enhanced catalytic ozonation of NO over black-TiO_2 catalyst under inadequate ozone (O_3/NO molar ratio=0.6). Chemical Engineering Research and Design 2018;136:219-29.

Hartmann W, Roemheld M, Rohde KD, Spiess FJ. Large area pulsed corona discharge in water for disinfection and pollution control. IEEE Transactions on Dielectrics and Electrical Insulation 2009;164:1061-5.

Innocent AJ, Chamhuri S, Hassain MD. Incineration and its implications: The need for a sustainable waste management system in Malaysia. International Journal of Environmental Science 2013;4(3):367-78.

Jiang X, Li Y, Yan J. Hazardous waste incineration in a rotary kiln: A review. Waste Disposal and Sustainable Energy 2019; 1(3):3-37.

Li CS, Jenq FT. Physical and chemical composition of hospital waste. Infection Control and Hospital Epidemiology 1993;143:145-50.

Lin F, Wang Z, Ma Q, He Y, Whiddon R, Zhu Y, et al. N_2O_5 formation mechanism during the ozone-based low-

temperature oxidation deNOX process. Energy and Fuels 2016;306:5101-7.

Lin F, Wang Z, Zhang Z, He Y, Zhu Y, Shao J, et al. Flue gas treatment with ozone oxidation: An overview on NO_x, organic pollutants, and mercury. Chemical Engineering Journal 2020;382:123030.

Liu B, Xu X, Liu L, Dai W, Jiang H, Yang F. Catalytic ozonation of NO with low concentration ozone over recycled SAPO-34 supported iron oxide. Industrial and Engineering Chemistry Research 2019;584:1525-34.

Ma Q, Wang Z, Lin F, Kuang M, Whiddon R, He Y, et al. Characteristics of O_3 oxidation for simultaneous desulfurization and denigration with limestone-gypsum wet scrubbing: Application in a carbon black drying kiln furnace. Energy and Fuels 2016;303:2302-8.

Ma J, Xu X, Zhao C, Yan P. A review of atmospheric chemistry research in China: Photochemical smog, haze pollution, and gas-aerosol interactions. Advances in Atmospheric Sciences 2012;295:1006-26.

National Research Council. Waste Incineration and Public Health. Washington, DC., USA: National Academies Press; 2000.

Olanrewaju O. Quantification and characterization of medical waste in public health care facilities within Akure Metropolis, Ondo State, Nigeria. EPH-International Journal of Agriculture and Environmental Research 2019;55:15-30.

Perera FP. Multiple threats to child health from fossil fuel combustion: Impacts of air pollution and climate change. Environmental Health Perspectives 2017;125:141-8.

Pollution Control Department (PCD). Thailand Statement of Pollution Report 2017. 1st ed. Bangkok, Thailand: Wongsawang Publishing and Printing; 2017.

Pollution control department (PCD). Thailand Statement of Pollution Report 2018. 1st ed. Bangkok, Thailand: Wongsawang Publishing and Printing; 2018.

Shao J, Xu C, Wang Z, Zhang J, Wang R, He Y, et al. NO_x reduction in a 130 t/h biomass-fired circulating fluid bed boiler using coupled ozonation and wet absorption technology. Industrial and Engineering Chemistry Research 2019; 5839:18134-40.

Si T, Wang C, Yan X, Zhang Y, Ren Y, Hu J, et al. Simultaneous removal of SO_2 and NO_x by a new combined spray-and-scattered-bubble technology based on preozonation: From lab scale to pilot scale. Applied Energy 2019;242:1528-38.

Sung TL, Teii S, Liu CM, Hsiao RC, Chen PC, Wu YH, et al. Effect of pulse power characteristics and gas flow rate on ozone production in a cylindrical dielectric barrier discharge ozonizer. Vacuum 2013;90:65-9.

United States Environmental Protection Agency (U.S. EPA). Wastewater Technology Fact Sheet: Ozone Disinfection. EPA/832-F-99-063. Washington, D.C., USA: EPA; 1999a.

United States Environmental Protection Agency (U.S. EPA). Nitrogen Oxides (NO_x): Why and How They are Controlled. EPA-456/F-99-006. Washington, D.C., USA: EPA; 1999b.

United States Environmental Protection Agency (U.S. EPA). Water Treatment Manual: Disinfection. Wexford, Ireland: Johnstown Castle Co.; 2011.

United States Environmental Protection Agency (U.S. EPA). Air pollutant emissions trends data [Internet]. 2019 [cited 2019 May 10]. Available from: https://.epa.gov/air-emissions-inventories/air-pollutant-emissions-trends-data.

Wang Z, Li B, Ehn A, Sun Z, Li Z, Bood J, et al. Investigation of flue-gas treatment with O_3 injection using NO and NO_2 planar laser-induced fluorescence. Fuel 2010;899:2346-52.

Wang Q, Tang M, Peng Y, Du C, Lu S. Ozone assisted oxidation of gaseous PCDD/Fs over CNTs-containing composite catalysts at low temperature. Chemosphere 2018;199:502-9.

Wang J, Zhong W. Simultaneous desulfurization and denitrification of sintering flue gas via composite absorbent. Chinese Journal of Chemical Engineering 2016;248:1104-11.

Wei L, Zhou J, Wang Z, Cen K. Kinetic modeling of homogeneous low-temperature multi-pollutant oxidation by ozone. Ozone: Science and Engineering 2007;293:207-14.

Xi H, Zhou S, Zhou J. New experimental results of NO removal from simulated marine engine exhaust gases by $Na_2S_2O_8$/urea solutions. Chemical Engineering Journal 2019;362:12-20.

Yamamoto Y, Yamamoto H, Takada D, Kuroki T, Fujishima H, Okubo M. Simultaneous removal of NO_x and SO_x from flue gas of a glass melting furnace using a combined ozone injection and semi-dry chemical process. Ozone: Science and Engineering 2016;383:211-8.

Young C, Jordan T. Cyanide remediation: Current and past technologies. Proceedings of the 10th Annual Conference on Hazardous Waste Research; 1995 May 23-24; Kansas State University, Manhattan: USA; 1995.

Yuan D, Wang Z, Ding C, He Y, Whiddon R, Cen K. Ozone production in parallel multichannel dielectric barrier discharge from oxygen and air: The influence of gas pressure. Journal of Physics D: Applied Physics 2016;49:455203.

Zhao L, Li C, Zhang X, Zeng G, Zhang J. A review on oxidation of elemental mercury from coal-fired flue gas with selective catalytic reduction catalysts. Catalysis Science and Technology 2015;57:3459-72.

Zhao W, Zhang S, Ding J, Deng Z, Guo L, Zhong Q. Enhanced catalytic ozonation for NO_x removal with $CuFe_2O_4$ nanoparticles and mechanism analysis. Journal of Molecular Catalysis A: Chemical 2016;424:153-61.

Zhou S, Zhou J, Feng Y, Zhu Y. Marine emission pollution abatement using ozone oxidation by a wet scrubbing method. Industrial and Engineering Chemistry Research 2016; 5520:5825-31.

Analysis of Landslide Occurrence using DTM-Based Weighted Overlay: A Case Study in Tropical Mountainous Forest of Cameron Highlands, Malaysia

Paul Lau Hua Ming* **and Azita Ahmad Zawawi**

Faculty of Forestry and Environment, Universiti Putra Malaysia, Serdang 43300, Malaysia

ARTICLE INFO

Received: 18 Apr 2021
Received in revised: 29 May 2021
Accepted: 8 Jun 2021
Published online: 21 Jul 2021
DOI: 10.32526/ennrj/19/202100069

Keywords:
Cameron Highlands/ Digital Terrain Model (DTM)/ Mountainous forest/ SAGA GIS/ Terrain assessment

*** Corresponding author:**
E-mail: paulau_94@hotmail.com

ABSTRACT

Landslides are massive natural disasters all around the world. In general, our society is only concerned with the landslides that can cause economic distress and impact human life. Landslides in remote areas such as mountainous forests have often been neglected. Referring to the historical disaster event, forest landslides have vast potential to cause unexpected ecological and social damage. This study reveals the terrain characteristics of the complex mountainous forest area of Cameron Highlands (CH), Malaysia, and demonstrates an approach to evaluate the terrain sensitivity of CH. Terrain assessment can be a powerful tool to prevent or reduce the risk of landslides. In this study, terrain features; elevation, slope gradient, aspect, topography wetness index (TWI), and length-slope factor (LS Factor) were extracted using a Digital Terrain Model (DTM) at 10 m resolution. The selected terrain features were incorporated using weighted overlay analysis to derive a terrain sensitivity map (TSM) using SAGA GIS software. The map identified five types of terrain sensitivity classified as very high sensitivity, high sensitivity, moderate sensitivity, low sensitivity, and very low sensitivity; these areas have a coverage of 0.78 km^2, 114.31 km^2, 107.50 km^2, 102.99 km^2, and 0.65 km^2, respectively. The findings suggest that the sensitive areas are scattered throughout all of the mountainous forests of CH; thus, this enhanced the risk of landslide. Results showed 79.25% accuracy, which is satisfactory to be a guideline for forest management planning and assist decision making in the respective region.

1. INTRODUCTION

Terrain is a complicated environmental factor that affects land use, human development, and localized ecology (Gong et al., 2017); and influences the water level as it contributes to total dissolved solid (Ostad-Ali-Askari and Shayannejad, 2021). In a more straightforward form, terrain refers to the features on the Earth's surface (Li and Hsu, 2020). Terrain characteristics can be studied by conducting terrain assessment. According to Beaven and Lawrence (1973), terrain assessment is a study of geo-morphology, terrain features, and limitations of a specific area. It can be applied in various fields. Ahmed and Rao (2019) conducted a terrain assessment to evaluate watershed conditions in Tuirini River, India, while Colby and Dobson (2010) evaluated flood patterns to develop a hazard prevention plan. Kim et al. (2017) conducted a terrain assessment to predict the wind flow in the montane area to identify a suitable spot for wind farm establishment. These studies emphasized that assessing terrain condition is crucial studying environmental phenomena, such as water flow and wind intensity, to evaluate and predict the land use potential.

In addition, terrain assessment can be useful to predict landslides. For example, Wawer and Nowocien (2003) conducted a terrain assessment to predict shallow landslides triggered by shallow groundwater in the Naleczow Plateau. Tarolli and Tarboton (2006) conducted a terrain assessment to find landslide initiation points in the Miozza

Citation: Lau PHM, Zawawi AA. Analysis of landslide occurrence using DTM-based weighted overlay: A case study in tropical mountainous forest of Cameron Highlands, Malaysia. Environ. Nat. Resour. J. 2021;19(5):358-370. (https://doi.org/10.32526/ennrj/19/202100069)

catchment area, Italy. Moreover, Gutierrez-Martin et al. (2019) conducted a terrain assessment to study the relationship between landslide susceptibility and heavy rainfall in Hundidero County, Spain. These studies aimed to forecast natural disasters by developing a model for terrain assessment in advance to pinpoint the potential landslide locations.

A landslide can occur naturally due to weathering processes or external triggers such as earthquakes, melting snow, and rainfall (Zhang et al., 2014). According to Cruden (1991) and Froude and Petley (2018), landslides are disaster events when land collapses and leads to soil sliding and rocks falling from the upper slope to lower slope due to gravity. Moreover, terrain with a high gradient of steepness tends to have a higher risk of landslide triggering than ground in flat conditions. These processes and external factors will initiate landslides in the area with high terrain sensitivity. According to Zhou et al. (2002), a landslide is closely related to the terrain condition and its geographical characteristics. Thus, landslides can occur when the land is used without wise management by neglecting the importance of terrain conditions. One of the examples is shown in a construction project at Malaysia Northern State that triggered a landslide as the building was constructed on a steep hill 75 m high and more than 25° steepness of slope, which is critical enough to initiate a landslide (Dermawan, 2019). In 1963, a large-scale landslide in Vajont, Italy caused 2,000 deaths. The high mortality was due to the tsunamis caused by the landslide of mountain parts into a lake (University of Cincinnati, 2018). These cases reflect the importance of terrain related study in order to avoid tragedy by conducting mitigation plans in advance.

Malaysia is one of the countries that are at high risk of landslide disasters (Matori et al., 2011). According to Sim et al. (2018), Malaysia is ranked tenth globally with a high frequency of landslides based on the landslide data between the years of 2007 to 2016. Several big scale landslides were recorded within the time frame. For instance, the landslide that occurred in Mount Kinabalu, Sabah in 2015 caused the death of 18 climbers and massive destruction to nearby farmland, houses, and bridges (Tongkul, 2015). In addition, a landslide tragedy occurred in Bukit Antarabangsa, Selangor in 2008 caused four deaths and destroyed 14 bungalows (The Star Online, 2008). Due to the high frequency of landslides, the Malaysia government had initiated landslide awareness systems such as the Early Warning System (EWS) and Kuala Lumpur Slope Information System (KuLSIS) (Wong, 2014; Zakiah et al., 2019). In addition, researchers had done extensive work by conducting an assessment on landslide occurrences in Malaysia, which covers various aspects such as correlation between the rainfall intensity and landslide frequency along public roads (Tay and Selaman, 2011); the effect of soil type and lithology factors towards landslide occurrence (Mohd et al., 2019); and the influence of land use towards landslide occurrence (Kamilia et al., 2016).

However, most of the landslide related study and prevention planning was focused on the urbanized area. Public and authorities show relatively less concern on landslide hazards in the mountainous region. According to the University of Cincinnati (2018), society tends to show less attention to landslide events in the natural area as these areas are often unpopulated. In fact, landslide risk in less populated areas will cause harm to the public as well. For example, a tourist tour which included 40 Malaysian tourists was trapped in Mount Rinjani, Indonesia due to an earthquake triggered by a landslide (Teh, 2019). This study focused on a detailed terrain sensitivity assessment in the natural area which should not be neglected.

Conventionally, terrain assessments are carried out manually where the information of terrains such as elevation and slope gradient are attained through Global Positioning System (GPS) (Kavitha et al., 2018). This method acquire data with relatively high accuracy, but it comes with higher labor costs, time-consumption, weather dependence, and limited accessibility. Today, terrain assessment can be conducted effectively using information derived from the Geography Information System (GIS) and Remote Sensing (RS). GIS is a powerful tool that is capable of enhancing terrain visualization and enables users to study the relationship of terrain features with its surroundings (Statuto et al., 2017). Through these technologies, terrain assessment can be conducted without physical access to the area. This study aims to develop a terrain sensitivity map through the DTM application and test its accuracy by verification to historical events. This work will provide a guideline for locating sensitive areas in a complex tropical mountainous area. Map outputs of this study may serve as a basis for forest managers, land developers, and policy makers in future planning to maintain sustainable forest resources.

2. METHODOLOGY

2.1 Study area

This study was conducted on the forest area of Cameron Highlands (CH), Peninsular Malaysia. The mountainous highland, which is characterized by dynamic terrain characteristics, plays essential roles in Malaysia's economic growth through the ecotourism sector, plantation, and agriculture production (Figure 1) (Azita et al., 2019). The rapid development of CH gives both positive and negative impacts on the environment, including landslides, where forest area plays as a stabilizer to the whole ecosystem. Being ranked as one of the mountainous regions listed as landslide hotspots in Malaysia, preservation of this mountainous forest highland is crucial for biodiversity and land stability, as well as community protection.

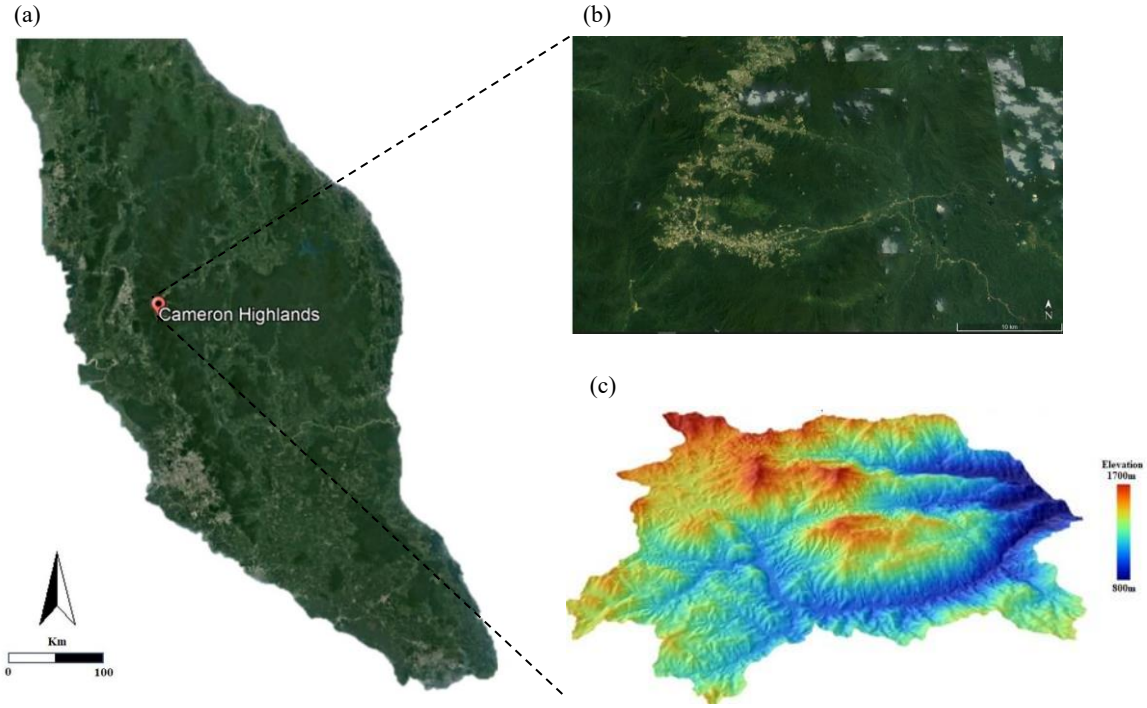

Figure 1. (a) Map of Peninsular Malaysia, (b) Landsat view of Cameron Highlands, and (c) three-dimensional (3D) terrain map of Cameron Highlands (4°31′26.99″N; 101°20′12.00″E)

The geographical characteristics of CH are shown in Table 1. CH possesses an elevation ranging from 1,070 to 1,870 m.a.s.l. It is a high precipitation area that receives an average of 2,852 mm of rainfall every year. According to Larsen and Simon (1993), the threshold value of rainfall to trigger a landslide in a tropical area is 2,000 mm/year. Countries that are located within wet tropic regions such as Malaysia and Indonesia tend to have the potential of landslides caused by heavy rainfall (Putra et al., 2021). In addition, the dynamic landform of CH and high precipitation makes it an area with high landslide susceptibility

Table 1. Geographical characteristics of Cameron Highlands

Characteristics	Attribute	Source
Coordinate	4°31′26.99″N, 101°20′12.00″E	Matori et al. (2011)
Area coverage	712 km^2	Zaini et al. (2014)
Elevation	1,070-1,870 m	Matori et al. (2011)
Precipitation	2,852 mm/year	Jerkins (2014)
Rainy day	236 day/year	Jerkins (2014)
Mean temperature	18.5°C	Jerkins (2014)
Forest distribution	Upper dipterocarp forest (750~1,200 m) Lower montane forest (1,200~1,500 m) Upper montane forest (>1,500 m)	Kumaran and Ainuddin (2006)

2.2 Research workflow and data acquirement

Figure 2 shows the entire workflow of the research.

2.3 Data acquirement

Spatial data were obtained from two agencies: the Forestry Department of Peninsular Malaysia (JPSM) and the Department of Survey and Mapping (JUPEM), as shown in Table 2. Malaysia is a country that has full coverage of clouds. Thus, the DTM obtained from JUPEM was generated through the technology of radargrammetry which utilises microwaves as data acquisition vectors as it can penetrate through the cloud cover to achieve relatively higher data accuracy (JUPEM, 2019).

Table 2. Resolution and source of spatial data

Spatial data	Year	Resolution	Agency
DTM	2018	10×10 m	JUPEM
Shape file of CH	2013	NA	JPSM
Topography map	2008	5×5 m	JUPEM

NA=Not Applicable

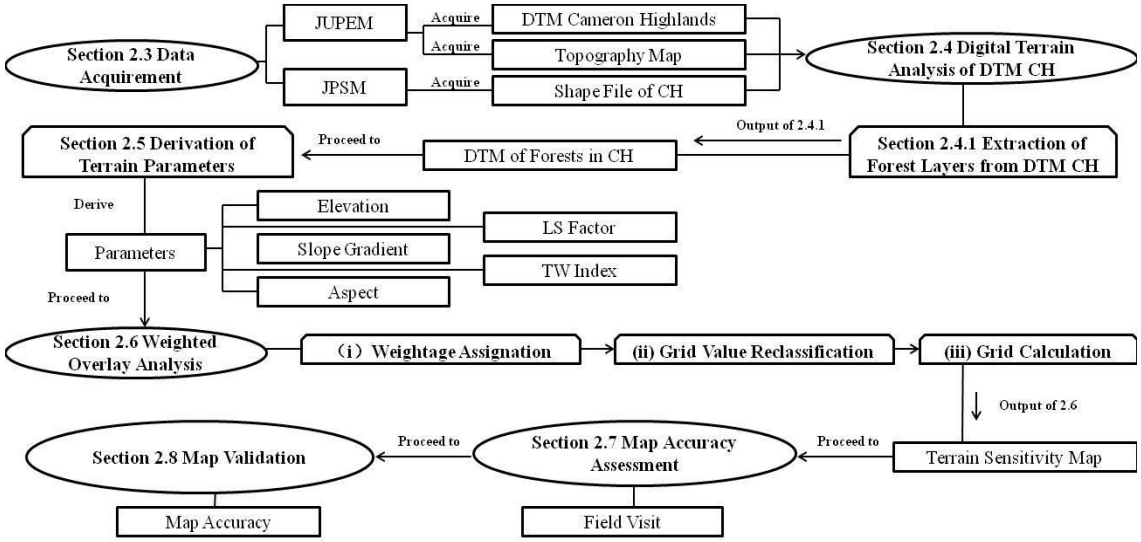

Figure 2. Flow of research methodology

2.4 Digital terrain analysis of DTM CH

2.4.1 Extraction of forest layer in Cameron Highlands

A total of 14 forest reserves were selected and extracted from the DTM of Cameron Highlands. Table 3 shows the extracted forest reserves and the digitized area of coverage.

2.5 Derivation of terrain parameters

This section shows the procedure to reveal the terrain characteristics of mountainous forest in CH. DTM-based terrain features were derived using module "basic terrain analysis" within SAGA GIS software (Conrad et al., 2015; Fisher et al., 2017). Selected terrain features were elevation, slope gradient, aspect, length-slope factor (LS Factor), and topography wetness index (TWI). These features exhibit the morphological setting of the terrain surface in the mountainous forests of CH. Table 4 shows terrain features and their respective significance.

Table 3. Forest reserves and their coverage area in Cameron Highlands

Forest Reserve (FR)	Area (km^2)
FR Terla	37.87
FR Gunung Siku	18.30
FR Sungai Wi	69.18
FR Hulu ICAT	7.14
FR Batu Gangan	10.17
FR Batu Gangan Tambahan	10.10
FR Sungai Kial	24.24
FR Hulu Bertan	7.44
FR Bukit Jerut	64.22
FR Mentigi	16.07
FR Mentigi Tambahan	2.87
FR Ringlet	14.29
FR Bertam	29.87
FR Gunung Berembun	15.48
Total	326.24

Table 4. Terrain features and their respective significance

Features	Description	Significant
Elevation (m)	Altitude of the slope above sea level	Climate, vegetation
Slope gradient (°)	Incline of terrain surface	Shear force, terrain steepness
Aspect (°)	Direction of terrain facing	Precipitation, effect of monsoon season, and sunlight exposure
LS factor (unit)	Impact of slope length and slope steepness. * LS Factor = $(\frac{m}{22.13})^t \times (\frac{\sin\beta}{0.0896})^{13}$	Rate of soil loss
TWI (unit)	Terrain moisture * TWI = $\ln(\frac{As}{\tan\beta})$	Relative size of upslope catchment area, condition of drainage channel, and runoff propensity

* Formula of terrain features

2.6 Weighted overlay analysis

This section shows the framework to derive terrain sensitivity maps that layout the terrain sensitivity spot in the mountainous forest of CH. After derivation of basic terrain features, five different map layers from Table 4 were stacked to generate a terrain sensitivity map. Three phases which were (i) weightage assignation, (ii) grid value reclassification and (iii) grid calculation were executed. Weighting classification method had been applied in various geographical and environmental studies and proven to be effective for susceptibility mapping (Panikkar and Subramaniyan, 1997; Shit et al., 2016; Kouhestani et al. 2016; Ostad-Ali-Askari et al., 2020).

(i) Weightage assignation

Each terrain feature was classified into subclasses and weightage values were assigned from 1 to 5 which represents low terrain sensitivity to high terrain sensitivity as shown in Table 5. Weightage assignation was adopted from Anbalagan (1992) and Matori et al., (2011).

Table 5. Classification and weightage of terrain features

Terrain Parameter		Subclass		Weightage
(a)	Elevation (m)	<805		1
		805-1,070		2
		1,070-1,335		5
		1,335-1,600		4
		>1,600		3
(b)	Slope gradient (°)	0-10.2		1
		10.2-20.4		2
		20.4-30.6		5
		30.6-40.8		4
		>40.8		3
(c)	Aspect (°)	-1	Flat	1
		0-22.5	North	2
		22.5-67.5	Northeast	5
		67.5-112.5	East	3
		112.5-157.5	Southeast	3
		157.5-202.5	South	3
		202.5-247.5	Southwest	4
		247.5-292.5	West	3
		292.5-337.5	Northwest	5
		337.5-360.0	North	2
(d)	LS Factor	<2.8		1
		2.8-5.6		2
		5.6-8.4		3
		8.4-11.2		4
		>11.2		5

Table 5. Classification and weightage of terrain features (cont.)

Terrain Parameter		Subclass	Weightage
(e)	TWI	<3.2	1
		3.2-6.4	2
		6.4-9.6	3
		9.6-12.8	4
		>12.8	5

Explanation on each terrain features and weightage assignation is elaborated as follows.

(a) Elevation

Elevation refers to the altitude of terrain. Based on Dou et al. (2015), the ground in different heights will have different sensitivity levels. A slope in low elevation will have lower terrain sensitivity as it is less likely to trigger landslides due to its gentle terrain. Thus, in this study, subclasses with <805 m and 805-1,070 m were assigned as 1 and 2. The terrain at intermediate level which is 1,070-1,335 m will have the most significant sensitivity due to the high accumulation of colluviums layer from the slope in higher elevation; thus, weightage 5 was assigned to this subclass (Wang et al., 2015). Terrain sensitivity decreases gradually at more upper elevation slope as colluviums material will displace from high elevation slope to intermediate slope from time to time (Roback et al., 2018). Thus, weightage 4 and 3 were assigned to high elevation slopes, which are subclass 1,335-1,600 m and >1,600 m respectively.

(b) Slope gradient

Slope gradient refers to terrain steepness. According to Dou et al. (2015) and Roback et al. (2018), low gradient slopes tend to have lower terrain sensitivity due to the low shear force. Terrain sensitivity increases with the slope gradient as well as shear force. Thus, subclass 0-10.2° and 10.2-20.4° were assigned as weightage 1 and 2 respectively. Terrain sensitivity tends to increase significantly at the intermediate subclass of slope gradient 20.4-30.6° as the slope in this level was loaded with enormous fine sediment from the high level subclass of slope gradient. The fine sediment can be landslide material that can be triggered anytime. Thus, subclass 20.4-30.6° was assigned as weightage 5. As slope gets steeper at high subclass which is 30.6-40.8° and >40.8°, the fine sediment is decreased due to the constant displacement to intermediate subclass of slope from time to time. Thus, subclass 30.6-40.8° and >40.8° were assigned as 4 and 3 respectively.

(c) Aspect

Malaysia is a country with high rainfall intensity. Referring to Matori et al. (2011), the frequency of landslide events is synchronized with rainfall intensity in CH; a high number of landslides were triggered with the increase of rainfall intensity. The weightage assignation of aspect refers to the previous landslide history and indicates the influence of rainfall towards the specific slope facing direction.

(d) Length-slope gradient (LS Factor)

LS Factor defines the soil loss potential regard to the slope length and slope steepness. Greater values of LS Factor indicate higher soil loss potential (Moses, 2017; Taghizadeh-Mehrjardi et al., 2019).

(e) Topography wetness index (TWI)

TWI defines slope runoff propensity. High TWI indicates high runoff propensity due to the large upslope catchment area associated with shallow or insufficient drainage channels (Quinn et al., 1991).

(ii) Grid value reclassification

Every map layer of features in Table 4 was reclassified to the weightage value in Table 5 using module "Grid Value Reclassification" in Saga GIS.

(iii) Grid calculation

These maps were then stacked together to produce a terrain sensitivity map (TSM) by using the following formula adopted from Tas (2016) and Chaudhari et al. (2018).

$$\frac{G1 + G2 + G3 + G4 + G5}{5}$$

Where; symbol "G" represents a single grid layer of terrain features. G1=elevation; G2=slope gradient; G3=aspect; G4=LS Factor; G5=TWI.

The generated TSM was divided into five classes which are (a) very high sensitivity, (b) high sensitivity, (c) moderate sensitivity, (d) low sensitivity, and (e) very low sensitivity. According to the Forest Practices Code of British Columbia (1999),

high-frequency landslides could be expected in areas plotted in sensitivity classes (a) and (b). Mild landslides or a small amount of landslides will be expected in the area plotted in sensitivity class (c) while no landslide will be expected in the area plotted in sensitivity classes (d) and (e).

2.7 Map accuracy assessment

Accuracy assessment was conducted by comparing simulated TSM and the field data obtained from the ground survey. The location of new and former landslides was recorded using Global Positioning System Garmin Montana 610/680.

2.8 Map validation

Accuracy of TSM was calculated based on the formula as follow:

$$\text{Accuracy} = \frac{\text{Amount of landslide in (a),(b)and (c)}}{\text{Total recorded number of landslide}}$$

The formula was referred to Forest Practices Code of British Columbia (1999), Sharir et al. (2017), and Simon et al. (2017). A study by Battistini et al. (2017) suggested that accuracy assessment or validation of landslide prediction models using geolocalized historical landslide events is possible.

3. RESULTS AND DISCUSSION

3.1 Terrain characteristic of mountainous forest in Cameron Highlands

Table 6 shows the terrain characteristics of mountainous forest in Cameron Highlands (CH). The minimum value (min) represents the lowest point of attribute, while maximum value (max) indicates otherwise. Mean values act as the representative figure of the selected attribute, while standard deviation (SD) represents the level of data dispersion. Figure 3 shows the map layer of selected terrain features, and Table 8 shows the forests' name with the respective code number.

Table 6. Terrain characteristics of Cameron Highlands

Attribute	Min	Max	Mean	SD
Elevation (m)	765.12	2,053.10	1,452.48	173.19
Slope gradient (°)	0.00	55.91	18.80	7.57
Aspect (°)	0.00	360.00	166.62	98.86
LS factor	0.00	66.51	5.32	2.78
TWI	1.93	22.41	5.55	1.54

The result indicates that the elevation value on the mountainous forest of CH is 1,452.48±173.19 m. Research by Kalimuthu et al. (2015) stated that more than 70% of CH's historical landslide was located at terrains on elevation higher than 1,200 m. The terrain beyond this point is considered a mountainous zone, and it tends to get unstable (Zainuddin et al., 2016; Azlini et al., 2018a). Thus, terrains in the mountainous forest of CH have high sensitivity in terms of elevation.

Based on Table 6, the slope in CH is considered as low sensitivity at the value of 18.80±7.57°. According to Sabah Environment Protection Department (2012), the threshold gradient for a slope to trigger a landslide is 20°. Thus, even though the slope in CH is relatively low steepness, it is essential to emphasize the total area of the slope that is steep enough to initiate a landslide event. The area coverage of different ranges of slope gradients in mountainous forests of CH is shown in Table 7. There is 43.23% of the area characterized by a slope gradient of more than 20°. The result shows a similar finding with the research of Azlini et al. (2018b) and Abdullah et al. (2019). These researches stated that CH suited only 30% to 60% of risky slopes that can initiate landslides. The percentage varied due to the different sizes of the study area. Thus, slopes in the mountainous forest of CH are risky in terms of slope gradient.

Table 7. Area coverage of different slope gradient ranges in mountainous forest of CH

Gradient (°)	Area (km^2)	Percentage (%)
0-10.2	47.60	14.59
10.2-20.4	137.61	42.18
20.4-30.6	123.19	37.76
30.6-40.8	17.45	5.35
>40.8	0.39	0.12

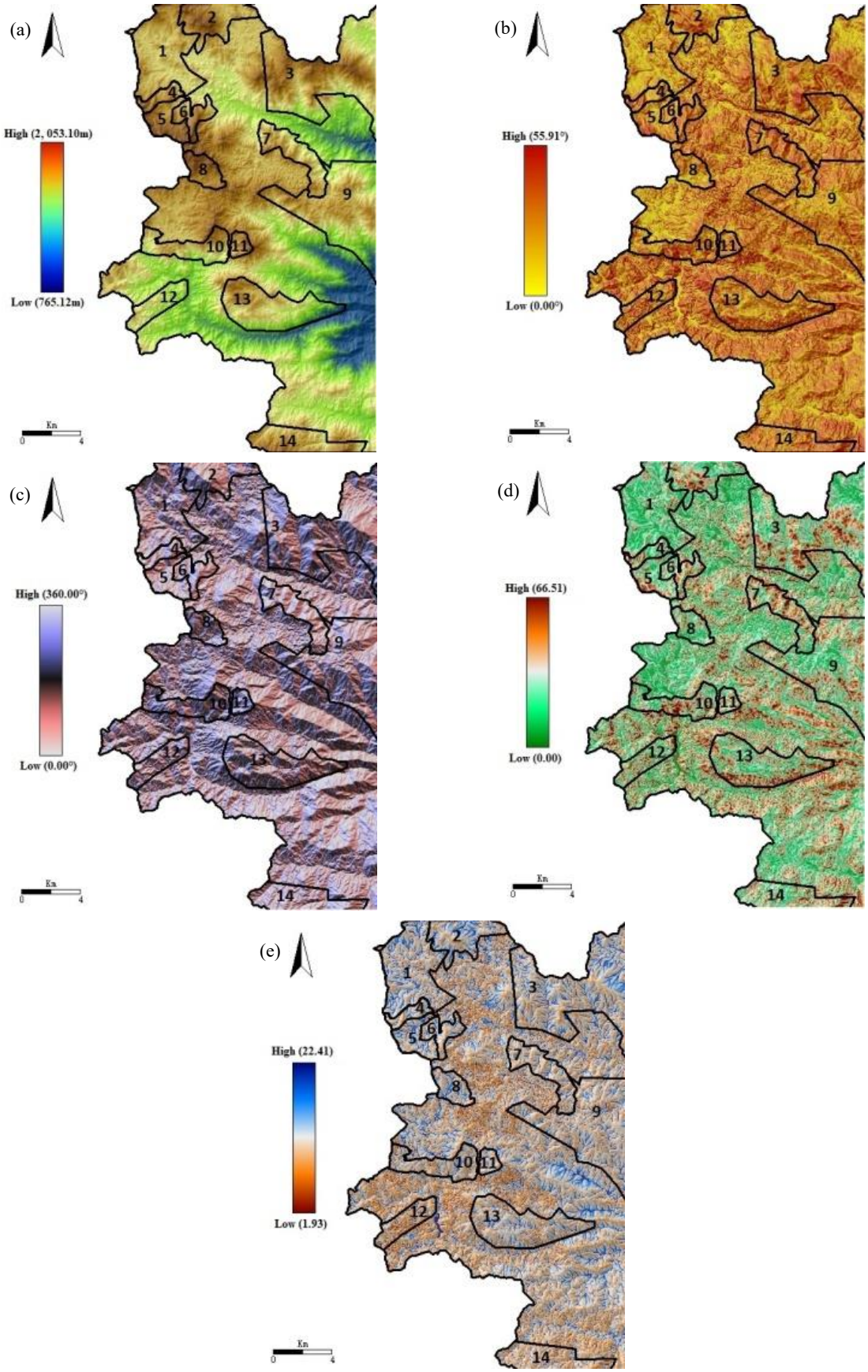

Figure 3. Map layer of (a) elevation, (b) slope gradient, (c) aspect, (d) LS Factor, and (e) TWI of mountainous forest in Cameron Highlands

Table 8. Forest Reserve (FR) in Cameron Highlands with their respective code number as presented in Figure 3.

Code	Forest Reserve (FR)	Code	Forest Reserve (FR)
1	FR Terla	8	FR Hulu Bertam
2	FR Gunung Siku	9	FR Bukit Jerut
3	FR Sungai Wi	10	FR Mentigi
4	FR Hulu ICAT	11	FR Mentigi Tambahan
5	FR Batu Gangan Tambahan	12	FR Ringlet
6	FR Batu Gangan	13	FR Bertam
7	FR Sungai Kial	14	FR Berembum

The mean value of aspect in the mountainous forest of CH is 166.62±98.86° (Table 6). This figure gives generalized information that most of the slope is southward facing. The terrain facing south has high exposure to sunlight since Malaysia is located just above the Earth's equator (Wu et al., 2006; Zakaria et al., 2019). These terrains tend to have relatively dry soil and drought conditions and lead to low vegetation (DeGraff and Romesburg, 1980). However, CH tends to receive a vast amount of rainfall as well. Jerkins (2014) reported that CH would experience 236 days of rain and average 2,852 mm of precipitation annually. Thus, this research assumed that drought and dry soil conditions caused by high sunlight exposure do not affect the terrain sensitivity.

LS Factor reflects the effect of length and steepness of slope towards soil loss. Based on Table 6, LS Factor shows a mean value of 5.32±2.78. According to the research of Mohamed et al. (2012), terrain with LS Factor of more than five is considered as the area with a high risk of slope failure; whereas, an area with LS value of more than ten is considered as a very high-risk area. Thus, mountainous forest in CH has a high risk of soil loss in the LS Factor aspect and deduced that the risk of landslide could be significantly enhanced whenever heavy rainfall is present.

TWI in the mountain forest of CH shows a mean value of 5.55±1.54°. Studies by Acharya et al. (2017) and Pourghasemi et al. (2013) stated that an area would have high water accumulation when its TWI is equal to or more than four, while it will cause a high frequency of landslides when an area is more or equal than seven. The finding suggested that the study area has a risk of landslide in terms of TWI.

3.2 Terrain sensitivity map of Cameron Highlands

The terrain sensitivity map of the mountainous forest in CH is presented in Figure 4. The results suggest that 35.28% (115.09 km^2) of the study area is considered as high sensitivity. Moderate sensitivity area covers 32.95% (107.50 km^2), while low sensitivity area covers 31.77% (103.64 km^2), as shown in Table 9. The result shows no dominant class of sensitivity area in CH. However, Figure 4, Table 10 shows that the high sensitivity area shows scatter distribution. The result is because the mountainous zone is characterized by dynamic landforms such as valleys, open areas, and ridges. Thus, high sensitivity areas are distributed in a sparse manner.

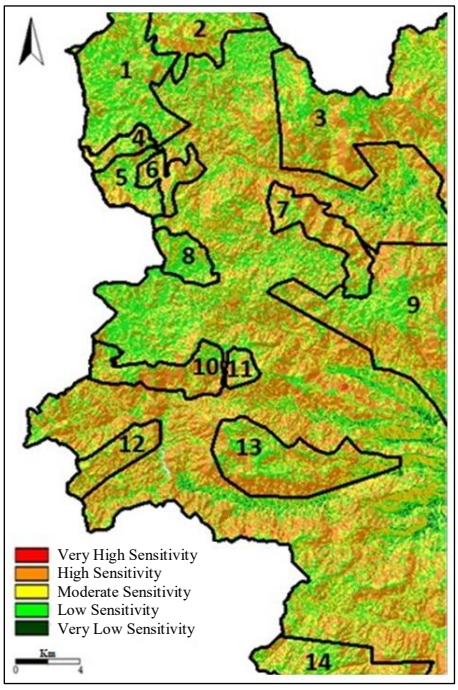

Figure 4. Terrain sensitivity map of mountainous forest in Cameron Highlands

Table 9. Classification of terrain sensitivity in mountainous forest of CH

Classification	Color code	Area (km^2)	Percentage (%)
Very low sensitivity	Dark green	0.65	0.20
Low sensitivity	Green	102.99	31.57
Moderate sensitivity	Yellow	107.50	32.95
High sensitivity	Orange	114.31	35.04
Very high sensitivity	Red	0.78	0.24

Table 10. Forest Reserve (FR) in Cameron Highlands with their respective code number as presented in Figure 4.

Code	Forest Reserve (FR)	Code	Forest Reserve (FR)
1	FR Terla	8	FR Hulu Bertam
2	FR Gunung Siku	9	FR Bukit Jerut
3	FR Sungai Wi	10	FR Mentigi
4	FR Hulu ICAT	11	FR Mentigi Tambahan
5	FR Batu Gangan Tambahan	12	FR Ringlet
6	FR Batu Gangan	13	FR Bertam
7	FR Sungai Kial	14	FR Berembum

3.3 Accuracy of terrain sensitivity map

Landslide distribution in the mountainous forest of CH is shown in Table 11. The total number of landslides located within zones of very high sensitivity, high sensitivity, and moderate sensitivity is 42.

Based on the calculation shown in Table 12, the simulated terrain sensitivity map indicated 79.25% accuracy, which is acceptable for the research purpose. The result is similar to the study of Muhammad et al. (2019), who reported that landslide assessment in CH could obtain accuracy as high as 78.0%. The author stated that the accuracy is acceptable and sufficient to be used as a guideline in a landslide mitigation plan. However, to obtain more accurate results, future studies should consider using higher spatial resolution data, with proper algorithms extraction features that may be effective for land use classification in environmental researches, as suggested by Pirnazar et al. (2018).

Table 11. Landslide distribution in different zones of sensitivity of the study area

Terrain sensitivity		Number of recorded landslide (point)
(a)	Very high sensitivity	0
(b)	High sensitivity	37
(c)	Moderate sensitivity	5
(d)	Low sensitivity	11
(e)	Very low sensitivity	0
Total		53

Table 12. Accuracy of terrain sensitivity map

Measure	Attribute
Landslide in zone of (a) + (b) + (c) (unit)	42
Total number of recorded landslide (unit)	53
Accuracy ($\frac{(a)+(b)+(c)}{T} \times 100\%$)	79.25%

Where; (a)=very high sensitivity, (b)=high sensitivity, (c)=moderate sensitivity and, T=total number of recorded landslides.

4. CONCLUSION

This study reveals mountainous forest terrain in CH in terms of elevation, slope gradient, aspect, LS Factor, and TWI. The mountainous forest of CH has a high elevation with a mean value of 1,452.48±173.19 m and 43.23% of the terrain is a steep slope which can easily trigger a landslide. In addition, most of the slopes are southward facing slopes with a mean value of 166.62±98.86°. Moreover, mountainous forests of CH possess a moderate level of soil loss potential (LS Factor) and runoff propensity (TWI) with mean values 5.32±2.78 and 5.55±1.54, respectively. In addition, this study demonstrated a practical application of digital terrain analysis using GIS tools on landslide assessment in the tropical mountainous forests. The simulated terrain sensitivity map shows that the mountainous forest of CH possesses 222.59 km^2, or 68.23% of the terrain, considered to be landslide-prone. The results showed 79.25% accuracy, which is suggested as acceptable and satisfactory. Due to the forests' complex terrain characteristics, this research highlights an alternative approach that is convenient to

carry out by researchers, forest planners, and decision-makers. In addition, the method provided is cost-effective, less time-consuming, and generates rapid results. The paper also reflects the importance of conserving mountainous forest areas due to the uneven distribution of susceptible areas. Any massive development and construction that might cause irreversible harm to the environment and put tourists, indigenous people, and residents at risk should be avoided.

ACKNOWLEDGEMENTS

We would like to show our appreciation to the Forestry Department of Peninsular Malaysia for their cooperation during field assessment and The Department of Survey and Mapping Malaysia for the contribution of spatial data. Our appreciation also extended to the Public Service Department of Malaysia (JPA) for students' scholarships. The research was funded by Geran GP-IPM/2017/955200.

REFERENCES

Abdullah AF, Aimrun W, Nasidi NM, Hazari SAF, Sidek M, Zalilah S. Modeling erosion and landslides induced by farming activities at hilly areas, Cameron Highlands, Malaysia. Jurnal Teknologi 2019;81(6):195-204.

Acharya TD, Yang IT, Lee DH. GIS-based landslide susceptibility mapping Bhotang, Nepal using frequency ration and statistical index methods. Journal of Korean Society of Surveying, Geodesy, Photogrammetry and Cartography 2017;35(5):357-64.

Ahmed F, Rao KS. Application of DEM and GIS in terrain analysis: A case study of Tuirini River Basin, NE India. International Journal of Geology and Earth Sciences 2019;5(1):1-20.

Anbalagan R. Landslide hazard evaluation and zonation mapping in mountainous terrain. Engineering Geology 1992;32:269-77.

Azita AZ, Muhammad-Shafeeq S, Thinaraj B, Paul L. Terrain characterization of mountainous forest area in Cameron Highland. The Malaysian Forester 2019;82(2):445-54.

Azlini R, Sharifah NSS, Suriyani A, Sarva MP, Emilia ZA. Land use change in highland area and its impact on river water quality: A review of case studies in Malaysia. Ecological Processes 2018a;7(19):1-17.

Azlini R, Sharifah NSS, Suriyani A, Sarva MP, Emilia ZA. Heavy metals contamination and potential health risk in highland river watershed (Malaysia). Malaysian Journal of Medicine and Health Sciences 2018b;14(2):45-55.

Battistini A, Rosi A, Segoni S, Lagomarsino D, Catani F, Casagli N. Validation of landslide hazard models using a semantic engine on online news. Applied Geography 2017;82:59-65.

Beaven PJ, Lawrance CJ. The Application of Terrain Evaluation to Road Engineering. Malaysia: Institution of Engineers, Public Works Department; 1973.

Chaudhari ARV, Lal BD, Dutta CS, Umrikar B, Halder ES. Weighted overlay analysis for delineation of ground water potential zone: A case study of Pirangut River basin. International Journal of Remote Sensing and Geoscience 2018;7(1):1-7.

Colby JD, Dobson JG. Flood modeling in the coastal plains and mountains: Analysis of terrain resolution. Natural Hazard Review 2010;11(1):19-25.

Conrad O, Bechtel B, Bock M, Dietrich H, Fischer E, Gerlitz L, et al. System for Automated Geoscientific Analyses (SAGA) v. 2.1.4. Geoscientific Model Development 2015;8:1991-2007.

Cruden DM. A simple definition of a landslide. Bulletin of the International Association of Engineering Geology 1991; 43(1):27-9.

DeGraff JV, Romesburg HC. Regional landslide-susceptibility assessment for wildland management. In: Coats DR, Vitek JD, editors. Thresholds in Geomorphology. London: George Allen and Unwin; 1980. p. 401-14.

Dermawan A. Findings of investigations into Jalan Bukit Kukus landslide tragedy must be made public-NGOs [Internet]. 2019 [cited 2019 Apr 24]. Available from: https://bit.ly/2FFMflb.

Dou J, Dieu TB, Yunus AP, Jia K, Song X, Revhaug I, et al. Optimization of causative factors for landslide susceptibility evaluation using remote sensing and GIS data in parts of Niigata, Japan. PLoS ONE 2015;10(7):1-29.

Fisher R, Hobgen S, Mandaya I, Kaho NR, Zulkarnain. Satellite Image Analysis and Terrain Modelling: A Practical Manual for Natural Resource Management, Disaster Risk and Development Planning Using Free Geospatial Data and Software. Charles Darwin University and Universitas Nusa Cendana dan Universitas Halu Oleo; 2017.

Forest Practices Code of British Columbia. Mapping and assessing terrain stability guidebook [Internet]. 1999 [cited 2020 Jan 12]. Available from: https://bit.ly/2FuruJh.

Froude MJ, Petley DN. Global fatal landslide occurrence from 2004 to 2016. Natural Hazards and Earth System Sciences 2018;18:2161-81.

Gong WF, Wang HB, Wang XF, Fan WY, Stott P. Effect of terrain on landscape patterns and ecological effects by a gradient-based RS and GIS Analysis. Journal of Forestry Research 2017;28:1061-72.

Gutierrez-Martin A, Herrada MA, Yenes JI, Castedo R. Development and validation of the terrain stability model for assessing landslide instability during heavy rain infiltration. Natural Hazards and Earth System Sciences 2019;19:721-36.

Jabatan Ukur dan Pemetaan Malaysia (JUPEM). How to get the JUPEM digital data? [Internet]. 2019 [cited 2019 Jun 12]. Available from: https://www.jupem.gov.my/soalan-lazim.

Jerkins E. Summary of weather in the Cameron Highlands-2nd edition. Regional Environmental Awareness Cameron Highland [Internet]. 2014 [cited 2019 Dec 18]. Available from: http://reach.org.my/2014/?p=709.

Kalimuthu H, Tan WN, Lim SL, Mohammad FAF. Assessing frequency ratio method for landslide susceptibility mapping in Cameron Highlands, Malaysia. Proceedings of the 2015 Institute of Electrical and Electronics Engineers Student Conference on Research and Development; 2015 Dec 13-14; Kuala Lumpur: Malaysia; 2015.

Kamilia S, Simon N, Rodeano R. Regional assessment on the influence of land use related factor on landslide occurrences in Kundasang, Sabah. Proceedings of the Universiti Kebangsaan Malaysia, Faculty of Science and Technology 2016 Postgraduate Colloquium; 2016 Apr 13-14; Universiti Kebangsaan Malaysia, Selangor: Malaysia; 2016.

Kavitha MNC, Viswanath R, Kavibharathi P, Aakash K, Balajimanikandan M. A comparative study of conventional surveying techniques with total station and GPS. International Journal of Civil Engineering and Technology 2018;9(1):440-6.

Kim H, Kang Y, Kim J. Evaluation of wind resource potential in mountainous region considering morphometric terrain characteristics. Wind Engineering 2017;41(2):114-23.

Kouhestani S, Eslamian SS, Abedi-Koupai J, Besalatpour AA. Projection of climate change impacts on precipitation using soft-computing techniques: A case study in Zayandeh-rud basin, Iran. Global and Planetary Change 2016;144:158-70.

Kumaran S, Ainuddin AN. Forest, water and climate of Cameron Highlands. In: Chan NW, editor. Cameron Highland: Issues and Challenges in Sustainable Development. Pulau Pinang: School of Humanities, Universiti Sains Malaysia; 2006. p. 1-11.

Larsen MC, Simon A. A rainfall intensity-duration threshold for landslides in a humid-tropical environment, Puerto Rico. Geografiska Annaler: Series A, Physical Geography 1993;75(1-2):13-23.

Li W, Hsu CY. Automated terrain feature identification from remote sensing imagery: A deep learning approach. International Journal of Geographical Information Science 2020;34(4):637-60.

Matori AN, Basith A, Harahap I. Study of regional monsoonal effects on landslide hazard zonation in Cameron Highlands, Malaysia. Arabian Journal of Geosciences 2011;5(5):1-16.

Mohamed K, Yoshino K, Setiawan Y. Assessment and mapping of soil erosion risk by water in Tunisia using time series MODIS data. Paddy and Water Environment 2012;10(1):59-73.

Mohd SS, Amir N, Noorbaya MS, Roslan ZA, Nirwani DM, Abdul HY. Landslide occurrences in Malaysia based on soil series and lithology factors. International Journal of Advances Science and Technology 2019;28(18):1-26.

Moses AN. GIS-based determination of RUSLE'S 'LS' factor for River Nzoia Basin in Kenya. International Journal of Innovative Research and Advanced Studies 2017;4(11):441-4.

Muhammad IMH, Solemon B, Omar R, Roslan R, Warishah AW, Intan NZB, et al. Landslide susceptibility assessment for Cameron Highland using analytical hierarchy process. International Journal of Engineering and Advanced Technology 2019;9(1):3494-9.

Ostad-Ali-Askari K, Shayannejad M. Quantity and quality modeling of groundwater to manage water resources in Isfahan-Borkhar Aquifer. Environment, Development and Sustainability 2021;23(3):1-17.

Ostad-Ali-Askari K, Kharazi HG, Shayannejad M, Zareian MJ. Effect of climate change on precipitation patterns in an arid region using GCM models: Case study of Isfahan-Borkhar plain. Natural Hazard Review 2020;21(2):1-6.

Panikkar S, Subramaniyan V. Landslide hazard analysis of the area around Dehra Dun and Mussoorie, Uttar Pradesh. Curricular Science 1997;73:1117-23.

Pirnazar M, Hasheminasab H, Qasemy Z, Hamedani MH, Mohri-Esfahani E, Eslamian S, et al. The evaluation of the usage of the fuzzy algorithms in increasing the accuracy of the extracted land use maps. International Journal of Global Environmental Issues 2018;17(4):307-21.

Pourghasemi HR, Jirandeh AG, Pradhan B, Chong X, Gokceoglu C. Landslide susceptibility mapping using support vector machine and GIS at the Golestan Province, Iran. Journal of Earth System Science 2013;122(2):349-69.

Putra AN, Nita I, Jauhary MRA, Nurhutami SR, Ismail MH. Landslide risk analysis on agriculture area in Pacitan Regency in East Java Indonesia using geospatial techniques. Environment and Natural Resources Journal 2021;19(2):141-52.

Quinn P, Beven K, Chevallier P, Planchon O. The prediction of hillslope flow paths for distributed hydrological modeling using digital terrain models. Hydrological Processes 1991;5:59-79.

Roback K, Clark MK, Joshua AW, Zekkos D, Li G, Gallen SF, et al. The size, distribution, and mobility of landslides caused by the 2015 Mw 7.8 Gorkha earthquake, Nepal. Geomorphology 2018;301:121-38.

Sabah Environment Protection Department. Environmental Impact Assessment (EIA): Guidelines for Construction on Hill Slopes. Sabah, Malaysia: Environment Protection Department; 2012.

Sharir K, Roslee R, Lee KE, Simon N. Landslide factors and susceptibility mapping on natural and artificial slopes in Kundasang, Sabah. Sains Malaysiana 2017;46(9):1531-40.

Shit PK, Bhunia GS, Maiti R. Potential landslide susceptibility mapping using weighted overlay model (WOM). Modelling Earth System and Environment 2016;2(21):2-10

Sim LL, Chan A, Trisha N. Malaysia among countries especially prone to landslides [Internet]. 2018 [cited 2019 Feb 22]. Available from: https://bit.ly/36FCRKv.

Simon N, Roslee R, Goh TL. Temporal landslide susceptibility assessment using landslide density technique. Geological Behaviour 2017;1(2):10-3.

Statuto D, Cillis G, Picuno P. Using historical maps within a GIS to analyze two centuries of rural landscape changes in Southern Italy. Land 2017;6(3):65.

Taghizadeh-Mehrjardi R, Bawa A, Kumar S, Zeraatpisheh M, Amirian-Chakan A, Akbarzadeh A. Soil erosion spatial prediction using digital soil mapping and RUSLE methods for Big Sioux River Watershed. Soil System 2019;3(43):1-15.

Tarolli P, Tarboton DG. A new method for determination of most likely landslide initiation points and the evaluation of digital terrain model scale in terrain stability mapping. Hydrology and Earth System Sciences 2006;10(5):663-77.

Tas E. Flood risk potential assessment in Akarcay Sinanpasa Subbasin using GIS Techniques. Proceedings of the 3rd International Conference of Geography, Environment and GIS, for Students and Young Researches; 2016 May 19-21; Targoviste: Romania; 2016.

Tay JE, Selaman OS. A study on the rainfall and landslides along Sarawak road using the antecedent rainfall analysis. UNIMAS E-Journal of Civil Engineering 2011;2(1):1-6.

Teh AY. Malaysians among 40 tourists trapped in deadly Lombok landslide [Internet]. 2019 [cited 2019 Feb 22]. Available from: https://bit.ly/2QYZFhH.

The Star Online. Ampang's hill of death [Internet]. 2008 [cited Apr 16]. Available from: https://bit.ly/30aj7vV.

Tongkul F. The 2015 Ranau earthquake: Cause and impact. Sabah Society Journal 2015;32:1-28.

University of Cincinnati. Nobody wins in a landslide [Internet]. 2018 [cited 2019 Jun 20]. Available from: https://bit.ly/2Ta6q30.

Wang Q, Li W, Chen W, Bai H. GIS-based assessment of landslide susceptibility using certainty factor and index of entropy models for the Qianyang Country of Baoji City, China. Journal of Earth System Science 2015;124(7):1399-415.

Wawer R, Nowocien E. Application of SINMAP terrain stability model to Grodarz stream watershed. Electronic Journal of Polish Agricultural Universities 2003;6(1):1-17.

Wong PM. Making new projects safe [Internet]. 2014 [cited 2019 Mar 21]. Available from: https://bit.ly/35FLKSK.

Wu CY, Qiao JP, Wang M. Landslides and slope aspect in the Three Gorges Reservoir area based on GIS and information value model. Wuhan University Journal of Natural Sciences 2006;11(4):773-9.

Zaini H, Che YA, Ahmad S, Khalik AW. Quantifying soil erosion and deposition rates in tea plantation area, Cameron Highlands, Malaysia using ^{137}Cs. Malaysian Journal of Analytical Sciences 2014;18(1):94-106.

Zainuddin MY, Nur AA, Haslinda N, Nik NND, Azlan AA. Engineering geological of an active slope in KM46 Simpang Pulai, Perak. Malaysian Journal of Civil Engineering 2016;28(1):35-41.

Zakaria A, Ooi JB, Thomas RL, Craig AL. Malaysia [Internet]. 2019 [cited 2019 Nov 12]. Available from: https://bit.ly/2N9JhKb.

Zakiah K, Lim R, Chung C, Liew JX. 26,000 new hotspots on watch list [Internet]. 2019 [cited 2020 Jan 4]. Available from: https://bit.ly/2s8SnPU.

Zhang S, Zhang LM, Glade T. Characteristics of earthquake and rain-induced landslides near the epicenter of Wenchuan earthquake. Engineering Geology 2014;175:57-73.

Zhou JX, Zhu CY, Zheng JM, Wang XH, Liu ZH. Landslide disaster in the loess area of China. Journal of Forestry Research 2002;13:157-61.

Sugarcane Bagasse-derived Hydrochar: Modification with Cations to Enhance Phosphate Removal

Usarat Thawornchaisit*, Tanrawee Onlamai, Nontakorn Phurkphong, and Rawiwan Sukharom

Faculty of Science, King Mongkut's Institute of Technology Ladkrabang, Bangkok 10520, Thailand

ARTICLE INFO

Received: 6 Mar 2021
Received in revised: 26 May 2021
Accepted: 8 Jun 2021
Published online: 15 Jul 2021
DOI: 10.32526/ennrj/19/202100036

Keywords:
Sugarcane bagasse/ Hydrothermal carbonization/ Engineered hydrochar/ Phosphate recovery

*** Corresponding author:**
E-mail: usarat.th@kmitl.ac.th

ABSTRACT

Cation modified hydrochars were synthesized by hydrothermal carbonization (HTC) of sugarcane bagasse, followed by impregnation of three different cations (Ca, Mg, and Fe) or co-precipitation of Fe^{3+} and Fe^{2+}. HTC enhanced the hydrochar surface area and increased the enrichment of oxygen functional groups on the hydrochar surface confirmed by FTIR. The oxygen functional groups further improve the adsorption capacity for cations during hydrochar chemical modification. Physical appearance, FTIR and XRF confirmed that Ca^{2+}, Mg^{2+} and Fe^{2+} or Fe^{3+} were well retained in the bagasse-derived hydrochar. The pH_{pzc} values of all chemically modified hydrochars were greater than the unmodified hydrochar or bagasse alone. Modification with different cations improved phosphate uptake capacity. The Fe-modified hydrochar with about 45-50% Fe content showed greater phosphate removal efficiency than Ca- and Mg-modified hydrochars. In addition, hydrochars decorated by impregnation of Fe^{3+} demonstrated better phosphate removal than ones produced by co-precipitation of Fe^{3+} and Fe^{2+}. Thus, chemically modified hydrochars could be used as an environmentally alternative adsorbent for phosphate removal from aqueous solutions.

1. INTRODUCTION

Sugarcane bagasse (SB), the solid fibrous material remaining from sugarcane juice extraction, is the main residue from the sugar industry. Approximately 270-280 tons of bagasse are generated from every 1,000 tons of processed sugarcane (Martinez-Hernandez et al., 2018). The world generated about 1,900 megatons of bagasse (mostly in Latin America and Asia) in the past five years (Mokhena et al., 2018). Bagasse availability is expected to increase, due to the increasing demand for sugar in households as well as industrial use. The bagasse is currently used as a biofuel within the sugar industry itself, and in biomass power plants for steam generation and electricity with a challenging operation issue related to its high moisture content, which is typically 40-50 percent (Congsomjit and Areeprasert, 2020). Considering 80-85% of sugarcane bagasse is used for energy generation within the plant, and about 15 to 20 percent of bagasse is left unused at some factories after energy needs are met (USDA, 2018), bagasse is an ideal raw material that needs to increase its added value.

Synthesis of hydrochar via hydrothermal carbonization (HTC) has been investigated as an approach for increasing biomass valued-products. Conversion of biomass waste to adsorbent for removal of organic and inorganic contaminants is an environmental aspect that has received considerable attention due to its simplicity and ability to produce hydrochars with attractive characteristics that promote effective use in dealing with pollutant contamination in aqueous solution (Jain et al., 2016; Nguyen et al., 2019). HTC is the thermochemical conversion technique in a closed reactor that uses moderate processing temperature (180-240°C) and water as carbonatization medium under self-generated pressures to react with wet/dry materials and convert the biomass into solid materials, namely hydrochar (Congsomjit and Areeprasert, 2020; Dai et al., 2014). HTC process offers significant advantages over pyrolysis, a conventional utilized process for biomass-to-carbon-based products conversion, in terms of mild reaction condition, lower energy consumption process, and the ability to deliver hydrochar with high concentrations of oxygenated

Citation: Thawornchaisit U, Onlamai T, Phurkphong N, Sukharom R. Sugarcane bagasse-derived hydrochar: Modification with cations to enhance phosphate removal. Environ. Nat. Resour. J. 2021;19(5):371-380. (https://doi.org/10.32526/ennrj/19/202100036)

functional groups (OFGs, i.e., carboxylic, hydroxyl, and phenolic) on the surface (Jain et al., 2016; Nguyen et al., 2019; Petrović et al., 2016). The relative abundance of OFGs on hydrochar's surface plays an important role in the adsorption capacity of hydrochar toward the given contaminants. Higher OFGs on the adsorbents resulted in higher adsorption capacity for the contaminants, especially positively charged contaminants, in an aqueous solution (Almarri et al., 2009; Hotová et al., 2020). This characteristic is a major reason for higher uptake capacity of hydrochar than biochar toward polar and nonpolar contaminants, including bisphenol-A, 17α-ethinyl estradiol, and phenanthrene (Sun et al., 2011), as well as methylene blue, iodine and copper ions (Jian et al., 2018). Although hydrochar showed a great potential adsorbent for cationic contaminants, the adsorption capacity for anions (i.e., phosphate, nitrate, arsenate) is very limited due to a large amount of OFGs, making the hydrochar's surface more negatively charged, subsequently repelling negatively charged compounds (Fang et al., 2015; He et al., 2019).

Phosphorus is an essential nutrient for the growth, functioning and reproduction of all life on earth, and is a non-renewable resource to produce phosphorus (P) based chemicals, mainly as mineral fertilizers (Tarayre et al., 2016). Phosphorus is naturally found in geological deposits of phosphate rock, which are found mostly in Morocco and Western Sahara (Cordell and White, 2013; Desmidt et al., 2015; USGS, 2021). In recent years, the depletion of phosphate rock natural reserves and phosphorus future availability has received great attention, thus phosphorus has been listed as one of the critical raw materials for the European Union since 2014 (European Commission, 2020). Apart from mineral reserves (i.e. phosphate rock), phosphorus has been found in natural water bodies (freshwater lakes, reservoirs and rivers). Phosphorus flow to an aquatic ecosystem is from soil erosion, agricultural runoff, and point source discharges. Discharge of municipal wastewaters and the effluent discharged from wastewater treatment plants (WWTPs) is an important point source of phosphorus loading (Kundu et al., 2015; Qin et al., 2015). Low concentrations of phosphorus benefit the biological productivity of the aquatic ecosystem, however excessive phosphorus inputs can cause eutrophication, a worldwide water quality deterioration. The phenomenon often leads to the reduction in oxygen concentrations, which affects not only benthic invertebrates but also the spawning success rate of some important fish species (Murray et al., 2019). To address the dual problems of phosphorus future availability and P-based eutrophication, technologies for removal and recovery of phosphorus from wastewater and its possible reuse is necessary and a long-term sustainable solution (Carrillo et al., 2020).

Application of natural agricultural residue for P-adsorption have been investigated, however the adsorption capacity of most natural materials is usually less than 1 mgP/g (Carrillo et al., 2020). Interest in agricultural hydrochars that are rich in oxygen-containing functional groups as adsorbents in water and wastewater treatment has increased. However, their ability for phosphate removal is quite low. To further enhance the phosphate sorption ability of hydrochar, several studies have investigated different methods of tailoring the hydrochar's surface structure. Deposition of mineral oxides and salts is one of the chemical modification methods that is widely applied to change the surface electrical properties of hydrochar (Azzaz et al., 2020). Research has shown that decorating hydrochar surface through impregnating or coating cationic minerals such as Fe, Mg, Ca, La, Al, Mg/Al, either before or after HTC, could develop effective adsorbents with improved adsorption capacity for anionic pollutants (Dai et al., 2014; He et al., 2019; Yu et al., 2019). However, the information about the effects of modifying cationic minerals on the phosphate removal capability of hydrochar is limited. In addition, growing concerns about phosphorus (P) future availability (Alewell et al., 2020; European Commission, 2017) as well as its detrimental environmental impacts like eutrophication, have made the recycling of P crucial to sustainable development (Cordell and White, 2013). Along with the presence of sugarcane bagasse as a common agricultural and industrial waste, this study demonstrates the utilization of hydrothermal carbonization as an approach for adding value to sugarcane bagasse. In addition, this study investigates the effects of different types of modifying agents on the efficiency and selectivity of sugarcane bagasse-modified hydrochar for phosphate adsorption.

2. METHODOLOGY

2.1 Materials and chemicals

Sugarcane bagasse was acquired from a roadside juice hawker in Bangkok, Thailand. After washing several times with tap water and deionized water (DI-water) to remove any adhering dirt, it was dried at 60°C for 24 h and cut into small pieces (about

25 mm length). The bagasse was ground, passed through a 70-mesh sieve, and then stored in a sealed container until use. All chemical reagents used in this study were analytical grade.

2.2 Preparation and modification of hydrochars

Hydrothermal carbonization of bagasse conducted in a 1 L Parr stirred pressure reactor with a 4848-reactor controller, following Hoekman et al. (2011). In a typical synthesis, 70 g of prepared bagasse was mixed with DI-water-1:8 bagasse/water ratio (w/v). The reactor and contents were then heated, while stirring, until the reaction temperature was at 230ºC and held for 1 h reaction time. At the end of the holding time, the vessel was cooled to 45ºC. The solid and aqueous products were separated by vacuum filtration, the hydrochars (HC) were then washed with DI-water, followed by oven drying at 105ºC for 24 h.

The hydochars were modified with Ca, Mg, and Fe, following Yang et al. (2018). To prepare the modified hydrochars, the solutions of calcium chloride ($CaCl_2$), magnesium chloride ($MgCl_2$), ferric chloride hexahydrate ($FeCl_3 \cdot 6H_2O$), and a mixture of ferric chloride hexahydrate ($FeCl_3 \cdot 6H_2O$) and ferrous sulfate heptahydrate ($FeSO_4 \cdot 7H_2O$) were prepared by dissolving a predetermined amount of each compound in DI-water. Subsequently, a measured amount of hydrochar was immersed in one of the solutions and stirred at 150 rpm for 10 min, followed by dropwise addition of 1 M NaOH until the pH was at 11. The suspension was continuously stirred for 45 min and aged without stirring for 24 h at room temperature. Then, the acquired mixtures were washed with deionized water to remove residual salts and loosely attached minerals until the pH of the washing solution equals the of the DI water (pH 6.0-6.5), followed by drying (105ºC, 24 h). The final products were labeled as Ca-HC, Mg-HC, Fe(III)-HC, and Fe(III)/Fe(II)-HC.

2.3 Characterization of sugarcane bagasse and hydrochars

The surface morphology of the bagasse and the hydrochars was characterized by a scanning electron microscope (SEM, QUANTA FEG-250, FEI, USA). C, H, and N compositions were determined by an elemental analyzer (LECO 628 series, LECO Corporation, USA). Methylene blue adsorption studies, following Nunes and Guerreiro (2011), were used to estimate the surface areas of biomass and hydrochars. A Fourier transform infrared spectrometer (FTIR, Spectrum GX, Perkin Elmer) within 400-4,000 cm^{-1} range, was used to identify surface functional groups. An X-ray Fluorescence Spectrometer (XRF, SRS3400, Bruker, Germany) was used to determine the composition of inorganics in hydrochar and the modified hydrochars. The pH at the point of zero charges (pH_{pzc}) was determined by using the pH drift method of 0.01 M NaCl with a pH interval of 1 and in the range of between 3 and 11 (Thawornchaisit et al., 2019).

2.4 Phosphate removal experiments

A stock phosphate solution was prepared by dissolving KH_2PO_4 in distilled water. The phosphate removal capability from aqueous solutions of bagasse and the hydrochars was measured by mixing a 0.1 g sample with 50 mL phosphate solution (pH 7, 25 mg P/L). The mixtures were mechanically shaken at a constant 150 rpm speed. At defined time intervals, the mixtures were immediately filtered through a 0.45 µm filter, and the concentration of phosphate in the filtrates was measured based on the 4500-PE: Ascorbic Acid Method (APHA et al., 2012).

3. RESULTS AND DISCUSSION

3.1 Physicochemical properties of hydrochars

3.1.1 Morphological and textural properties

Bagasse samples were a pale creamy yellow color (Figure 1(a)). Hydrothermal carbonization at 230ºC for 1 h turned the hydrochar into grayish-black solids (Figure 1(b)), confirming the success of lignocellulosic biomass conversion to carbon-rich materials.

(a) (b)

Figure 1. Images of (a) sugarcane bagasse and (b) the derived hydrochar.

Bagasse SEM images show relatively well-defined surfaces with little flaking observed on the surface (Figure 2(a)). In contrast, the image, labeled (b), of the sugarcane bagasse-dervied hydrochar shows a high degree of surface roughness and numerous microspheres with different shapes and sizes indicating destruction and degradation of the cell wall. The new microspheres on the hydrochar surface were ascribed to the decomposition of hemicellulose, as well as

depolymerization of cellulose and partial degradation of lignin (Cai et al., 2016; Jain et al., 2016).

3.1.2 Elemental composition

CHN elemental analysis showed that hydrochar had significantly higher carbon content than the raw bagasse, as a result of carbonization (Table 1). The C content increased from 45% in sugarcane bagasse to 61% in the hydrochar. On the other hand, a slight reduction in hydrogen content was observed in the hydrochar compared to its content in the sugarcane bagasse. Dehydration and decarboxylation were reported to be the paths that were responsible for the reduction of hydrogen and oxygen contents in hydrochar (Cai et al., 2016). Meanwhile, the nitrogen contents of the hydrochar increase, which were consistent with that reported by Congsomjit and Areeprasert (2020) and the HTC of other kinds of lignocellulosic biomass (Xiao et al., 2012; Cai et al., 2016).

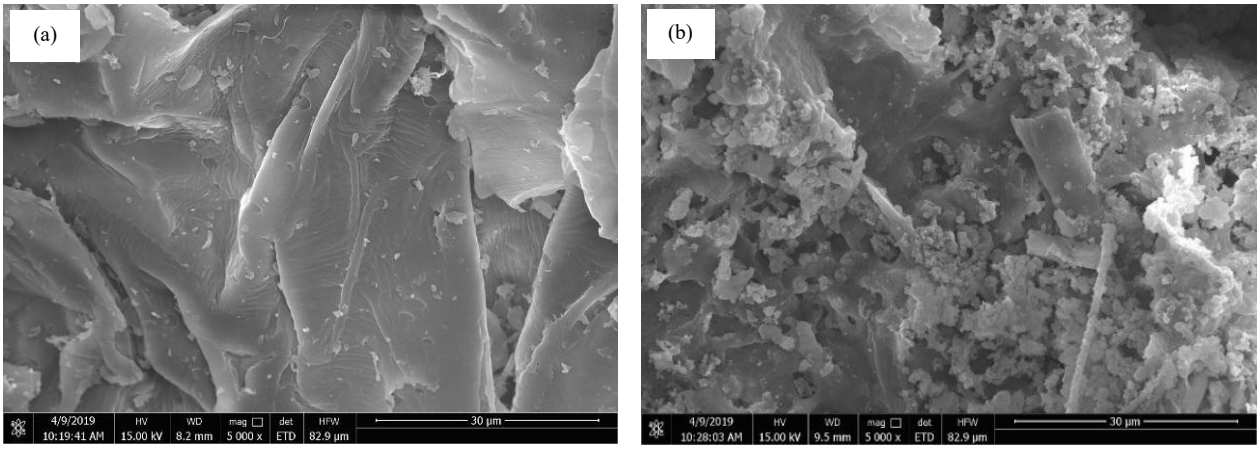

Figure 2. SEM images of sugarcane bagasse (a) and the derived hydrochar (b).

Table 1. Composition of sugarcane bagasse and hydrochars determined by CHN elemental analysis

Sample	Elements (%)		
	C	H	N
SB	45.44	6.29	0.12
HC	60.99	5.64	0.23

3.1.3 Surface functionality

FTIR were recorded to understand chemical changes in the bagasse and the derived hydrochars during HTC. As shown in Figure 3, the IR spectra of the hydrochars were quite similar to that of the raw biomass. The OH-group stretching vibration at 3,346-3,416 cm^{-1}, was ascribed to the hydroxyl group, and the C-H stretching vibration appears at 2,923-2,929 cm^{-1}, indicating a presence of aliphatic structures, identified in both bagasse and hydrochar samples. The 1,733 cm^{-1} band, ascribed to C=O stretching vibrations in the hemicellulose (Wang et al., 2017), disappeared from the hydrochar. In contrast, the 1,112 cm^{-1} band, associated with cellulose (Guo et al., 2015) was sharper in HC when compared to the raw materials. This confirmed hydrolysis of hemicellulose content with hydrothermal carbonization of the bagasse. The 1,510 cm^{-1} peak, attributed to aromatic ring stretching vibration (Guo et al., 2015), was also sharper in the hydrochar. This showed removal of the amorphous fraction in the biomass as suggested by Guo et al. (2015). In contrast, the peak at 1,699 cm^{-1}, corresponding to the carboxyl, carbonyl, or ester groups, was observed only in the hydrochar samples. Wang et al. (2017) noted that the 1,699 cm^{-1} peak indicated the presence of oxygen-containing functional groups, confirming that HTC enhanced oxygen group content and further improved the reactivity of the hydrochar.

3.1.4 Specific surface area

Methylene blue number (MBN) was 40±11 mg/g for bagasse and 101±18 mg/g for the hydrochar. The higher number for the hydrochar showed that HTC increased the biomass surface area. This is consistent with other studies of HTC of lignocellulosic materials (Cai et al., 2016; Niinipuu et al., 2020) and was attributed to the disintegration of the physical structure of biomass, followed by degradation of hemicellulose and cellulose (Jain et al., 2016).

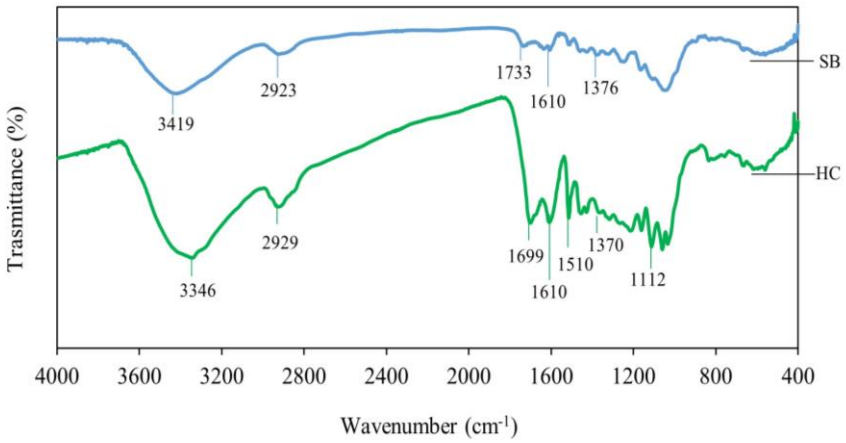

Figure 3. FTIR spectra of sugarcane bagasse (SB) and the derived hydrochar (HC).

3.2 Physicochemical properties of metal modified hydrochars

3.2.1 Physical appearance

Images of modified hydrochar are presented in Figure 4. In the case of Ca-HC and Mg-HC, the material color was completely black compared with the sugarcane-derived hydrochar (Figure 1(b)). On the contrary, when Fe^{3+} and a combination of Fe^{3+} and Fe^{2+} were added to a hydrochar, the products had an orange-red tone, which indicated successful mineral impregnation or coating.

(a) (b) (c) (d)

Figure 4. Images of cation-modified hydrochars (a) Ca^{2+}, (b) Mg^{2+}, (c) Fe^{3+}/ Fe^{2+} and (d) Fe^{3+}.

3.2.2 Elemental composition by XRF

Data obtained from XRF revealed that the major mineral in the hydrochar was silica (Si), with a SiO_2 content of 52.7% (Table 2). Si content in the hydrochar dropped after impregnation or coating with metals. A significant reduction of SiO_2 was attributed to the release of silicon components during NaOH post-treatment of the metal impregnation or co-precipitation process in Equation (1) (Tang et al., 2019).

$$nSiO_2 + 2NaOH \rightarrow Na_2O \cdot nSiO_2 + H_2O \quad (1)$$

Compared to the original hydrochar, compositions of Ca, Mg, and Fe were higher confirming the surface modification of the hydrochar with these cations. In addition, Fe content in both Fe modified hydrochars was relatively greater than Ca or Mg contents. This was related to the metal affinity with the oxygenated functional groups in hydrochar. Fe, especially Fe^{3+}, has a greater ionic charge than Ca^{2+} and Mg^{2+}. Subsequently, interaction between Fe^{3+} and oxygen functional groups of hydrochar would be more favorable.

Table 2. Elemental compositions of hydrochar and modified hydrochars determined by XRF.

Elements	Contents (%)				
	HC	Ca-HC	Mg-HC	Fe(III)/Fe(II)-HC	Fe(III)-HC
SiO_2	52.7	ND	ND	ND	ND
Al_2O_3	9.94	35.0	77.9	18.3	19.3
Fe_2O_3	4.02	ND	ND	54.0	43.8
CaO	1.37	19.9	ND	ND	ND
MgO	5.05	ND	14.93	ND	ND
Na_2O	ND	8.95	2.09	9.87	10.4

Table 2. Elemental compositions of hydrochar and modified hydrochars determined by XRF (cont.).

Elements	Contents (%)				
	HC	Ca-HC	Mg-HC	Fe(III)/Fe(II)-HC	Fe(III)-HC
K_2O	3.38	4.15	3.46	3.89	2.88
CoO	ND	ND	1.02	ND	ND
CuO	2.54	ND	0.460	0.406	0.291
ZnO	ND	ND	ND	ND	0.175
P_2O_5	5.52	ND	ND	ND	ND
Cl	3.99	17.8	ND	4.73	7.79
SO_3	12.3	5.90	ND	9.03	7.54

3.2.3 Surface functionality

To understand chemical changes in hydrochars after surface modification with different cations, FTIR spectra were recorded for the original hydrochar and cation-impregnated hydrochars. As shown in Figure 5, the 1,699 cm^{-1} band, ascribed to the carboxyl, carbonyl, or ester groups on the hydrochar surface, was noticeably weakened, especially in Ca-, and Fe-hydrochars. The band at 757 cm^{-1} became stronger in the Ca-HC, confirming the interaction of the cation with the oxygenated functional groups on hydrochar. On the contrary, the characteristic peaks of Mg-HC were similar to those of the unmodified hydrochar. Fang et al. (2014) also observed this when corn-derived biochar was impregnated with $MgCl_2$, and their explanation was given that the magnesium nanoparticles did not affect the structural formation of organic functional groups in Mg-modified biochar. For Fe-modified hydrochars, Fe incorporation was confirmed by bands at 550 cm^{-1} and 460 cm^{-1}, representing hematite (Mahmoud, 2017). These two bands were found in all hydrochars decorated by Fe^{3+} (Fe(III)-HC) or a combination of Fe^{3+} and Fe^{2+}(Fe(III)/Fe(II)-HC). A peak of Fe-O at 580 cm^{-1} was also found in Fe(III)/Fe(II)-HC. This was also reported in Yang et al. (2018), confirming that Fe^{3+}/Fe^{2+} had been coated on the hydrochars.

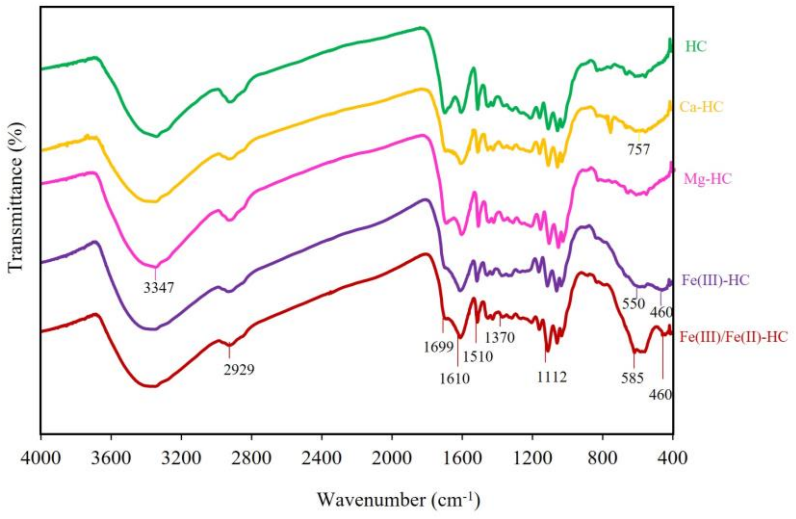

Figure 5. FTIR spectra of hydrochar (HC) and Mg^{2+}-modified hydrochar (Mg-HC), Ca^{2+}-modified hydrochar (Ca-HC), Fe^{3+}/Fe^{2+} modified hydrochar (Fe(III)/Fe(II)-HC) and Fe^{3+} modified hydrochar (Fe(III)-HC).

3.2.4 pH_{pzc}

Points of zero charge (pH_{pzc}) were determined for bagasse and the modified hydrochars using the pH drift method, measuring pH where the material behaves as a neutral species. The values of pH differences (final pH-initial pH, ΔpH) were plotted versus their corresponding initial pH (pH_i)-see Figure 6. From the graphs, pH_{pzc} of the materials were determined from the point of intersection on the x-axis in Figure 6.

Figure 6 shows that bagasse and its derived hydrochars had acidic surfaces, with pH_{pzc} approximately 4. Thus, binding of cations was favored for $pH>pH_{pzc}$, due to deprotonation of the surface

functional groups, resulting in a negatively charged surface which attracts cations. After cations were added by either impregnation or co-precipitation, the surfaces were less acidic, as seen from the shift of pH_{pzc} to the higher value (Figure 6). The pH_{pzc} of Ca-HC and Mg-HC were similar at approximately 7, while the points of zero charge (pzc) were at pH 5.6 for Fe(III)/Fe(II)-HC and pH 8.0 for Fe(III)-HC. The presence of sulfate in the materials used to synthesize Fe(III)/Fe(II)-HC could be the reason for shifting the Fe(III)/Fe(II)-HC pH_{pzc} to lower pH as reported by Kosmulski (2016). The higher pH_{pzc} of the metal-modified hydrochars compared to bagasse and the original hydrochar indicated that phosphate removal was feasible below this pH, because the net positively charged surfaces was favorable and facilitated the removal of anions.

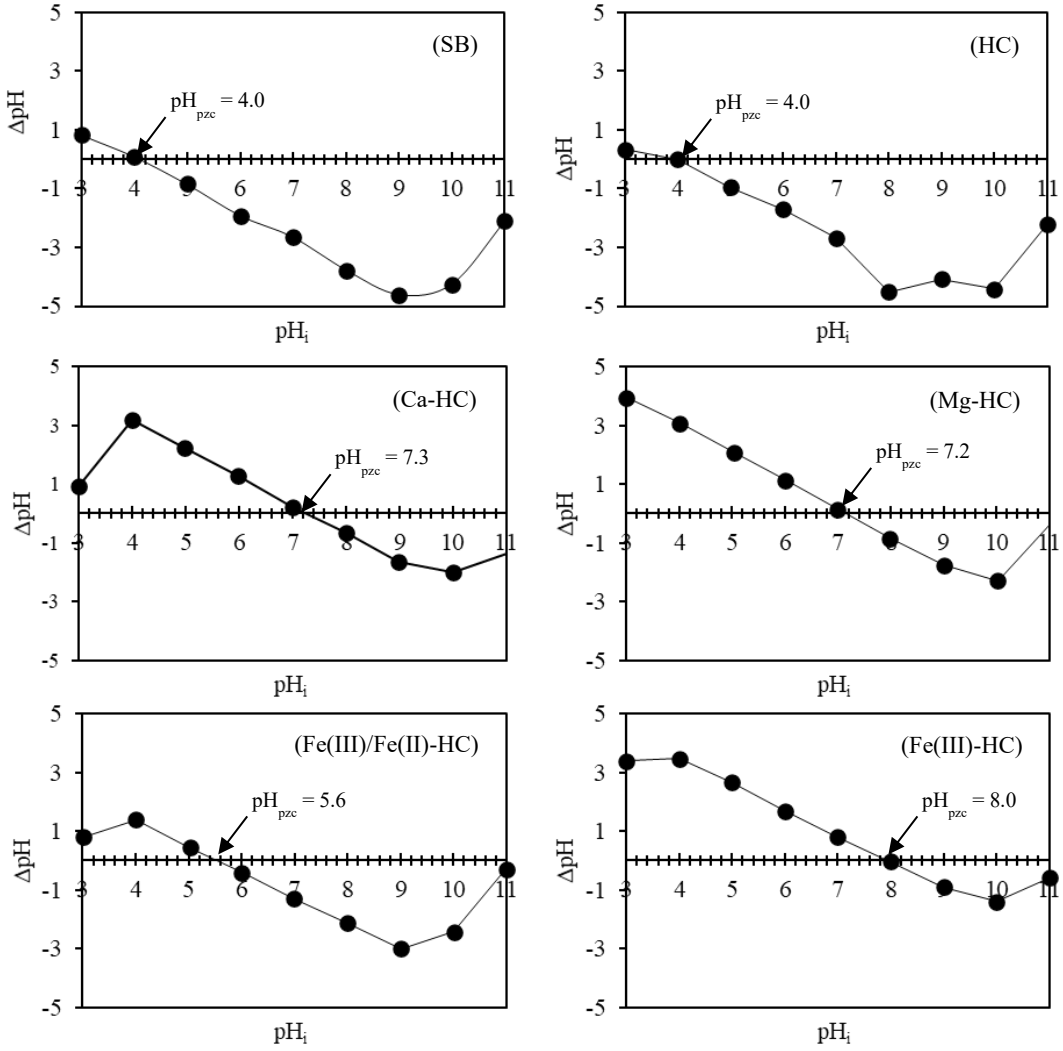

Figure 6. Plot to determine pH_{pzc}: SB=sugarcane bagasse, HC=unaltered and modified hydrochars, Ca-HC=Ca^{2+}, Mg-HC=Mg^{2+}, Fe(III)/Fe(II)-HC=Fe^{3+}/Fe^{2+}, and Fe(III)-HC=Fe^{3+}.

3.3 Phosphate removal capacity

Figure 7 shows the phosphate removal efficiency of the hydrochars. It can be seen that hydrothermal carbonization followed by chemical impregnation or coating transforms sugarcane bagasse into an effective phosphate adsorbent. Phosphate was removed more effective by the hydrochar than the raw material (Figure 8). The surface roughness and numerous microspheres on the hydrochar surface facilitated physisorption of phosphorus from aqueous solution.

The modifying cations enhanced phosphate removal: phosphate removal efficiencies were greater than the unmodified hydrochar (Figure 7 and 8). Phosphate removal was efficient when Fe-modified hydrochars, especially Fe^{3+}-modified hydrochar, were used, yielding the highest adsorption capacity (Figure 8). Moreover, hydrochar decorated with Fe^{3+} in

alkaline conditions showed higher phosphate removal than hydrochars decorated with co-precipitation of Fe^{3+}/Fe^{2+}. A similar observation was reported when rice straw biochar was decorated by impregnation of Fe^{3+} compared to biochar decorated by co-precipitation of Fe^{3+}/Fe^{2+} (Thawornchaisit et al., 2019). The high phosphate removal by Fe(III)-HC was attributed to the presence of $Fe(OH)_3$ and Fe_2O_3 that existed in the Fe^{3+}-modified hydrochar (Yang et al., 2018). In addition, the difference in phosphate removal capacity between the Fe(III)-HC and Fe(III)/Fe(II)-HC could be related to the pHpzc values. pHpzc values were 5.6 for Fe(III)/Fe(II)-HC and 8.0 for Fe(III)-HC. The charge on the Fe(III)-HC surface was more positive, since phosphates removal experiments were conducted at pH<pHpzc, then the phosphate interaction occurred more favorably for Fe(III)-HC.

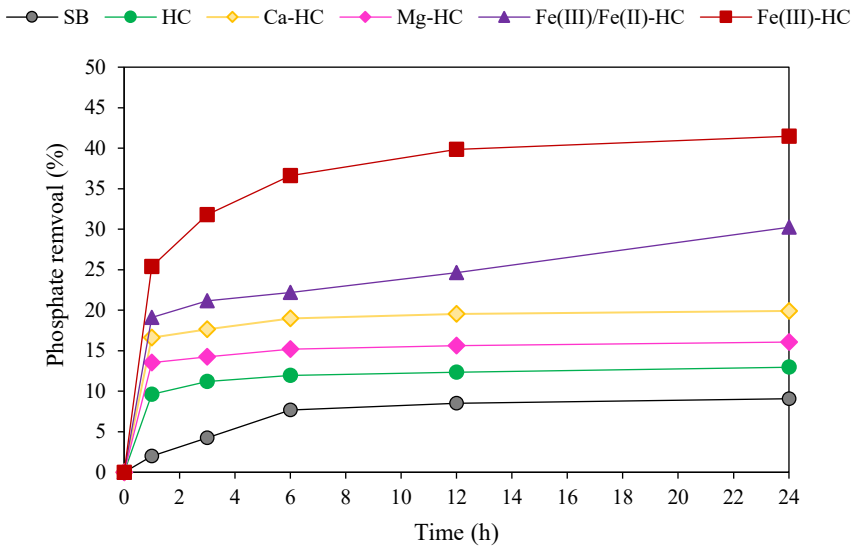

Figure 7. Effect of different modifying cations on phosphate removal ability of sugarcane bagasse (SB), hydrochar (HC), and cation-modified hydrochars.

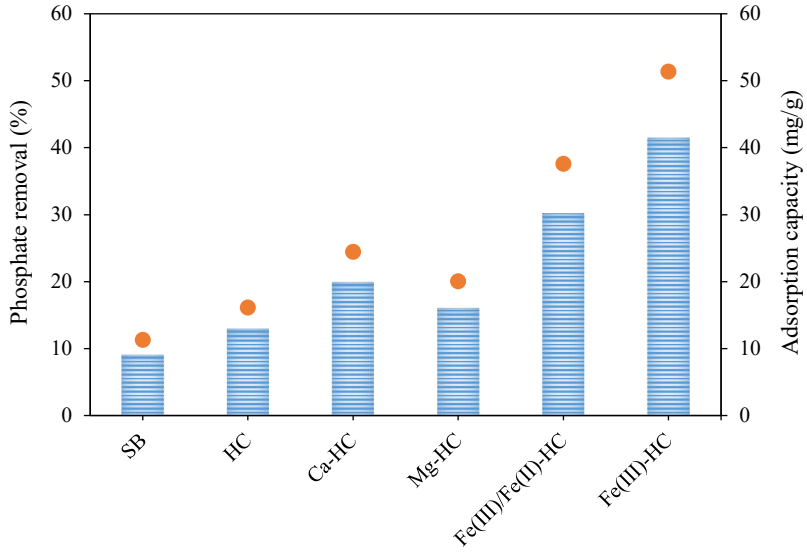

Figure 8. Phosphate removal ability (bar) and phosphate adsorption capacity (orange dot) of cation-modified hydrochars in contact with a 25 mg P/L of KH_2PO_4 solution for 24 hours.

In the Mg- and Ca-modified hydrochars, phosphate removal was observed but less than Fe-modified hydrochars. This phenomenon was attributed to the different valence states: Fe^{3+} with a higher charge density and considered to be a hard acid, would have a greater affinity for a hard base, like PO_4^{3-}, than Ca^{2+} or Mg^{2+}. Therefore, reaction between PO_4^{3-} and Fe^{3+} would be more favorable through a combination

of electrostatic attraction, surface complex formation and anion exchange as reported by Yang et al. (2018). In addition, the amount of Fe in the hydrochar also played an important role in phosphate removal. XRF analysis (see Table 2) revealed that Fe modified hydrochar had higher Fe concentration than Ca- and Mg-modified biochar, thus it removed phosphate more efficiently.

4. CONCLUSION

Hydrothermal carbonization (HTC), followed with impregnating or coating with cations including Ca, Mg or Fe was applied to sugarcane bagasse for producing a solid char product, or hydrochar, with improving phosphate removal capability. Bagasse surfaces became much rougher with more fragmentation than the starting materials after HTC. Higher methylene blue number in hydrochars compared with bagasse showed an increased surface area for adsorption of contaminants. HTC also improved reactivity through the formation of oxygenated functional groups on the hydrochar, which made it an effective precursor for the production of cation-modified hydrochars. Phosphate removal was improved when hydrochars were decorated with Ca^{2+}, Mg^{2+}, Fe^{3+}, and Fe^{3+}+Fe^{2+} under alkaline conditions. Fe-rich hydrochars demonstrated better phosphate removal capacity. We concluded that impregnation or coating on the hydrochar surface after HTC was able to produce effective functional adsorbent for anionic pollutants, like phosphates.

ACKNOWLEDGEMENTS

The authors would like to thank the Department of Chemistry, Faculty of Science, KMITL for financial support for a student's Special Project of TO, NP and RS. Special thanks to John Morris, the author of "Keep it Simple: a guide to English Technical writing" and a member of the Research Clinic, KMITL Research and Innovation Services (KRIS) for shortening and removing unnecessary color from the paper.

REFERENCES

Alewell C, Ringeval B, Ballabio C, Robin son DA, Panagos P, Borrelli P. Global phosphorus shortage will be aggravated by soil erosion. Nature Communications 2020;11:4546.

Almarri M, Ma X, Song C. Role of surface oxygen-containing functional groups in liquid-phase adsorption of nitrogen compounds on carbon-based adsorbents. Energy and Fuels 2009;23(8):3940-7.

American Public Health Association (APHA), American Water Works Association (AWWA), and Water Environment Federation (WEF). Standard Methods for the Examination of Water and Wastewater. 22nd ed. Washington, D.C., USA: APHA-AWWA-WEF; 2012. p. 153-5.

Azzaz AA, Khiari B, Jellali S, Ghimbeu CM, Jeguirim M. Hydrochars production, characterization and application for wastewater treatment: A review. Renewable and Sustainable Energy Reviews 2020;127:109882.

Cai J, Li B, Chen C, Wang J, Zhao M, Zhang K. Hydrothermal carbonization of tobacco stalk for fuel application. Bioresource Technology 2016;220:305-11.

Carrillo V, Fuentes B, Gomez G, Vidal G. Characterization and recovery of phosphorus from wastewater by combined technologies. Reviews in Environmental Science and Biotechnology 2020;19:389-418.

Congsomjit D, Areeprasert C. Hydrochar-derived activated carbon from sugar cane bagasse employing hydrothermal carbonization and steam activation for syrup decolorization. Biomass Conversion and Biorefinery 2020;In press.

Cordell D, White S. Sustainable phosphorus measures: Strategies and technologies for achieving phosphorus security. Argonomy 2013;3:86-116.

Dai L, Wu B, Tan F, He M, Wang W, Qin H, et al. Engineered hydrochar composites for phosphorus removal/recovery: Lanthanum doped hydrochar prepared by hydrothermal carbonization of lanthanum pretreated rice straw. Bioresource Technology 2014;161:327-32.

Desmidt E, Ghyselbrecht K, Zhang Y, Pinoy L, Van der Bruggen B, Verstraete W, et al. Global phosphorus scarcity and full-scale P-recovery techniques: A review. Critical Reviews in Environmental Science and Technology 2015;45:336-84.

European Commission. Study on the Review of the List of Critical Raw Materials: Criticality Assessments. Luxembourg: Publications Office of the European Union; 2017.

European Commission. Study on the EU's List of Critical Raw Materials (2020): Final Report. Luxembourg: Publications Office of the European Union; 2020.

Fang J, Gao B, Chen J, Zimmerman AR. Hydrochars derived from plant biomass under various conditions: Characterization and potential applications and impacts. Chemical Engineering Journal 2015;267:253-9.

Fang C, Zhang T, Li P, Jiang R-F, Wang Y-C. Application of magnesium modified corn biochar for phosphorus removal and recovery from swine wastewater. International Journal of Environmental Research and Public Health 2014; 11(9):9217-37.

Guo S, Dong X, Wu T, Shi F, Zhu C. Characteristic evolution of hydrochar from hydrothermal carbonization of corn stalk. Journal of Analytical and Applied Pyrolysis 2015;116:1-9.

He H, Zhang N, Chen N, Lei Z, Shimizu K, Zhang Z. Efficient phosphate removal from wastewater by MgAl-LDHs modified hydrochar derived from tobacco stalk. Bioresource Technology Reports 2019;8:100348.

Hoekman SK, Broch A, Robbins C. Hydrothermal carbonization (HTC) of lignocellulosic biomass. Energy Fuels 2011; 25(4):1802-10.

Hotová G, Slovák V, Zelenka T, Maršálek R, Parchaňská A. The role of the oxygen functional groups in adsorption of copper (II) on carbon surface. Science of The Total Environment 2020;711:135436.

Jain A, Balasubramanian R, Srinivasan MP. Hydrothermal conversion of biomass waste to activated carbon with high porosity: A review. Chemical Engineering Journal 2016; 283:789-805.

Jian X, Zhuang X, Li B, Xu X, Wei Z, Song Y, et al. Comparison of characterization and adsorption of biochars produced from hydrothermal carbonization and pyrolysis. Environmental Technology and Innovation 2018;10:27-35.

Kosmulski M. Isoelectric points and points of zero charge of metal (hydr)oxides: 50 years after Parks' review. Advances in Colloid and Interface Science 2016;238:1-61.

Kundu S, Coumar MV, Rajendiran S, Kumar A, Rao AS. Phosphates from detergents and eutrophication of surface water ecosystem in India. Current Science 2015;108(7),1320-5.

Mahmoud ZH. The magnetic properties of alpha phase for iron oxide NPs that prepared from its salt by novel photolysis method. Journal of Chemical and Pharmaceutical Research 2017;9(8):29-33.

Martinez-Hernandez E, Amezcua-Allieri MA, Sadhukhan J, Anell JA. Sugarcane bagasse valorization strategies for bioethanol and energy production. In: de Oliveira AB, editor. Sugarcane-Technology and Research. London, UK: IntechOpen; 2018. p. 71-83.

Mokhena TC, Mochane MJ, Motaung TE, Linganiso LZ, Thekisoe OM, Songca SP. Sugarcane bagasse and cellulose polymer composites. In: de Oliveira AB, editor. Sugarcane-Technology and Research. London, UK: IntechOpen; 2018. p. 225-40.

Murray CJ, Müller-Karulis B, Carstensen J, Conley DJ, Gustafsson BG, Andersen JH. Past, present and future eutrophication status of the Baltic Sea. Frontiers in Marine Science 2019;6:No.2.

Nguyen DH, Tran HN, Chao H-P, Lin C-C. Effect of nitric acid oxidation on the surface of hydrochars to sorb methylene blue: An adsorption mechanism comparison. Adsorption Science and Technology 2019;37(7-8):607-22.

Niinipuu M, Latham KG, Boily J-F, Bergknut M, Jansson S. The impact of hydrothermal carbonization on the surface functionalities of wet waste materials for water treatment applications. Environmental Science and Pollution Research 2020;27(19):24369-79.

Nunes CA, Guerreiro MC. Estimation of surface area and pore volume of activated carbons by methylene blue and iodine numbers. Química Nova 2011;34(3):472-6.

Qin C, Liu H, Liu L, Smith S, Sedlak DL, Gu AZ. Bioavailability and characterization of dissolved organic nitrogen and dissolved organic phosphorus in wastewater effluents. Science of the Total Environment 2015;511:47-53.

Petrović JT, Stojanović MD, Milojković JV, Petrović MS, Šoštarić TD, Laušević MD, et al. Alkali modified hydrochar of grape pomace as a perspective adsorbent of Pb^{2+} from aqueous solution. Journal of Environmental Management 2016; 182:292-300.

Sun K, Ro K, Guo M, Novak J, Mashayekhi H, Xing B. Sorption of bisphenol A, 17α-ethinyl estradiol and phenanthrene on thermally and hydrothermally produced biochars. Bioresource Technology 2011;102(10):5757-63.

Tang Q, Shi C, Shi W, Huang X, Ye Y, Jiang W, et al. Preferable phosphate removal by nano-La(III) hydroxides modified mesoporous rice husk biochars: Role of the host pore structure and point of zero charge. Science of the Total Environment 2019;662:511-20.

Tarayre C, De Clercq L, Charlier R, Michels E, Meers E, Camargo-Valero M, et al. New perspectives for the design of sustainable bioprocesses for phosphorus recovery from waste. Bioresource Technology 2016;206:264-74.

Thawornchaisit U, Donnok K, Samphoanoi N, Pholsil P. Iron-modified biochar derived from rice straw for aqueous phosphate removal. Current Applied Science and Technology 2019;19(3):263-75.

United States Department of Agriculture (USDA). Adding value to sugar crop trash and byproduct [Internet]. 2018 [cited 2021 Feb 4]. Available from: https://agresearchmag.ars.usda.gov/2018/feb/sugar.

United States Geological Survey (USGS). Phosphate rock [Internet]. 2021 [cited 2021 May 25]. Available from: https://pubs.usgs.gov/periodicals/mcs2021/mcs2021-phosphate.pdf.

Wang T, Zhai Y, Zhu Y, Peng C, Xu B, Wang T, et al. Acetic acid and sodium hydroxide-aided hydrothermal carbonization of woody biomass for enhanced pelletization and fuel properties. Energy Fuels 2017;31(11):12200-8.

Xiao L-P, Shi Z-J, Xu F, Sun R-C. Hydrothermal carbonization of lignocellulosic biomass. Bioresource Technology 2012; 118:619-23.

Yang Q, Wang X, Luo W, Sun J, Xu Q, Chen F, et al. Effectiveness and mechanisms of phosphate adsorption on iron-modified biochars derived from waste activated sludge. Bioresource Technology 2018;247:537-44.

Yu Y, Yang X, Lei Z, Yu R, Shimizu K, Chen N, et al. Effects of three microelement cations on P mobility and speciation in sewage sludge derived hydrochar by using hydrothermal treatment. Bioresource Technology Reports 2019;7:100231.

Effects of Nano-Scale Zero Valent Iron Fresh and Aged Particles on Environmental Microbes

Papitcha Jongwachirachai[1] and Pijit Jiemvarangkul[2*]

[1]*Department of Clinical Microbiology and Applied Technology, Faculty of Medical Technology, Mahidol University, Bangkok 10700, Thailand*

[2]*Department of Civil Engineering, King Mongkut's University of Technology North Bangkok, Bangkok 10800, Thailand*

ARTICLE INFO

Received: 4 Mar 2021
Received in revised: 6 Jun 2021
Accepted: 9 Jun 2021
Published online: 8 Jul 2021
DOI: 10.32526/ennrj/19/202100031

Keywords:
Nano-scale zero valent iron particles (nZVI)/ nZVI toxicity/ Environmental microorganism/ Bacteria/ Aged nZVI particles

*** Corresponding author:**
E-mail: pijit.j@eng.kmutnb.ac.th

ABSTRACT

Currently, nano-scale zero valent iron particles (nZVI) are being increasingly used in many types of environmental remediation. Due to their usage, nZVI can be left in the environment and may cause toxic effects to living beings, especially surrounding microorganisms. Environmental bacteria in soil and water are some of the main factors affecting plant productivity and other microorganisms in ecosystems. This study evaluated the toxicological effects of nZVI and aged nZVI on bacteria commonly found in the environment. Bacterial, namely *E. coli*, *P. aeruginosa*, *S. aureus*, *B. subtilis*, and *Rhodococcus* sp., were treated with different concentrations of nZVI at different times of exposure in *in vitro* conditions, and bacterial cell viability was determined in order to analyze the toxic effects of nZVI over the course of treatments. The data revealed that at the highest nZVI concentration (1,000 mg/L), *B. subtilis* and *Rhodococcus* sp. had the highest resistance to nZVI (49.35% and 48.31% viability) and less resistance in *P. aeruginosa* (2.26%) and *E. coli* (0.50%) was observed. The growth of microorganisms significantly increased after exposure with seven and 14-day aged nZVI particles. Therefore, the toxicity of aged nZVI to microbial organisms was reduced. Hence, this study demonstrated the toxic effects of nZVI and aged nZVI particles on several species of bacteria *in vitro*. Less toxicity to bacteria was observed in aged nZVI. These findings provide more understanding in the toxic effect of nZVI to microorganisms.

1. INTRODUCTION

Nanotechnology is a rapidly growing scientific area. There are several industrial applications using nanomaterials for development of many commercial products and environmental remediation (Li et al., 2006; Pulit-Prociak et al., 2015). Since 1996, zero-valent iron nanoparticles (nZVI) have been presented as remediation material for removing environmental hazardous contaminants (Wang and Zhang, 1997; Zhang et al., 1998; Lien and Zhang, 1999). For instance, nZVI have been used for removing heavy metals such as cadmium, mercury, silver and nickel, as well as chlorinated hydrocarbons, from contaminated soil and water (Barzan et al., 2014). nZVI particles smaller than 100 nm can be successfully used in degrading chemical contaminants including organic and inorganic pollutants in wastewater and ground water (Diao and Yao, 2009).

In 2005, more than 10 trichloroethane (TCE) contaminated sites in USA were treated by using nZVI (NSCEP, 2005). Mueller et al. (2012) reported the use of nZVI to remove chlorinated hydrocarbon from contaminated sites in Germany and Czech Republic. More recently, nZVI has been used to clean many contaminated fields including both soil and groundwater (Chowdhury et al., 2015; Galdames et al., 2020). Therefore, the increasing use of nZVI can lead to their presence in the environment. The residual nZVI may come from its direct injection into the contaminant sources such as underground or in underwater sludge. After use, the reacted nZVI has been discarded in the treated areas.

Citation: Jongwachirachai P, Jiemvarangkul P. Effects of nano-scale zero valent iron fresh and aged particles on environmental microbes. Environ. Nat. Resour. J. 2021;19(5):381-390. (https://doi.org/10.32526/ennrj/19/202100031)

Some research shows that microorganism viability in contaminated water exposed with nZVI can be decreased, but the effect depends on many conditions such as exposure time and microorganism species (Lee et al., 2008; Chen et al., 2013; Bensaida et al., 2021). The toxicity level of nZVI is related to the composition and structure of the cell in different types of microorganisms. Gram-positive cells showed more resistance than Gram-negative cells. Some previous research also suggested that the different resistance of Gram-positive and Gram-negative bacteria to nZVI was due to the difference in their ability to fight reactive oxidative species (ROS) created by nZVI reactions with the surrounding environment. nZVI particles have been shown to be able to react with O_2 and H_2O in the environment to produce Fe(II) and H_2O_2, which continuously create hydroxyl radicals (OH·) and other ROS by Fenton reaction (Wu et al., 2014). The resistance ability was related to the metalloregulatory protein and ROS scavenger production (Chen et al., 2013). Moreover, the effect of nZVI on bacteria was not only dependent upon genus and strain but also growth phase, where the toxicity to the bacterial cells was higher in exponential and decline phases than in lag and stationary phases (Chaithawiwat et al., 2016). There are several *in vitro* reports of the antibacterial effect of nZVI and a decrease of enzyme activity in microorganisms including *Escherichia coli*, *Staphylococcus aureus*, and *Dehalococcoides* spp. (Pawlett et al., 2013). The effect of nZVI on soil microbial communities was dependent on the level of organic matter and soil mineral type. It was also found that the nanoparticles did not change the soil composition or the organic carbon in the soil extract, but affected the soil bacterial community composition (Ben-Moshe et al., 2013). These studies have confirmed the toxic effect of nZVI on surrounding microorganisms. However, nZVI has still been used due to its ability to efficiently and quickly remove many hazardous contaminants in the environment.

Due to the large areas of contamination, high amounts of nZVI (in the form of sludge) have been directly injected at the contaminant sources to create high concentrations (>1,000 mg/L) in the contamination site (Li et al., 2006; Chowdhury et al., 2015; Galdames et al., 2020). After use, a large quantity of used nZVI has been discarded in the remediation sites. Therefore, this research focused to study and compare the toxicity of both fresh nZVI and aged nZVI (used nZVI) to bacterial viability that live in natural environment in vary concentrations especially at high concentration and exposure times. The results of this study will reveal the safety and reliability of using nZVI as a material to remove several hazardous substances contaminating the environment.

2. METHODOLOGY

2.1 Chemicals and materials

Ferric chloride ($FeCl_3$) was obtained from Alfa Aesar. Sodium borohydride ($NaBH_4$) with 98% purity was used in this work. Pentane (99%), spectrophotometric grade was obtained from Sigma-Aldrich. Ethanol (95%) was purchased from Pharmco-AAper.

2.2 nZVI synthesis

The nZVI synthesis method in this research followed previous publications (Sun et al., 2006; Sun et al., 2007; Jiemvarangkul et al., 2011; Padungthon et al., 2020). Briefly, nZVI particles were manufactured by titration of $FeCl_3$ solution (1.6140 g/L $FeCl_3 \cdot 6H_2O$ dissolved in 120 mL distilled water) with $NaBH_4$ solution (0.9108 g/ L $NaBH_4$ dissolved in 120 mL distilled water) rapidly, while mixing by overhead stirrer at a stirring speed of 400 rpm. The mixing was continuously performed until the color of the mixing solution turned from yellow to black particles. The synthesis reaction is presented as follows:

$$4Fe^{3+}_{(aq)} + 3BH_4^-{}_{(aq)} + 9H_2O \rightarrow 4Fe^0_{(s)} + 3H_2BO_3^-{}_{(aq)} + 12H^+_{(aq)} + 6H_{2(g)} \quad (1)$$

At least 10 minutes of mixing time were needed to complete the reaction above. The nanoparticles were collected by vacuum filtration through 0.4 µm filter papers and were then washed by 5% ethanol solution. The average size of the particles was around 60-70 nm, as measured by transmission electron microscopy (TEM) and a combined acoustic/electro-acoustic spectrometer (Sun et al., 2006). The harvested particles were washed by 5% ethanol and kept submerged in ethanol at low temperature in a sealed polyethylene container. The moisture of contained particles was usually about 70%. nZVI solution (1,000 mg/L) was prepared by mixing 10 mg of filtered nZVI particles with 2 mL sterile water into a homogeneous solution, then adding 8 mL of sterile water, and mixing by vortex for five minutes. nZVI solution was prepared to create three conditions of 10, 100, and 1,000 mg/L. All nZVI solutions were incubated at

room temperature on a Horizontal shaker for seven days and 14 days to prepare aged nZVI.

2.3 Transmission electron microscopy (TEM)

The images of nZVI were taken by a Philips EM 400T TEM (Philips Electronics Co., Eindhoven, Netherlands) operated at 100 kV. The particle samples for TEM were set by placing three droplets of the sample suspension solution onto a holey carbon film (Ernest Fullam, Inc., Latham, NY), which was completely dried in a fume hood before taking TEM images (Sun et al., 2006).

2.4 Luria-Bertani broth (LB broth) and Luria-Bertani agar (LB agar) preparation

Luria-Bertani broth contained 10 g/L of tryptone, 5 g/L of yeast extract, and 5 g/L NaCl. The solution pH (7.0) of LB broth was measured by a pH meter and sterilized by autoclave at 121°C, 15 lbs/in^2 for 15 minutes. Luria-Bertani agar (LB agar) was prepared with 4 g LB agar powder with 1 L of distilled water at pH 7.0 and sterilized by autoclave. LB agar solution was poured in Petri dishes to form LB agar, and they were kept at 4°C if not immediately used.

2.5 Bacterial suspension and yeast suspension

Bacterial suspension dilutions for *E. coli*, *P. aeruginosa*, *S. aureus*, *B. subtilis*, and *Rhodococcus* sp. were prepared by inoculation of cultured bacteria from LB agar for 18-24 h, 35±2°C with 3 mL sterile water pH 7.4. The bacterial solution concentration was adjusted to 0.5 McFarland standard, then diluted into 10^7, 10^6, and 10^5 CFU/mL. For bacterial suspension dilution, yeast suspension dilutions for *C. albicans* were prepared following the same procedure with the strain cultured on Luria-Bertani agar and preparing a final concentration dilution to 10^5 CFU/mL. All microorganisms used in this research have been easily found in natural waters and environments. They were chosen to represent both Gram-positive and Gram-negative bacteria and yeast (Phopin et al., 2016).

2.6 Effects of nZVI on microbes

The bacterial dilution (10^5 CFU/mL) and yeast dilution (10^5 CFU/mL) of each strain were prepared in four conditions: (i) 1 mL of suspension without nZVI solution for control group; (ii) 1 mL of suspension with 10 mL of 10 mg/L nZVI solution; (iii) 1 mL of suspension with 10 mL of 100 mg/L nZVI solution; and (iv) 1 mL of suspension with 10 mL of 1,000 mg/L nZVI solution. Each condition, after mixing by vortex for five minutes, was transferred onto two LB agar plates, and then incubated at 35±2°C for 24 h. for *E. coli*, *P. aeruginosa*, *S. aureus*, and *B. subtilis*, but 48 h. for *Rhodococcus* sp. and *C. albicans*. Viable colony counts were determined at the end of incubation time. The treatments were compared with the control group, and the experiments were made in triplicate for accuracy. Statistical T-test analyses and One-Way Analysis of Variance (ANOVA) were conducted to compare the treatments at percent confidence of 95% (α=0.05) and *p*-values were calculated.

3. RESULTS AND DISCUSSION

3.1 nZVI properties

The color of nZVI particles sludge was black. After drying, it appeared be a black powder. The average pH of the solution containing 0.5 g of nZVI in 100 mL of deionized water was around 7.8 and the moisture of harvested nZVI was around 70%. TEM image showed a cluster of small particles with a chain-like form (Figure 1). The small individual particles had a diameter less than 100 nm (Figure 1).

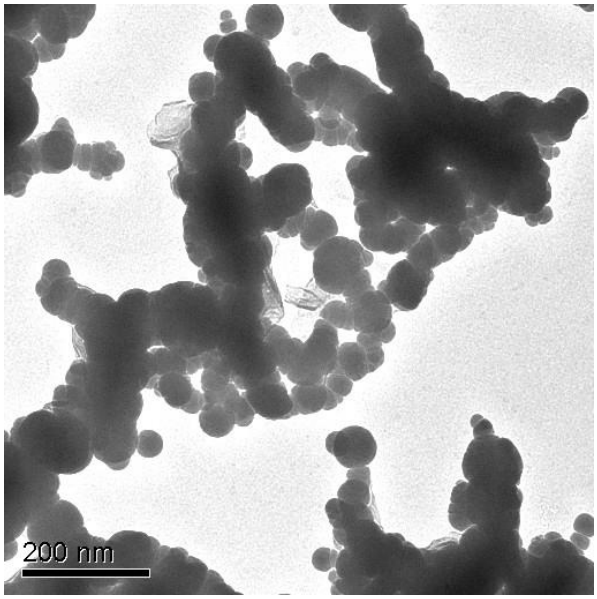

Figure 1. TEM images of nZVI particles obtained in this study.

3.2 nZVI toxicity to microorganisms

Using cytotoxicity assay to analyze the effect of nZVI on bacterial and yeast, high nZVI concentration significantly decreased microorganism viability. The results of nZVI toxicity on tested microbes are presented in Figure 2. With the high concentration of 1,000 mg/L of nZVI, the viability of *E. coli*, *P. aeruginosa*, *S. aureus*, and *C. albiacans* decreased to 0.50%, 2.26%, 7.92%, and 12.49%, respectively. *B.*

subtilis and *Rhodococcus* sp. were more resistant to toxicity with viability of 49.35% and 48.31%. Thus, the results revealed that nZVI toxicity was related to the genus or species of microbes. With nZVI concentration at 1,000 mg/L, the highest resistance was observed in the Gram-positive group (*B. Subtilis* at 49.35% and *Rhodococcus* sp. at 48.31%) and less resistance was observed in Gram-negative (*P. aeruginosa* at 2.26% and *E. coli* at 0.50%) (Figure 2).

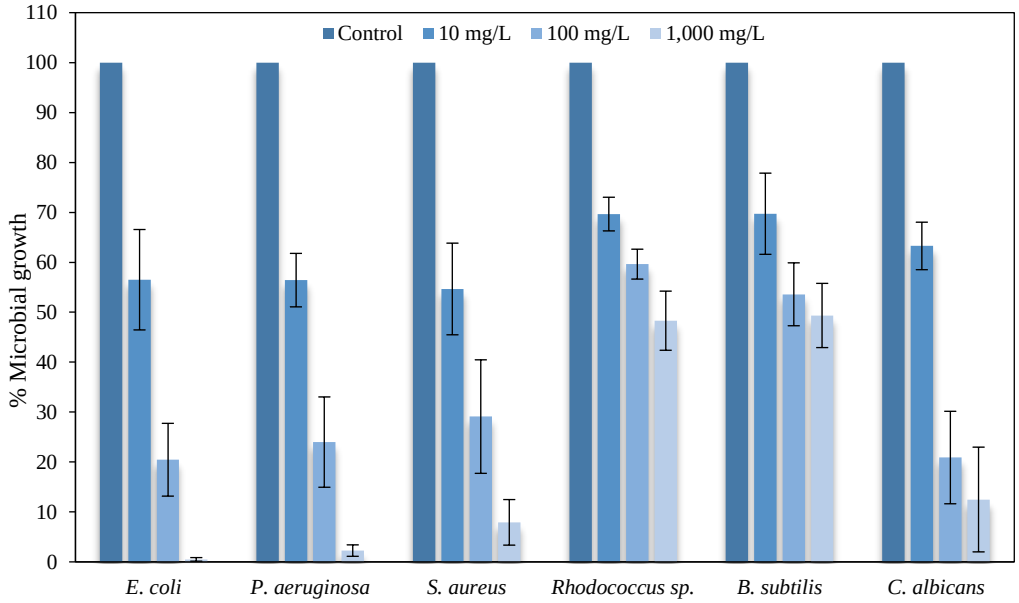

Figure 2. Percent of bacterial colony count compared to the control group after incubating with nZVI

Figure 3 shows the toxic effect of nZVI at various concentration to microorganisms. The growth of bacterial strains (except *C. albicans* as yeast) was linearized with logarithm of concentration. The correlation R^2 of all group data were higher than 0.95 indicating the toxic effect relationship with nZVI concentration. Moreover, based on Figure 3, the results showed the clear picture of the different strains of bacteria resistance to nZVI effects. The upper group of data presents Gram-positive bacteria with higher growth percent compared with the lower group which was Gram-negative. The statistical t-test of percent growth of the Gram-positive group showed a significant difference than Gram-negative bacteria with *p*-value less than 0.05 (*p*-value=0.0048).

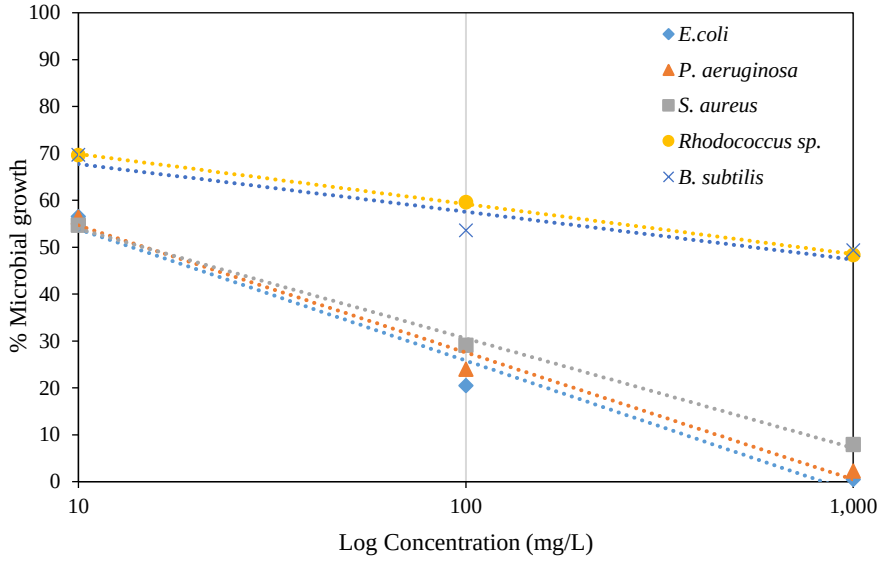

Figure 3. Bacteria strains and nZVI concentration relation with percentages of microbial growth.

The toxicity of nZVI to bacteria could be explained as a cytotoxicity mechanism related to the reactive oxidative species (ROS) production, the oxidative stress, and the liberation of toxic Fe(II), which disturbs the electronic and/or ion transport activity in the cell membrane (Kumar et al., 2017). The oxidation reaction of nZVI particles with intracellular oxygen could produce Fe(II) and hydrogen peroxide that induced oxidative stress by producing ROS (Lee et al., 2008; Kim et al., 2010; Wu et al., 2014). Diao and Yao (2009) found that nZVI particles attached to *B. subtilis* cell walls and coated their surface. Fe(II) released due to nZVI reaction may be able to enter the cytoplasm of cells and create oxidative stress, which can damage the cell membrane, leading to cell death. Cell death occurred because of DNA injuries *in vivo* and membrane damage by ROS (Sacca et al., 2014). However, the toxic effect was dependent on the bacterial species and the environmental stress level. Gram-positive and Gram-negative bacteria might have different ROS confrontation mechanisms (Chen et al., 2013). The mechanism model of nZVI particles causing toxicity to bacteria cells is proposed in Figure 4. After nZVI particles enter into the bacteria environment, they are able to cover the surface of the bacteria cell and react with oxygen in the surrounding environment to produce Fe(II) and H_2O_2, which are able to be transported into the inner cell through cell wall. Then, Fe(II) and H_2O_2 create activities to form ROS, which are harmful to bacteria.

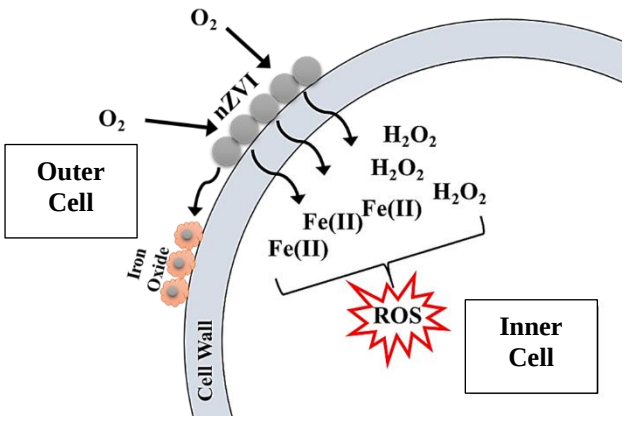

Figure 4. The proposed mechanism model of nZVI activities to cause toxicity to bacterial cell

Due to bacterial characteristics, the Gram-positive cell wall, a 20-80 nm peptidoglycan layer, is 10 times thicker than the Gram-negative cell wall, resulting in additional protection to nZVI toxicity in the Gram-positive bacteria (Silhavy et al., 2010; Chen et al., 2011). Therefore, lipoteichoic acid, a component of the cell wall of Gram-positive bacteria, might have an important role in the toxic resistance when forming a chelating complex with nZVI (Chen et al., 2013). The greater resistance of *B. subtilis* and *Rhodococcus* sp. in this study was caused by their cell wall, as well as the endospore production of *B. subtilis* and mycolic acid of *Rhodococcus* sp. *B. subtilis*, a Gram-positive bacterium with a thick cell wall has a better defense system against environmental stress. Although *B. subtilis* was treated with 1,000 mg/L of nZVI, they were still able to growth with 49.39% viability. The thicker cell wall of Gram-positive bacteria may absorb most of Fe(II) and H_2O_2 released from nZVI reaction with O_2 in solution, so they cannot enter the inner cell to produce ROS as in Figure 4. On the other hand, the lower resistance of Gram-negative bacteria such as *E. coli* may be due to their thinner cell wall that cannot block Fe(II) and H_2O_2 to go inside their cells.

Based upon the results, *C. albicans*, a yeast, was able to resist the effect of nZVI particles better than all Gram-negative bacteria, but its resistance was still less than Gram-positive bacteria, even though *C. albicans* had thicker cell wall (average around 150 nm) than Gram-positive bacteria cell wall (20-80 nm) (Plaine et al., 2008; Silhavy et al., 2010; Klis et al., 2014). The cell wall of *C. albicans* consists of two-layers, and the major structures of its cell wall are beta-glucan and chitin (Plaine et al., 2008). However, there was a discovery that the thickness of *C. albicans* cell wall was able to be changed by its environmental stress (Klis et al., 2014). The different mechanism and structure composition of *C. albicans* cell wall may be factors to its ability to resist the toxicity of nZVI particles. The specific study of nZVI effects on yeast such as *C. albicans* may be needed to explain the mechanism.

3.3 nZVI toxicity on microbes of aged nZVI

To better understand the toxicity effects of the residual nZVI, the colony count cytotoxicity assay was used on different types of microorganisms: *E. coli* and *P. aeruginosa* represented Gram negative bacteria, *S. aureus, B. Subtilis*, and *Rhodococcus* sp. represented Gram positive: and *C. albicans* represented yeast. Microorganisms with different nZVI treatments and exposure times were compared with the control group (not exposed to nZVI particles). The treatment results are shown in Figures 5-10.

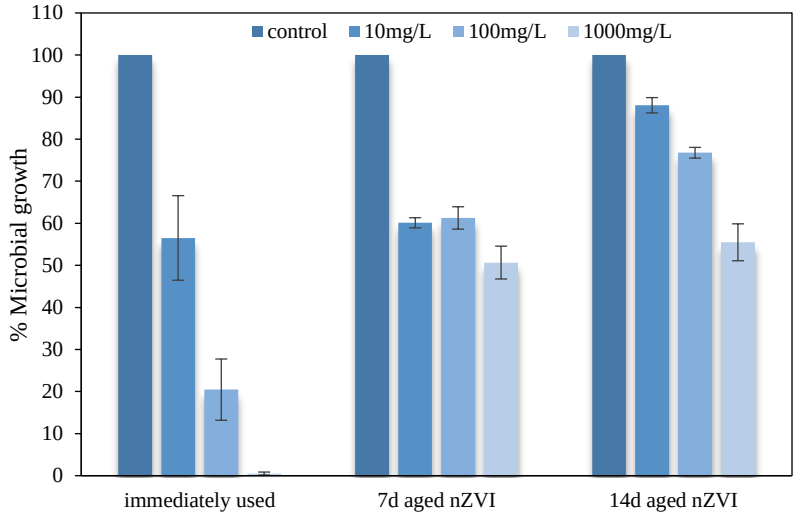

Figure 5. Percent *E. coli* growth in nZVI concentrations (10, 100, and 1,000 mg/L) at 0, 7, and 14 days aged nZVI.

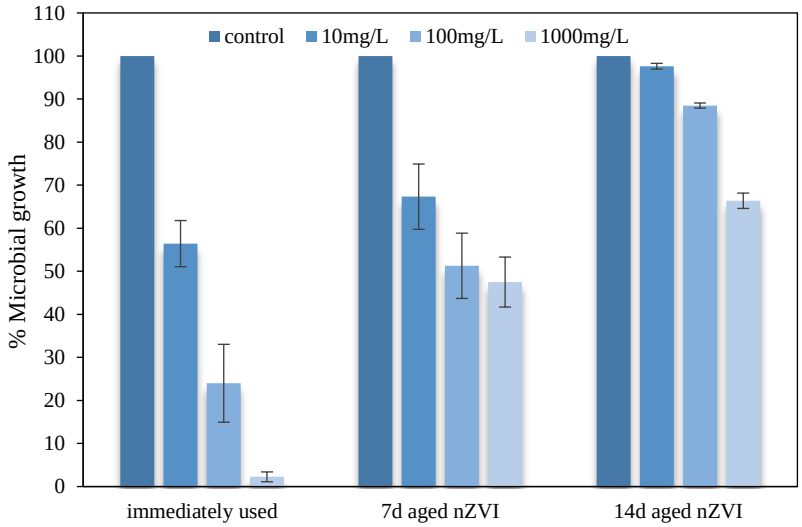

Figure 6. Percent *P. aeruginosa* growth in nZVI concentrations (10, 100, and 1,000 mg/L) at 0, 7, and 14 days aged nZVI.

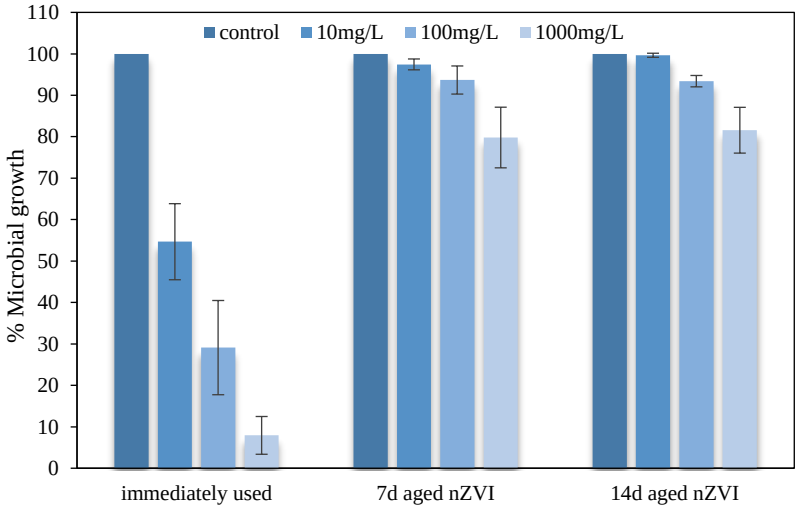

Figure 7. Percent *S. aureus* growth in nZVI concentrations (10, 100, and 1,000 mg/L) at 0, 7, and 14 days aged nZVI.

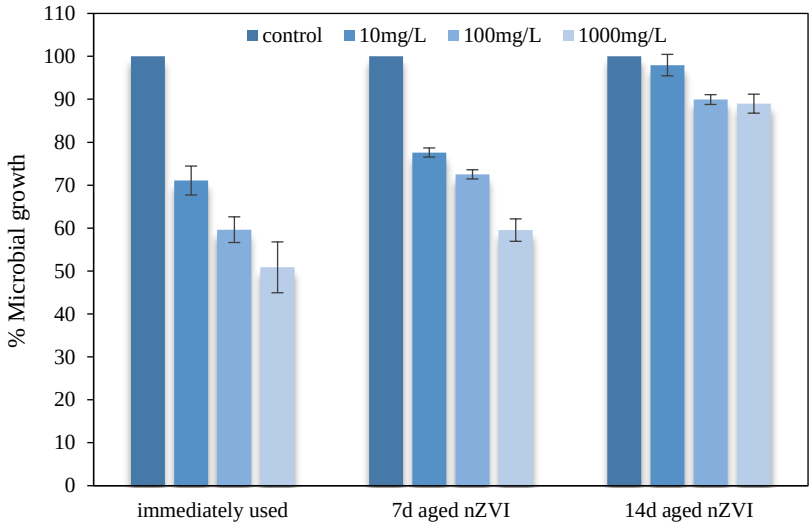

Figure 8. Percent *Rhodococcus* sp. growth in nZVI concentrations (10, 100, and 1,000 mg/L) at 0, 7, and 14 days aged nZVI.

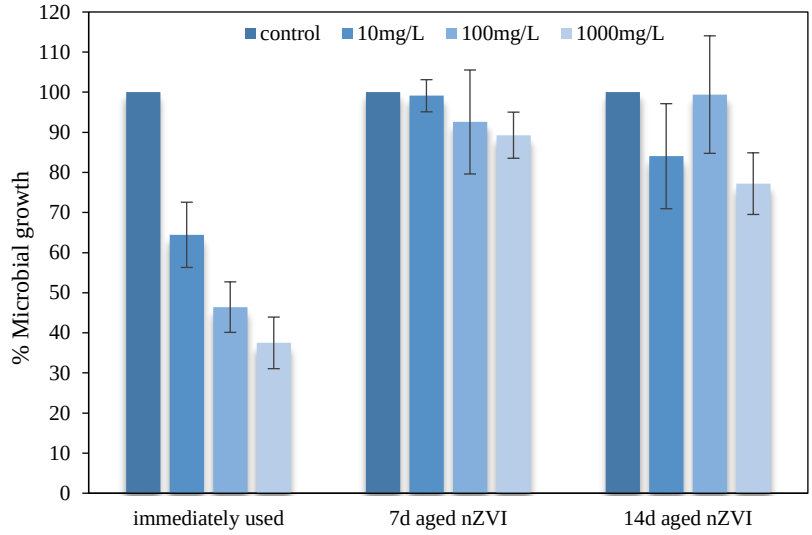

Figure 9. Percent *B. subtilis* growth in nZVI concentrations (10, 100, and 1,000 mg/L) at 0, 7, and 14 days aged nZVI.

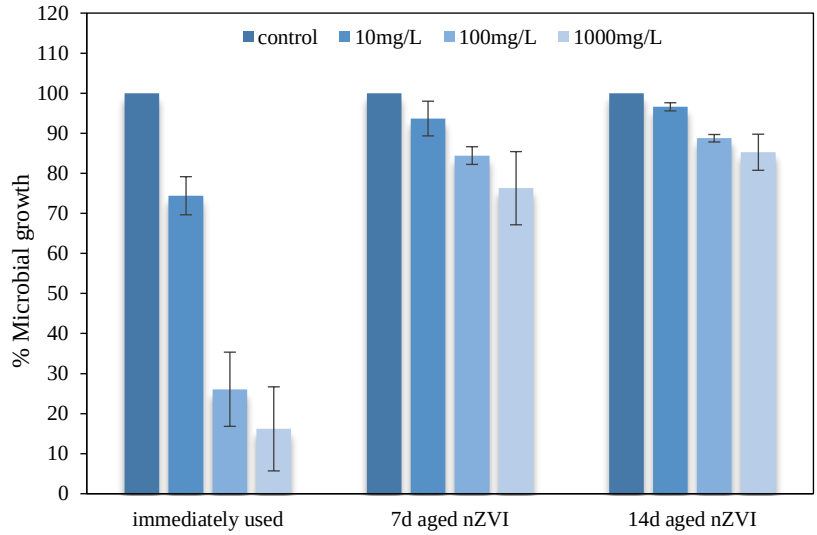

Figure 10. Percent *C. albicans* growth in nZVI concentrations (10, 100, and 1,000 mg/L) at 0, 7, and 14 days aged nZVI.

The bacteria were exposed to 7-day and 14-day old nZVI particles at different concentrations (10, 100, and 1,000 mg/L). As the results show, the toxicity was low in the nZVI long exposure groups. At 14-day aged nZVI, the results show that only minor effect was found even at the highest concentration (1,000 mg/L). Figure 11 presents the percentage of microbial growth with long-time exposure with 1,000 mg/L nZVI.

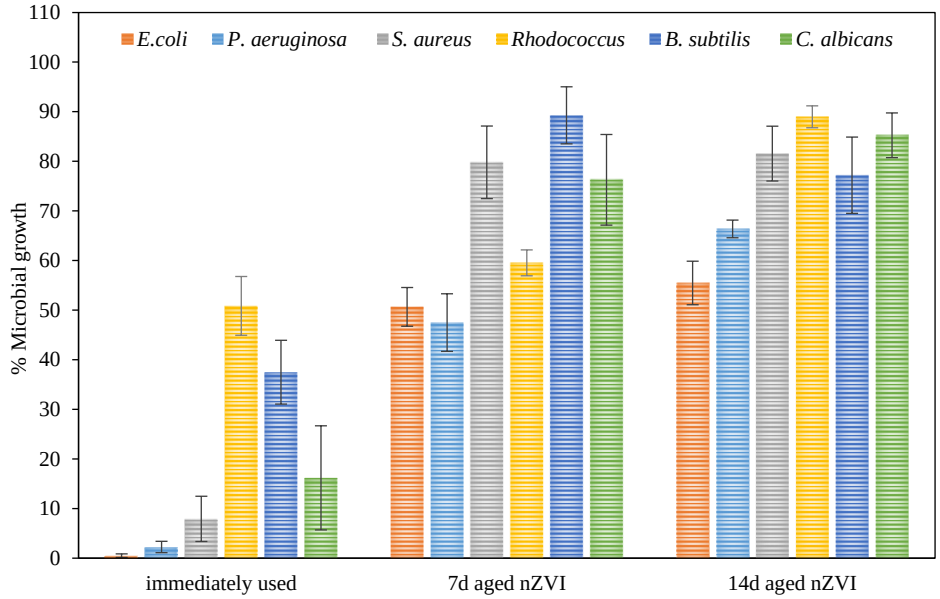

Figure 11. Microbial growth percent with long time exposure at 1,000 mg/L aged nZVI.

According to Figure 11, the percent growth of microorganism increased with aged nZVI particles exposing for 7 and 14 days, respectively. ANOVA statistical test for the three treatments showed significant differences at *p*-value less than 0.05 (*p*-value=0.00007). Therefore, the toxicity of nZVI particles to microbial growth was reduced after aging for long time. Therefore, the toxicity of aged nZVI particles had an inverse relation with microbial growth. All Gram positive bacteria were able to grow with 7-day aged nZVI and almost grew normally with 14-day aged nZVI. The reduction of toxicity of aged nZVI particles may be due to the change of the composition of particles. The outer shell of nZVI particles, which already reacted with surrounding environment, was changed to iron oxide, which has lower reactivity than fresh nZVI particles. The fresh particles shell consisted of Fe(0) that was ready to react (Li and Zhang, 2006; Yan et al., 2010). As seen in Figure 4, the reacted nZVI particle changed to iron oxide particles. Even though iron oxide particles were also able to produce ROS, their toxicity was far less than fresh nZVI particles (Diao and Yao, 2009).

Based on the results, the toxic effect of nZVI was dependent on the Gram type of bacteria as mentioned in the previous section. Moreover, the results also showed that the toxic effect of nZVI on microbial growth was only the instant effect. After the reactive power of the particles decreased, the toxic effect was much reduced. A significant decrease of aged nZVI toxicity to microorganism indicates that nZVI application to remediate contamination is not a long-term effect with small toxicity to microorganisms and nZVI particles will be naturally decomposed by the environment to iron oxide (iron rust), which is found normally in nature (Slunský, 2013).

However, there are many modifications of nZVI to increase its ability such as surface modification for increasing the particle mobility and bimetallic modification for increase the reactive power (Jiemvarangkul et al., 2011; O'Carroll et al., 2013; Bhuvaneshwari et al., 2017; Bensaida et al., 2021). These modified nZVI had higher reactivity and combined with other dangerous chemicals such as heavy metals. Moreover, residual wastes, that were created from used nZVI especially heavy metal adsorbed particles may be dumped into the environments with careless unsecured management. These modified nZVI and nZVI wastes can be expected to be the hazardous waste that is toxic to microorganism in natural environments. Therefore, studying the toxic effects of those particles and wastes to environmental microorganisms will be very important issues in the future.

There are many studies reporting the toxic effects of nZVI exposure in other microorganisms in the environment. A toxic effect of nZVI has been found in Pb-polluted soil treated by nZVI. After aged nZVI exposure in Pd-polluted soil, the ecotoxicological standardised test on *Caenorhabditis elegans* (*C. elegans*), a soil-dwelling bacterivorous nematode, indicated a decrease in the growth of *C. elegans*. However, a different event occurred in Zn-polluted soils treated by nZVI. There was no change in soil biodiversity and *C. elegans* were still able to growth after aged nZVI exposure. These specify that nZVI interaction with various types of pollutants should be considered to be a factor affecting microbial growth. The nZVI reaction significantly reducing *C. elegans* existence may be due to an increase in ROS concentration and the subsequent oxidative stress (Fajardo et al., 2015). nZVI inhibiting *C. elegans* growth was also found to be related to the particle concentration (Sacca et al., 2014). Reproductive toxicity assays presented that carboxymethyl cellulose (CMC)-stabilized nZVI (CMC-nZVI), nanoscale iron oxide (nFe_3O_4), and ferrous ion ($Fe(II)_{aq}$), a group of nZVI products, also significantly decreased the offspring of *C. elegans* due to the increase of reactive oxygen species (ROS) levels in its cells (Yang et al., 2016). These reports showed a similar trend with the results in this research and confirmed that the toxicity of nZVI was just an instant effect.

4. CONCLUSION

The experimental study presents that nZVI exposure to microorganisms affected the bacterial and yeast growth. The effect of nZVI on bacteria is related to type of microorganism and nZVI concentration. Gram-positive bacteria and yeast show more resistance to nZVI toxicity than Gram-negative bacteria. The toxicity effect of nZVI on bacteria is described by cytotoxicity mechanism: reactive oxidative species (ROS) production and oxidative stress. Additionally, the toxic effect of nZVI on microbial is a temporal effect. After a long period of exposure, the toxicity is significantly reduced. This research can confirm that nZVI particles, used in contamination treatment, have no long-term environment effect to microorganism. However, there still are several types of modified nZVI, such as surface modification, combined bimetallic particles and residual waste of nZVI, which need to be evaluated for their toxicity to microbes in the environment.

ACKNOWLEDGEMENTS

This research is financially supported by Faculty of Engineering, King Mongkut's University of Technology North Bangkok, Thailand.

REFERENCES

Barzan E, Mehrabian S, Irian S. Antimicrobial and genotoxicity effects of zero-valent iron nanoparticles. Jundishapur Journal of Microbiology 2014;7(5):e10054.

Ben-Moshe T, Frenk S, Dror I, Minz D, Berkowitz B. Effects of metal oxide nanoparticles on soil properties. Chemosphere 2013;90(2):640-6.

Bensaida K, Eljamal R, Eljamal K, Sughihara Y, Eljamal O. The impact of iron bimetallic nanoparticles on bulk microbial growth in wastewater. Journal of Water Process Engineering 2021;40:101825.

Bhuvaneshwari M, Kumar D, Roy R, Chakraborty S, Parashar A, Mukherjee A, et al. Toxicity, accumulation, and trophic transfer of chemically and biologically synthesized nano zero valent iron in a two species freshwater food chain. Aquatic Toxicology 2017;183:63-75.

Chaithawiwat K, Vangnai A, McEvoy J, Pruess B, Krajangpan S, Khan E. Impact of nanoscale zero valent iron on bacteria is growth phase dependent. Chemosphere 2016;144:352-9.

Chen J, Xiu Z, Lowry GV, Alvarez PJ. Effect of natural organic matter on toxicity and reactivity of nano-scale zero-valent iron. Water Research 2011;45(5):1995-2001.

Chen Q, Li J, Wu Y, Shen F, Yao M. Biological responses of Gram-positive and Gram-negative bacteria to nZVI (Fe^0), Fe^{2+} and Fe^{3+}. RSC Advances 2013;3(33):13835-42.

Chowdhury AIA, Krol MM, Kocur CM, Boparai HK, Weber KP, Sleep BE, et al. nZVI injection into variably saturated soils: Field and modeling study. Journal of Contaminant Hydrology 2015;183:16-28.

Diao M, Yao M. Use of zero-valent iron nanoparticles in inactivating microbes. Water Research 2009;43(20):5243-51.

Fajardo C, Gil-Diaz M, Costa G, Alonso J, Guerrero AM, Nande M, et al. Residual impact of aged nZVI on heavy metal-polluted soils. Science of the Total Environment 2015;535:79-84.

Galdames A, Ruiz-Rubio L, Orueta M, Sánchez-Arzalluz M,Vilas-Vilela JL. Zero-valent iron nanoparticles for soil and groundwater remediation. International Journal of Environmental Research and Public Health 2020;17(16):5817.

Jiemvarangkul P, Zhang W-X, Lien H-L. Enhanced transport of polyelectrolyte stabilized nanoscale zero-valent iron (nZVI) in porous media. Chemical Engineering Journal 2011;170(2): 482-91.

Kim JY, Park HJ, Lee C, Nelson KL, Sedlak DL, Yoon J. Inactivation of *Escherichia coli* by nanoparticulate zerovalent iron and ferrous ion. Applied and Environmental Microbiology 2010;76(22):7668-70.

Klis FM, de Koster CG, Brul S. Cell wall-related bionumbers and bioestimates of *Saccharomyces cerevisiae* and *Candida albicans*. Eukaryot Cell 2014;13(1):2-9.

Kumar D, Roy R, Parashar A, Raichur AM, Chandrasekaran N, Mukherjee A, et al. Toxicity assessment of zero valent iron nanoparticles on *Artemia salina*. Environmental Toxicology 2017;32(5):1617-27.

Lee C, Kim JY, Lee WI, Nelson KL, Yoon J, Sedlak DL. Bactericidal effect of zero-valent iron nanoparticles on

Escherichia coli. Environmental Science and Technology 2008;42(13):4927-33.

Li XQ, Elliott DW, Zhang WX. Zero-valent iron nanoparticles for abatement of environmental pollutants: Materials and engineering aspects. Critical Reviews in Solid State and Materials Sciences 2006;31(4):111122.

Li XQ, Zhang WX. Iron nanoparticles: the core-shell structure and unique properties for Ni(II) sequestration. Langmuir 2006; 22(10):4638-42.

Lien HL, Zhang WX. Transformation of chlorinated methanes by nanoscale iron particles. Journal of Environmental Engineering-Asce 1999;125(11):1042-7.

Mueller NC, Braun J, Bruns J, Černík M, Rissing P, Rickerby D, et al. Application of nanoscale zero valent iron (NZVI) for groundwater remediation in Europe. Environmental Science and Pollution Research 2012;19(2):550-8.

National Service Center for Environmental Publications (NSCEP). U.S. EPA Workshop on Nanotechnology for Site Remediation: U.S. Department of Commerce. Washington, D.C., USA: Environmental Protection Agency; 2005.

O'Carroll D, Sleep B, Krol M, Boparai H, Kocur C. Nanoscale zero valent iron and bimetallic particles for contaminated site remediation. Advances in Water Resources 2013;51:104-22.

Padungthon S, Pranudta A, El-Moselhy MM, Kidkhunthod P, Amonpattaratkit P, Jiemvarangkule P. The capability of nano-scale zero valent iron particles for removal of concentrated lead in spent acidic regeneration solution. Desalination and Water Treatment 2020;194:160-71.

Pawlett M, Ritz K, Dorey RA, Rocks S, Ramsden J, Harris JA. The impact of zero-valent iron nanoparticles upon soil microbial communities is context dependent. Environmental Science and Pollution Research International 2013;20(2):1041-9.

Phopin K, Sinthupoom N, Treeratanapiboon L, Kunwittaya S, Prachayasittikul S, Ruchirawat S, et al. Antimalarial and antimicrobial activities of 8-Aminoquinoline-Uracils metal complexes. EXCLI Journal 2016;15:144-52.

Plaine A, Walker L, Da Costa G, Mora-Montes HM, McKinnon A, Gow NAR, et al. Functional analysis of *Candida albicans* GPI-anchored proteins: Roles in cell wall integrity and caspofungin sensitivity. Fungal Genetics and Biology 2008;45(10):1404-14.

Pulit-Prociak J, Stokłosa K, Banach M. Nanosilver products and toxicity. Environmental Chemistry Letters 2015;13(1):59-68.

Sacca ML, Fajardo C, Costa G, Lobo C, Nande M, Martin M. Integrating classical and molecular approaches to evaluate the impact of nanosized zero-valent iron (nZVI) on soil organisms. Chemosphere 2014;104:184-9.

Silhavy TJ, Kahne D, Walker S. The bacterial cell envelope. Cold Spring Harbor Perspectives in Biology 2010;2(5):a000414.

Slunský J. Utilization of Zero-Valent Iron Nanoparticles (nZVI) for in-situ groundwater remediation including recent field scale application and remediation experience. Proccedings of the Inaugural Conference on the Applications of Nanotechnology for Safe and Sustainable Environmental Remediations (Nano-4-Rem-aNssERs); Southeastern Louisiana University, Hammond, Louisiana: USA; 2013.

Sun Y-P, Li X-Q, Cao J, Zhang W-X,Wang HP. Characterization of zero-valent iron nanoparticles. Advances in Colloid and Interface Science 2006;120(1):47-56.

Sun Y-P, Li X-Q, Zhang W-X, Wang HP. A method for the preparation of stable dispersion of zero-valent iron nanoparticles. Colloids and Surfaces A: Physicochemical and Engineering Aspects 2007;308(1):60-6.

Wang CB, Zhang WX. Synthesizing nanoscale iron particles for rapid and complete dechlorination of TCE and PCBs. Environmental Science and Technology 1997;31(7):2154-6.

Wu H, Yin J-J, Wamer WG, Zeng M, Lo YM. Reactive oxygen species-related activities of nano-iron metal and nano-iron oxides. Journal of Food and Drug Analysis 2014;22(1):86-94.

Yan W, Herzing AA, Kiely CJ, Zhang W-X. Nanoscale zero-valent iron (nZVI): Aspects of the core-shell structure and reactions with inorganic species in water. Journal of Contaminant Hydrology 2010;118(3):96-104.

Yang YF, Chen PJ, Liao VH. Nanoscale zerovalent iron (nZVI) at environmentally relevant concentrations induced multigenerational reproductive toxicity in Caenorhabditis elegans. Chemosphere 2016;150:615-23.

Zhang WX, Wang CB, Lien HL. Treatment of chlorinated organic contaminants with nanoscale bimetallic particles. Catalysis Today 1998;40(4):387-95.

Presence of Biosynthetic Gene Clusters (NRPS/PKS) in Actinomycetes of Mangrove Sediment in Semarang and Karimunjawa, Indonesia

Amelia Cahya Anggelina, Delianis Pringgenies*, and Wilis Ari Setyati

Department of Marine Sciences, Faculty of Fisheries and Marine Sciences, Diponegoro University, Semarang 50275, Indonesia

ARTICLE INFO

Received: 31 Mar 2021
Received in revised: 9 Jun 2021
Accepted: 9 Jun 2021
Published online: 26 Jul 2021
DOI: 10.32526/ennrj/19/202100050

Keywords:
Antibiotic/ Actinomycetes/ Pathogenic bacteria/ Sediments

*** Corresponding author:**
E-mail: delianispringgenies @lecturer.undip.ac.id

ABSTRACT

Actinomycetes are a group of bacteria that are widely distributed in soil, litter, water, and other natural sources. These Gram positive bacteria can produce hundreds of bioactive compounds, especially antibiotics. This research isolated culturable actinomycetes from mangrove sediments in the Semarang and Karimunjawa Island areas. The isolates that produce potential antibacterial compounds were identified by qualitative screening using the Biosynthetic Gene Cluster (NRPS/PKS) prediction approach. This research was conducted from June to November 2020. A total of 19 actinomycetes from Semarang and 17 actinomycetes from Karimunjawa were found to have at least one type of Biosynthetic Gene Cluster (NRPS, Type I or Type II PKS), but only three isolates had antibacterial activity against *S. aureus*, *E. coli*, and *L. monocytogenes*. Molecular identification found that the bacteria were similar to *Brachybacterium paraconglomeratum* (99.92%), *Streptomyces pluripotens* (100%), and *Micromonospora chersina* (99.08%). Results of the study concluded that the three bacterial isolates that had bacterial activity have similar genes with known antibiotic-producing genes and can potentially provide new antibiotic candidates.

1. INTRODUCTION

Mangroves have many marine organisms (Ariyanto et al., 2020) and have good nutrition sources (Ariyanto, 2019) and amino acid contents (Ningsih et al., 2020). This is supported by the physicochemical factors and litter dynamics of mangroves (Ariyanto et al., 2019) and the decomposition of leaves over time (Ariyanto et al., 2018). Pathogenic microbes in the world have evolved for their survival, such as the development of resistance mechanisms to drug compounds. Pathogenic microbial resistance is predicted to kill 10 million people by 2050 if not handled immediately (Romano et al., 2018). However, there is a solution if humans can adeptly utilize natural conditions because nature is the main provider of bioactive materials needed by humans to overcome various kinds of disease (Sharma and Thakur, 2020). More than 100,000 types of natural bioactive compounds during the last 150 years have been identified, such as polyketides, alkaloids, non-ribosomal peptides, isoprenoids, and phenylpropanoids (Carbonell et al., 2016). Some types of natural bioactive compounds that have been identified have come from the actinomycetes group of microorganisms. Natural materials produced by microorganisms are very structurally diverse and are considered important sources in the search for new drugs for various diseases in humans including infections and cancer (Sekurova et al., 2019).

Actinomycetes are Gram-positive bacteria that are known to be capable of producing potential compounds, especially in pharmacology. Some of the compounds produced by actinomycetes are used as antibiotics and can kill cancer cells. The bioactive compounds produced by actinomycetes are proven to be useful as drugs for infections caused by fungi, viruses, and bacteria. They are also used as drugs to treat various types of cancer. Bioactive compounds are usually formed as products of secondary metabolites of organisms, thus they are often referred to as secondary metabolites. According to Katz and Baltz (2016), one type of actinomycetes can produce 30-50 types of secondary metabolite compounds based on the information from the genomic sequences results.

Citation: Anggelina AC, Pringgenies D, Setyati WA. Presence of Biosynthetic Gene Clusters (NRPS/PKS) in actinomycetes of mangrove sediment in Semarang and Karimunjawa, Indonesia. Environ. Nat. Resour. J. 2021;19(5):391-401. (https://doi.org/10.32526/ennrj/19/202100050)

In general, secondary metabolite compounds are produced by enzymes encoded in Biosynthetic Gene Groups (Biosynthetic Gene Clusters) (Romano et al., 2018). Examples of biosynthetic gene groups frequently found are PKS and NRPS.

Actinomycetes are commonly found growing naturally on land and water, including in mangrove sediments. Sediment from mangrove ecosystems is known to be a good place to live for various types of microorganisms because it provides various kinds of nutrients that can be used by actinomycetes to live (Thatoi et al., 2012). Hence, the target location of this research was in the mangrove ecosystem area of Semarang waters and Karimunjawa Islands (Nyamuk island), Central Java. Accordingly, the research objectives were to identify a number culturable-actinomycetes isolated from mangrove sediments in the Semarang and Karimunjawa Island areas. Isolates with the potential to produce anti-bacterial compounds were found by using Biosynthetic Gene Cluster (NRPS / PKS) prediction approach.

2. METHODOLOGY

2.1 Study material

This research was conducted from June to November 2020. Sediment samples were collected from Tapak, Tugurejo Village, Semarang mangrove forest and Nyamuk Island, Karimunjawa mangrove forest. Samples were inserted into sterile ziplock bags, then dried at 26-32°C for two weeks in the laboratory. The treatment method used to isolate actinomycetes from the sediment samples was a modification of the method of Davies-Bolorunduro et al. (2019). Isolation of actinomycetes was done using spread plate method by serial dilution. Each 1 g dry sediment sample was diluted into 9 mL of sterile seawater, then 1 mL of the solution diluted into 9 mL of sterile seawater repeatedly to make a 10^{-3} dilution series. A total of 50 µL from the sample dilutions was flattened on the surface of different medium types, namely Zobell (Zobell 2216 (HiMedia, India)) 40.25 g; agar (Oxoid, England) 15 g), Zobell + Humic Acid (humic acid 1 g (diluted in 10 mL 0.2 N NaOH)), International Streptomyces Project 1 (ISP 1) (yeast extract 3 g; tryptone 5 g; agar (Oxoid, England) 15 g), ISP 1 + Humic Acid (humic acid 1 g (diluted in 10 mL 0.2 N NaOH)), and Humic Acid Vitamin Agar (HVA) (humic acid 1 g (diluted in 10 mL 0.2 N NaOH); Na_2HPO_4 0.5 g; KCl 1.71 g; $MgSO_47H_2O$ 0.05 g; $FeSO_47H_2O$ 0.01 g; vitamin B complex 3.75 mg; $CaCO_3$ 0.02 g; agar (Oxoid, England) 18 g) (Hayakawa and Nonomura, 1987). Each medium was added with 60 mg/L of antibiotic compounds (Nalidixic Acid and Nystatin). Samples were incubated at 29-37°C for 1-5 weeks. Representative isolates were grown on new medium using the streak plate method until pure cultures were obtained.

2.2 Antibacterial activity screening

Actinomycetes antibacterial screening was carried out by modifying the agar plug method (Messaoudi et al., 2020). Actinomycetes cultures grown for two weeks were cut into a cylindrical shape (about 8 mm in diameter), then affixed to the surface of Mueller Hinton Agar (MHA) medium that had been inoculated, which include the types of: (*Staphylococcus aureus*, *Escherichia coli*, and *Listeria monocytogenes*). The test sample was incubated at 29-34°C.

2.3 DNA extraction

Bacterial DNA extraction was carried out using Chelex method. Bacterial colonies were included in a mixture of 500 µL of 0.5% saponin solution (in Phosphate Buffer Saline) and 100 µL of ddH_2O. Samples were soaked for 12-24 h at 4°C in order to lyse the bacterial cell walls. Samples that had been soaked in saponins were centrifuged at 9,000 rpm for 15 min. The supernatant from centrifugation was discarded, then the pellets were added with 1 mL of PBS solution, then vortexed until homogeneous. The homogeneous mixture of natant and PBS was then centrifuged again for 10 min. The supernatant was discarded again. 100 µL of ddH_2O and 50 µL of 20% Chelex solution (vortex Chelex solution before use) were added. The samples were then heated at 95°C for 5 min then vortexed, then heated again at 95°C for 5 min. The samples were re-centrifuged for 15 min, then the supernatants were transferred to new 1.5 mL microtubes ready for use as a DNA Template.

2.4 NRPS and PKS gene type II cluster amplification

NRPS gene cluster detection was done using Thermo Scientific 2X Phire Plant Direct PCR Master Mix with A2gam F (5´-AAGGCNGGCGSBGCSTAY STGCC-3´) and A3gamR (5´-TTGGGBIKBCCGGTS GINCCSGAGGTG-3´) primer pair (Radjasa et al., 2005). The PCR condition was 98°C for 5 min for initial denaturation; then 40 cycles consisting of a denaturation stage at 98°C for 5 sec, annealing stage at 70°C for 5 sec, extension stage at 72°C for 1 min,

and a final extension stage at 72°C for 1 min and cooling stage at 4°C.

Type I PKS gene cluster detection was used Thermo Scientific 2X Phire Plant Direct PCR Master Mix with MDPQQR f (5'-RTRGAYCCNCAGCAIC G-3') and HGTGT r (5'-VGTNCCNGTGCCRTG-3') primer pair (El Samak et al., 2018). The PCR condition was 98°C for 5 min for initial denaturation; then 10 cycles consisting of a denaturation stage at 98°C for 5 sec, annealing stage at 60°C (temperature reduced 2°C per cycle) for 5 sec, extension stage at 72°C for 1 min, followed with 30 cycles with a denaturation stage at 98°C for 1 min, annealing stage at 40°C for 5 sec, extension stages at 72°C for 1 min, and a final extension stage at 72°C for 1 min and a cooling stage at 4°C.

PKS-II gene amplification was carried out by mixing the primary pair of PF6 (5'-TSGCSTGCTTGG AYGCSATC-3 ') and PR6 (5'TGGAANCCGCCGAA BCCGCT-3') (El Samak et al., 2018), 1 µL each at a concentration of 10 mM, with 1 µL of extracted template DNA, 10 µL of Thermo Scientific2X Phire Plant Direct PCR Master Mix, and 8 µL of ddH_2O. PCR amplification process was carried out in 40 cycles with the following stages: initial denaturation stage (98°C, 5 min), followed by denaturation (98°C, 5 sec), annealing (70°C, 5 sec), extension stage (72°C, 1 min), and the final extension (72°C, 1 min).

2.5 Amplification of 16S rRNA from active isolates and DNA visualization

Amplification of the 16S rRNA gene was carried out by mixing 1 µL of template DNA, primary pair of 27F (5'-AGAGTTTGATCCTGGCTCAG-3') and 1429R (5'-GGTTACCTTGTTACGACTT-3') (El Samak et al., 2018), 1 µL each at a concentration of 10 mM, 12.5 µL of Thermo Scientific2X Phire Plant Direct PCR Master Mix, and 9.5 µL of ddH_2O. PCR process was carried out in 40 cycles with the following stages: initial denaturation (98°C, 5 min), denaturation (98°C, 5 sec), annealing (55°C, 5 sec), extension (72°C, 1 min), and final extension (72°C, 1 min).

Electrophoresis of the DNA samples was done in an agarose gel medium. The agarose gel concentration used in this research was 1% agarose gel in a buffer solution of TAE (Tris Acetate EDTA) mixed with GelRed dye to make it easier to visualize with UV light. The electrophoresis process was carried out at a voltage of 100 volts and a strong current of 400 A for 30 min. Then, the agarose gel is transferred to a UV Transilluminator to process the visualization of the formed DNA bands.

The amplified sample was carried out in sequencing process that aims to determine the nucleotide bases sequence using Sanger Deoxy Method. The sequencing data were edited using MEGA 7.0 software, then the data from 16s rDNA primers were matched with the data from GenBank NCBI. The 16S rRNA sequence data from the samples were deposited on GenBank with access numbers MW750399, MW750400, and MW750401.

2.6 Biosynthetic Gene Cluster (BGC) mapping simulation

Biosynthetic Gene Cluster (BCG) mapping simulation was carried out by submitting the whole genome sequence of actinomycetes species which was similar to the result of molecular identification of active isolates in the AntiSMASH 6.0 program (https://antismash.secondarymetabolites.org/).

3. RESULTS AND DISCUSSION

3.1 Actinomycetes isolation and Biosynthetic Gene Cluster (BGC) screening

Thirty six actinomycetes isolates were successfully obtained from the mangrove sediments of Semarang and Karimunjawa with five different growth medium (Zobell, Zobell + Humic Acid, ISP 1, ISP 1 + Humic Acid, and Humic Acid Vitamin Agar (HVA)), namely 19 isolates from Semarang consisting of 3 isolates growing from ISP 1 medium; 1 isolate grown from Zobell medium; 9 isolates grown from HVA medium; 6 isolates grew from ISP 1 + Humic Acid medium and 17 Karimunjawa Isolates consisting of 3 isolates grown from ISP 1 medium; 4 isolates grown from Zobell medium; 5 isolates grew from HVA medium; 2 isolates grew from ISP 1 medium + Humic Acid; and 3 isolates grown from Zobell + Humic Acid medium (Figure 1(a) and (b)).

Selective media is an important step to enhance the isolation process. Furthermore, growth medium composition affects the biological activities for the isolates, for example, antimicrobial properties (Dhanasekaran et al., 2009). HVA has been indicated as the best medium for isolating actinomycetes from mangrove sediments based on the number of actinomycetes isolates obtained from the two sampling locations compared to the other four types of medium. This is because the HVA media is specifically designed to isolate actinomycetes from the

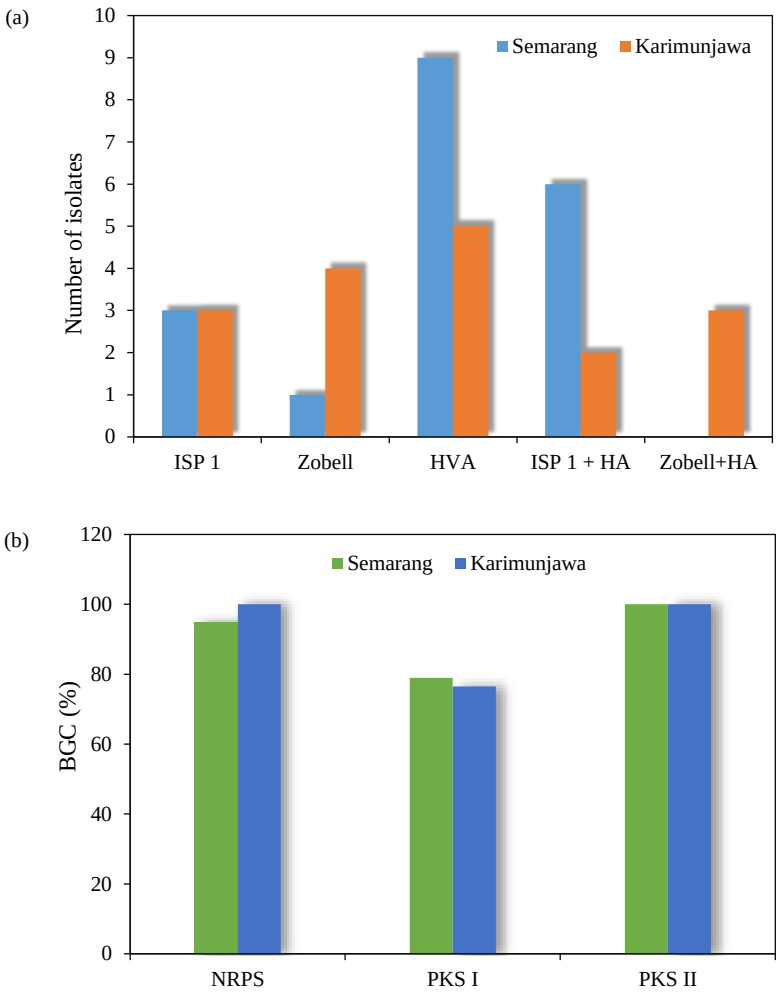

Figure 1. (a) Number of actinomycetes isolates successfully grown based on the type of growth medium and (b) percentage of the number of actinomycetes isolates detected to have Biosynthesis Gene Clusters (BGC) from Semarang and Karimunjawa

soil by providing sufficient nutrients to support growth and sporulation for actinomycetes and to inhibit the development of other bacteria (Hayakawa and Nonomura, 1987). ISP 1 contains tryptone and yeast extract provides nutrition that is necessary for bacterial metabolism (https://himedialabs.com/TD/M356.pdf). Zobell medium contains peptone and yeast as nutrients as well as minerals like seawater. Some actinomycetes have adapted to the salinity of marine areas (seawater and sediments). High salinity adaptation is needed to survive and grow as a fundamental biological process (Rashad et al., 2015). Furthermore, the average number of actinomycetes isolated from the modified ISP 1 + Humic Acid medium was greater than the average number of actinomycetes isolated from the ISP 1 medium. Meanwhile, the average number of actinomycetes isolated from Zobell + Humic Acid modified medium was less than the average number of actinomycetes from Zobell medium. This means that the addition of humic acid as one of the soil constituent components has a more positive effect when it is added to actinomycetes isolation medium (ISP 1) compared to when it is added to the isolation medium of universal marine bacteria (Zobell).

The number of actinomycetes isolated from the mangrove sediments of Tapak, Tugurejo, Semarang was higher than the number of actinomycetes isolated from the mangrove sediments of Nyamuk Island, Karimunjawa. This can be caused by the supply of nutrients derived from factory waste, household waste, shipping activity waste, and waste from various other human activities in Semarang (Siregar and Koropitan, 2016) which provide more nutrients for actinomycetes when compared to nutrients in the waters of Nyamuk Island which are not yet abundant. It is influenced by human activities due to its relatively smaller population, less diverse community activities in terms of industry, and the remote location of the islands (Karimunjawa National Park, 2019).

Screening results for the presence of Biosynthetic Gene Clusters (BGC) consisting of NRPS genes, PKS type I genes, and PKS type II genes in actinomycetes isolates that were isolated from mangrove sediments in Tapak, Tugurejo, Semarang and Nyamuk Island, Karimunjawa obtained detailed results; 18 out of 19 (94.74%) actinomycetes isolates from Semarang were detected to have the NRPS gene while all Karimunjawa actinomycetes isolates (100%) were detected to have the NRPS gene. Results of PKS type I genes detection from Semarang isolates showed that 15 out of 19 (78.95%) isolates had genes detected, while 13 out of 17 (76.47%) of Karimunjawa isolates had these genes. Results of PKS type II genes detection showed that all isolates (100%) from both locations were detected to have the gene.

3.2 Antibacterial activity

Inhibition zone values from the antibacterial activity screening of mangrove sediment actinomycetes isolates in Semarang and Karimunjawa against pathogenic bacteria *Staphylococcus aureus* (PN.SB.11:1.67±0 cm), *Escherichia coli* (PN.SB. 11.1:0.57±0.15 m), and *Listeria monocytogenes* (S.SK.8.1:0.65±0.40 cm; PN.SB.11.3:1.72±0.29 cm) are shown in Figure 2.

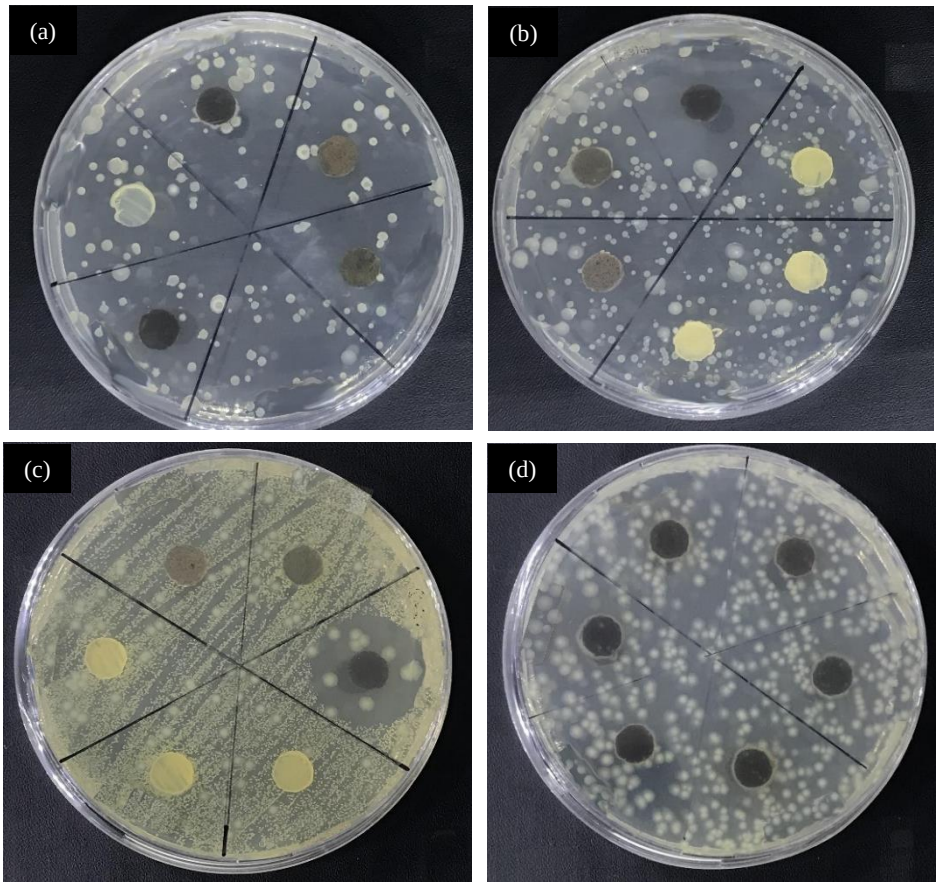

Figure 2. Antibacterial activity screening clear zone data of actinomycetes isolates (a) S.SK.8.1 against *L. monocytogenes*, (b) PN.SB.11.3 against *L. monocytogenes*, (c) PN.SB.11.3 against *S. Aureus*, and (d) PN.SB.11.1 against *E. coli*

Although all isolates were detected to have Biosynthetic Gene Clusters (BGC), only three actinomycetes isolates had antibacterial activity with the tested bacteria of *E. coli*, *S. aureus*, and *L. monocytogenes*. The actinomycetes isolate of mangrove sediment from Semarang which has antibacterial activity against *L. monocytogenes* was the isolate designated by code S.SK.8.1. Actinomycetes isolates of mangrove sediment from Karimunjawa that were able to inhibit the growth of pathogenic bacteria were the isolate code PN.SB.11.1 against *E. coli* and isolate code PN.SB.11.3 against *S. aureus* and *L. monocytogenes*. Although almost all isolates were detected to have a Biosynthetic Gene Cluster, the causes of the lack of active isolates against pathogenic bacteria have been reported in several previous studies. It has been stated that the presence of Biosynthetic Gene Clusters (PKS and NRPS) in the

genomic DNA of an organism is an indication of the organism's potential to produce bioactive compounds, however, the products produced by these organisms might have other activities besides antibacterial, such as antioxidants or antitumors (El Samak et al., 2018). It can also be caused by Biosynthetic Gene Clusters that are not expressed (silent) under laboratory culture conditions (*in vitro*) (Kalkreuter et al., 2019).

3.3 Molecular identification of 16S rRNA active isolates

Molecular identification results of actinomycetes active isolates that were isolated from the mangrove sediments of Tapak, Tugurejo, Semarang and Nyamuk Island, Karimunjawa based on 16S rRNA gene sequencing are shown in Table 1.

Table 1. Bacteria identification results at different locations

Isolate code	Species identification (BLAST)	Access number	Sequence length (bp)	Ident (%)	Query cover (%)
S.SK.8.1	*Brachybacterium paraconglomeratum*	MW750399	870	99.08%	100%
PN.SB.11.1	*Streptomyces pluripotens*	MW750400	1354	100%	100%
PN.SB.11.3	*Micromonospora chersina*	MW750401	1316	99.92%	100%

Notes: S.SK=Semarang; PN.SB=Nyamuk Island, Karimunjawa

The active actinomycetes isolates of mangrove sediment from Semarang with code S.SK.8.1 was identified molecularly as *Brachybacterium paraconglomeratum* with the data equation in MT214268.1 sequence at 99.08%. Meanwhile, the actinomycetes isolate code PN.SB.11.1 was identified molecularly as *Streptomyces pluripotens* with a 100% similarity percentage to the data with access number CP022433.1. Actinomycetes code PN.SB.11.3 was identified as *Micromonospora chersina* with a 99.92% similarity percentage to GenBank data with access number EU274367.1.

Brachybacterium paraconglomeratum is a gram-positive bacterium belonging to the actinobacteria phylum which was first introduced by (Takeuchi et al., 1995). This actinobacteria species is anaerobic facultative, pale brown, with coccoid-shaped cells during the stationary phase, and irregular rod-shaped during the exponential phase. *Streptomyces pluripotent* is a species of actinomycetes belonging to the genus Streptomyces which was first isolated from mangrove sediments (Lee et al., 2014). This species is reported to be able to produce Bacteriocin compounds (compounds that can inhibit the growth of MRSA bacteria). *Micromonospora chersina* is a species of actinomycetes belonging to the genus Micromonospora. The genus has characteristics such as gram-positive, spore-forming capability, generally aerobic, and ability to form branched mycelium. Several species of the genus are known as important sources of antibiotics (Hirsch and Valdés, 2010).

3.4 Biosynthetic Gene Cluster (BGC) mapping simulation using AntiSMASH 6.0 program

Mapping simulation results of Biosynthetic Gene Cluster (BGC) in the whole genome from GenBank of the same species with the molecular identification results of the *Brachybacterium paraconglomeratum* sample (NZ_QOCI00000000.1) are shown in Table 2.

Table 2. Mapping simulation of Biosynthetic Gene Cluster (BGC)

Region	Region location (Nucleotides)	Type	Most similar known cluster	Similarity	References
6.1	177714-211682	NAA, Ectoine	Ectoine	75%	Zaccai et al. (2016)
10.1	141523-152335	Siderophore	-	-	-
16.1	141523-152335	Terpene	Carotenoid	50%	Maoka (2019)

Mapping simulation of Biosynthetic Gene Cluster (BGC) using AntiSMASH 6.0 in the whole genome of the same species with the *Brachybacterium paraconglomeratum* sample (S.SK.8.1) has detected three secondary metabolite producing regions with estimates that the resulting product was included in the NAPAA (Non-Alpha Poly-Amino group Acids), ectoine, siderophore group, and terpene group. The

three regions have similarities with the gene clusters that produce active compounds including the cosmetic active ingredient compound Ectoine at 75% (Region 6.1) (Zaccai et al., 2016) and carotenoid pigment compounds at 50% (Region 10.1) (Maoka, 2019). Another region, namely Region 10.1, which was thought to produce sideropore compounds, has not yet been known to have similarities with the gene clusters that produce other secondary metabolite compounds.

Mapping simulation results of Biosynthetic Gene Cluster (BGC) using AntiSMASH 6.0 in the whole genome of the same species with *Streptomyces pluripotens* sample (PN.SB.11.1) has detected 31 BGC regions with estimates of the composing products in the types of butyrolactone, lanthipeptide-class iii, terpene, PKS Type 3, PKS Type 2, PKS Type 1, NRPS, betalactone, hglE-KS (heterocyst glycolipid synthase-like PKS), ectoine, LAP (Linear Azol (in) e-containing Petide), melanin, siderophore, ladderane, RiPP-like, NRPS-like, lanthipeptide-class v, thiopeptide, and nucleoside (Table 3). Some of these regions had similarities with the gene clusters that produce antibiotic compounds such as Cyphomycin at 5% (Region 1) (Chevrette et al., 2019), Cinnamycin at 14% (Region 6) (Widdick et al., 2003), Enduracidin at 10% (Region 7) (Inoue et al., 2010), Glycinocin A at 16% (Region 15) (Corcilius et al., 2018), Alba-flavenone at 100% (Region 16) (PubChem NCBI), Toxoflavin/Fervenulin at 14% (Region 21) (Lee et al., 2016), Formicamycins AM at 11% (Region 24) (Qin et al., 2017), Daptomycin at 6% (Region 27) (WHO, 2018), Platencin at 9% (Region 30) (PubChem NCBI), and Toyocamycin at 30% (Region 31) (PubChem NCBI) as shown in Table 3.

Table 3. Mapping simulation results of the Biosynthetic Gene Cluster (BGC) of the *Streptomyces pluripotens* sample

Regions	Region location (Nucleotides)	Type	Most simillar known cluster	Similarity	Reference
Region 1	72991-81978	Butyrolactone	Cyphomycin	5%	Chevrette et al. (2019)
Region 2	490073-512793	Lanthipeptide-class-iii	Informatipeptin	85%	-
Region 3	702613-724773	Terpene	Isorenieratene	54%	Maresca et al. (2008)
Region 4	771946-811237	Type 3 PKS	Herboxidiene	6%	Hasegawa et al. (2011)
Region 5	823634-935178	Type 1 PKS, NRPS, Betalactone	Sporolide A/B	46%	Nicolaou et al. (2009)
Region 6	953402-1003799	Type 1 PKS, hgIE-KS	Cinnamycin	14%	Widdick et al. (2003)
Region 7	1006575-1060635	NRPS	Enduracidin	10%	Inoue et al. (2010)
Region 8	1694597-1705001	Ectoine	Ectoine	100%	Zaccai et al. (2016)
Region 9	2013395-2085904	Type 2 PKS, LAP	Spore pigment	83%	-
Region 10	2584611-2593666	Melanin	Melanin	60%	El Obeid et al. (2017)
Region 11	2692924-2703013	Siderophore	Desferrioxamin B/E	83%	Hoffman et al. (2013)
Region 12	3134085-3176400	Ladderane	-	-	-
Region 13	3178040-3227594	NRPS	Caniferolide A/B/C/D	4%	Alvarino et al. (2019)
Region 14	4120523-4131467	Butyrolactone	Scieric Acid	29%	-
Region 15	4881960-4962501	NRPS	Glycinocin A	16%	Corcilius et al. (2018)
Region 16	5214968-5235513	Terpene	Albaflavenone	100%	PubChem NCBI
Region 17	5851988-5862506	Siderophore	-	-	-
Region 18	5974148-6040769	Type 1 PKS	4-Z-Annimycin	77%	Kalan et al. (2013)
Region 19	6256914-6266782	RiPP-Like	-	-	-
Region 20	6285291-6303587	Terpene	Geosmin	100%	Neff (2018)
Region 21	6357767-6400888	NRPS-Like	Toxoflavin/Fervenulin	14%	Lee et al. (2016)
Region 22	6437681-6450991	Siderophore	-	-	-
Region 23	6475041-6486984	RiPP-Like	-	-	-
Region 24	6489293-6533506	Lanthipeptide-class-v and ii	Formicamycins A-M	11%	Qin et al. (2017)
Region 25	6733259-6759994	Terpene	Hopene	92%	PubChem NCBI
Region 26	6870824-6959482	Type 1 PKS	E-837	100%	PubChem NCBI
Region 27	6994914-7036098	Type 3 PKS	Daptomycin	6%	WHO (2018)

Table 3. Mapping simulation results of the Biosynthetic Gene Cluster (BGC) of the *Streptomyces pluripotens* sample (cont.)

Regions	Region location (Nucleotides)	Type	Most simillar known cluster	Similarity	Reference
Region 28	7229421-7239861	Melanin	Melanin	71%	El Obeid et al. (2017)
Region 29	7376037-7480384	NRPS, Type 1 PKS	Antimycin	100%	Seipke and Hutchings (2013)
Region 30	7482780-7511674	Thiopeptide, LAP	Platencin	9%	PubChem NCBI
Region 31	7516137-7536499	Nucleoside	Toyocamycin	30%	PubChem NCBI

Table 3 reveals the similarity level from region 1 to region 31, ranging from 0% to 100%. Based on the similarity level in the database, it showed a similarity level of 0%, which means the function of the gene sequence has not yet been known. This can be seen in Region 22 which was 0%, in contrast to regions 7, 16, 20, and 26 which showed 100% similarity, meaning that it can be utilized. Meanwhile, other regions had similarities with the pigment-producing gene clusters consisting of Isorenieratene at 54% (Region 3); *spore pigment* at 83% (Region 9); also Melanin at 60% and 71% (Region 10 and 28), Herboxidiene antitumor at 6% (Region 4), cosmetic active ingredients of Ectoine at 100% (Region 8), Fe and Al Desferrioxamin B/E binders at 83% of (Region 11), Caniferolide A-D antioxidant at 4% (Region 13), Annymycin 4-Z sporulation inhibitor at 77% (Region 18), Antimycin toxin at 100% (Region 29), earthy aroma Geosmin, and several other compounds those function has not yet known.

Based on the mapping simulation of Biosynthetic Gene Cluster (BGC) in the whole genome of the same species on *Micromonospora chersina sample* (PN.SB.11.3) (Table 4), 18 regions of the gene clusters that produce secondary metabolites were estimated to have products included in the types of PKS Type 3, NRPS, PKS Type 2, PKS Type 1, lanthipeptide-class i and iii, terpenes, betalactone, siderophore, RiPP-like, and PKS-like.

Table 4. Mapping simulation results of Biosynthetic Gene Cluster (BGC) on *Micromonospora chersina* samples

Regions	Region location (Nucleotides)	Type	Most simillar known cluster	Similarity	Reference
Region 1	36142-152907	Type 3 PKS, NRPS	Enduracidin	33%	Inoue et al. (2010)
Region 2	242721-315352	Type 2 PKS	Pradimicin-A	25%	PubChem NCBI
Region 3	489117-511699	Lanthipeptide-class-iii	SapB	100%	PubChem NCBI
Region 4	655663-675976	Terpene	-	-	-
Region 5	1101595-1122775	Lanthipeptide-class-i	-	-	-
Region 6	1216411-1244997	Betalactone	Cyphomicin	2%	Chevrette et al. (2019)
Region 7	1620792-1687557	NRPS, Type 1 PKS	Nostopeptolide A2	25%	PubChem NCBI
Region 8	2026564-2038336	Siderophore	Desferrioxamin B/E	100%	Hoffman et al. (2013)
Region 9	2176471-2235139	NRPS	Lysocin	9%	Hamamoto et al. (2015)
Region 10	2237017-2299646	NRPS, Type 1 PKS	Bleomycin	6%	Hindra et al. (2017)
Region 11	3364961-3379746	NAGGN	-	-	-
Region 12	3930661-3951079	Terpene	Phosphonoglycans	3%	Yu et al. (2014)
Region 13	4018620-4039932	Terpene	Isorenieratene	25%	Maresca et al. (2008)
Region 14	4468081-4513783	Type 1 PKS	Dynemicin A	55%	Tuttle et al. (2005)
Region 15	4669198-4710247	Type 3 PKS	Alkyl-O-dihidrogeranyl-methoxyhydroquinones	71%	PubChem NCBI
Region 16	6186452-6207402	Terpene	-	-	-
Region 17	6345774-6356598	RiPP-Like	Lymphostin/Neolymphostinol B/ Lymphostinol/Neolymphostin B	33%	Miyanaga et al. (2011)
Region 18	6508782-6549804	PKS-Like	-	-	-

Table 4 also shows the simulation of the level of similarity in the Biosynthetic Gene Cluster (BGC) on *Micromonospora chersina* samples. The results showed that Region 2 and Region 8 have 100% similarity. However, a 0% similarity level was also found, namely Region 4, Region 5, Region 11, Region 16, and Region 18. The higher the Mapping simulation results of Biosynthetic Gene Cluster (BGC) on *Micromonospora chersina* samples, the greater the usefulness value and vice versa.

There were several regions similar to the antibiotic-producing regions such as Enduracidin at 33% (Region 1), Cyphomycin at 2% (Region 6), and Lysocin at 9% (Region 9). In addition to regions that were similar to those producing antibiotics, it has also detected that several regions were similar to other active compounds producers such as antifungal Pradimicin A at 25% (Region 2) (PubChem NCBI), an important compound in the formation of aerial mycelium SapB at 100% (Region 3), Fe and Al Desferrioxamin E binders at 100% (Region 8), Bleomycin anticancer at 6% (Region 10), Polysaccharides Phosphonoglycans at 3% (Region 12), Isorenieratene pigment at 25% (Region 13), Dynemicin A antitumor at 55% (Region 14), *Lymphostin immunosuppressant* at 33% (Region 17), and several other compounds those function has not yet known.

BGC mapping simulation results are used to estimate the compounds that can be produced by actinomycetes isolates based on the sequence of nucleic bases in their genome. The three actinomycetes isolates were detected to have gene regions that are similar to the antibiotic-producing genes. Thus, based on the BGC mapping simulation, it can be seen that the active isolates of actinomycetes may potentially produce new candidates of antibiotic compounds. It is necessary to do further research on the types of compounds that have antibacterial activity produced by each of these actinomycetes isolates.

4. CONCLUSION

The number of culturable-actinomycetes isolates of mangrove sediment in the Semarang was 19 isolates that consist of 3 isolates grown from ISP 1 medium; 1 isolate grown from Zobell medium; 9 isolates grown from HVA medium; 6 isolates grown from ISP 1 + Humic Acid medium and in Karimunjawa was 17 isolates that consist 3 isolates grown from ISP 1 medium; 4 isolates grown from Zobell medium; 5 isolates grown from HVA medium; 2 isolates grown from ISP 1 + Humic Acid medium, and 3 isolates grown from Zobell + Humic Acid medium. All isolates were detected to have at least one type of Biosynthetic Gene Cluster, but only three isolates had antibacterial activity against *S. aureus*, *E. coli*, and *L. monocytogenes*, namely one isolate from Semarang and two isolates from Nyamuk Island, Karimunjawa. Results of molecular identification found the types of *Brachybacterium paraconglomeratum* (99.08%), *Streptomyces pluripotens* (100%), and *Micromonospora chersina* (99.92%). Biosynthetic Gene Cluster (BGC) mapping simulation results showed that these three species have similar genes with antibiotics producing genes that potentially could be new antibiotic candidates.

ACKNOWLEDGEMENTS

Part of this paper covers the work conducted for the author's Master degree at Diponegoro University, Semarang-Indonesia. The authors would like to express gratitude to Mrs. Desy Wulan Triningsih (Toyama Prefectural University, Japan) for her technical support.

REFERENCES

Alvarino R, Alonso E, Lacret R, Oves-Costales D, Genilloud O, Reyes F, et al. Caniferolide A, a macrolide from *Streptomyces caniferus*, attenuates neuroinflammation, oxidative stress, amyloid-beta, and tau pathology in vitro. Molecular Pharmaceutics 2019;16:1456-66.

Ariyanto D, Bengen DG, Prartono T, Wardiatno Y. Short communication: The relationship between content of particular metabolites of fallen mangrove leaves and the rate at which the leaves decompose over time. Biodiversitas 2018;19(3):780-5.

Ariyanto D. Food preference on *Telescopium telescopium* (Mollusca: Gastropoda) based on food sources in mangrove. Plant Archives 2019;19(1):913-6.

Ariyanto D, Bengen DG, Prartono T, Wardiatno Y. The physicochemical factors and litter dynamics (*Rhizophora mucronata* lam. and *Rhizophora stylos*a griff) of replanted Mangroves, Rembang, Central Java, Indonesia. Environment and Natural Resources Journal 2019;17(4):11-29.

Ariyanto D, Bengen DG, Prartono T, Wardiatno Y. Distribution and abundance of *Cerithideopsilla djadjariensis* (Martin 1899) (potamididae) on avicennia marina in Rembang, Central Java, Indonesia. Egyptian Journal of Aquatic Biology and Fisheries 2020;24(3):323-32.

Carbonell P, Currin A, Jervis AJ, Rattray NJW, Swainston N, Yan C, et al. Bioinformatics for the synthetic biology of natural products: Integrating across the Design-Build-Test cycle. Natural Product Reports 2016;33(8):925-32.

Chevrette MG, Carlson CM, Ortega HE, Thomas C, Ananiev GE, Barns KJ, et al. The antimicrobial potential of Streptomyces from insect microbiomes. Nature Communications 2019; 10(516):1-11.

Corcilius L, Liu DY, Ochoa JL, Linington RG, Payne RJ. Synthesis and evaluation of analogues of the glycinocin family of calcium-dependent antibiotics. Organic and Biomolecular Chemistry 2018;16(29):5310-20.

Davies-Bolorunduro OF, Adeleye IA, Akinleye MO, Wang PG. Anticancer potential of metabolic compounds from marine actinomycetes isolated from Lagos Lagoon sediment. Journal of Pharmaceutical Analysis 2019;9:201-8.

Dhanasekaran D, Thajuddin N, Panneerselvam A. Distribution and ecobiology of antagonistic Streptomyces from agriculture and coastal soil in Tamil Nadu, India. Journal of Culture Collections 2009;6:10-20.

El Samak M, Solyman SM, Hanora A. Antimicrobial activity of bacteria isolated from Red Sea marine invertebrates. Biotechnology Reports 2018;19:e00275.

El Obeid AS, Kamal-Eldin A, Abdelhalim MAK, Haseeb AM. Pharmacological properties of melanin and its function in health. Basic and Clinical Pharmacology and Toxicology 2017;120(6):515-22.

Hamamoto H, Urai M, Ishii K, Yasukawa J, Paudel A, Murai M, et al. Lysocine is a new antibiotic that targets menaquinone in the bacterial membrane. Nature Chemical Biology 2015; 11:127-33.

Hasegawa M, Miura T, Kuzuya K, Inoue A, Ki SW, Horinouchi S, et al. Identification of SAP155 as the target of GEX1A (Herboxidiene), an antitumor natural product. ACS Chemical Biology 2011;6:229-33.

Hayakawa M, Nonomura H. Humic acid-vitamin agar, a new medium for the selective isolation of soil actinomycetes. Journal of Fermentation Technology 1987;65(5):501-9.

Hindra, Yang D, Teng Q, Dong L, Huang T, Ge H, et al. Genome mining of *Streptomyces mobaraensis* dsm40847 as a bleomycin producer providing a biotechnology platform to engineer designer bleomycin analogues. Organic Letters 2017;19(6):1386-9.

Hirsch AM, Valdés M. Micromonospora: An important microbe for biomedicine and potentially for biocontrol and biofuels. Soil Biology and Biochemistry 2010;42:536-42.

Hoffman R, Benz E, Silberstein L, Heslop H, Weitz J, Anastasi J. Hematology: Diagnosis and Treatment. 6th ed. Churchill Livingstone; 2013. p. 311.

Inoue K, Hattori Y, Hino T, Oka H. An approach to on-line electrospray mass spectrometric detection of polypeptide antibiotics of enramycin for high-speed counter-current chromatographic separation. Journal of Pharmaceutical and Biomedical Analysis 2010;51:1154-60.

Kalan L, Gessner A, Thaker MN, Waglechner N, Zhu X, Szawiola A, et al. A cryptic polyene biosynthetic gene cluster in *Streptomyces calvus* is expressed upon complementation with a functional bldA gene. Chemistry and Biology 2013; 20:1214-24.

Kalkreuter E, Pan G, Cepeda AJ, Shen B. Targeting bacterial genomes for natural product discovery. Trends in Pharmacological Sciences 2019;41(1):13-26.

Karimunjawa National Park. Final Report Karimunjawa: A Community-Based Islandscape Initiative. Kota Kita, Pulau kita, Indonesia: 2019. p. 1-71.

Katz L, Baltz RH. Natural product discovery: Past, present, and future. Journal of Industrial Microbiology and Biotechnology 2016;43(2-3):155-76.

Lee J, Park J, Kim S, Park I, Seo Y. Differential regulation of toxoflavin production and its role in the enhanced virulence of *Burkholderia gladioli*. Molecular Plant Pathology 2016; 17(1):165-76.

Lee L, Zainal N, Azman A, Eng S, Mutalib NA, Yin W, et al. *Streptomyces pluripotens* sp . nov ., a bacteriocin-producing streptomycete that inhibits meticillin-resistant *Staphylococcus aureus*. International Journal of Systematic and Evolutionary Microbiology 2014;64:3297-306.

Maoka T. Carotenoids as natural functional pigments. Journal of Natural Medicines 2019;74:1-16.

Maresca JA, Romberger SP, Bryant DA. Isorenieratene biosynthesis in green sulfur bacteria requires the cooperative actions of two carotenoid cyclases. Journal of Bacteriology 2008;190(19):6384-91.

Messaoudi O, Wink J, Bendahou M. Diversity of actinobacteria isolated from date palms rhizosphere and saline environments: Isolation, identification, and biological activity evaluation. Microorganisms 2020;8(1853):1-19.

Miyanaga A, Janso E, Mcdonald L, He M, Liu H, Barbieri L, et al. Discovery and assembly-line biosynthesis of the lymphostin *Salinispora* bacteria. Journal of the American Chemical Society 2011;133:13311-3.

Neff EP. Stop and smell the geosmin. Lab Animal Nature 2018;47:267-72.

Nicolaou KC, Tang Y, Wang J. Total synthesis of Sporolide B. Angewandte Chemie International Edition 2009;48(19): 3449-53.

Ningsih SS, Ariyanto D, Puspitasari D, Jayanegara A, Hamim Hamim H, Gunawan H. The amino acid contents in mangrove *Rhizophora mucronata* leaves in Asahan, North Sumatra, Indonesia. E3S Web of Conferences 2020;151(01047):1-3

Qin Z, Munnoch JT, Devine R, Holmes NA, Seipke RF, Wilkinson KA , et al. Formicamycins, antibacterial polyketides produced by Streptomyces formicae isolated from African Tetraponera plant-ants. Chemical Science 2017;8(4):3218-27.

Radjasa OK, Martens T, Grossart HP, Sabdono A, Simon M, Bachtiar T. Antibacterial property of a coral-associated bacterium pseudoalteromonas luteoviolacea against shrimp pathogenic *Vibrio harveyi* (In Vitro Study). HAYATI Journal of Biosciences 2005;12(2):77-81.

Rashad FM, Fathy HM, El-Zayat AS, Elghonaimy AM. Isolation and characterization of multifunctional Streptomyces species with antimicrobial, nematicidal, and phytohormone activities from marine environments in Egypt. Microbiological Research 2015;175:34-7.

Romano S, Jackson SA, Patry S, Dobson ADW. Extending the one strain many compounds (OSMAC) principle to marine microorganisms. Marine Drugs 2018;16(7):1-29.

Seipke RF, Hutchings MI. The regulation and biosynthesis of antimycins. Beilstein Journal of Organic Chemistry 2013;9:2556-63.

Sekurova ON, Schneider O, Zotchev SB. Novel bioactive natural products from bacteria via bioprospecting, genome mining and metabolic engineering. Microbial Biotechnology 2019; 12(5):828-44.

Sharma P, Thakur D. Antimicrobial biosynthetic potential and diversity of culturable soil actinobacteria from forest ecosystems of Northeast India. Scientific Reports 2020; 10(1):1-18.

Siregar V, Koropitan AF. Land use change and its impact to marine primary production in Semarang Waters. Procedia Environmental Sciences 2016;33:520-31.

Takeuchi M, Fang CX, Yokota A. Taxonomic Study of the Genus Brachybacterium : Proposal of *Brachybacterium conglomeratum* sp. nov., nom. rev., B*rachybacteriurn paraconglorneratum* sp. nov., and *Brachybacterium rhamnosum* sp. nov. International Journal of Systematic Bacteriology 1995;45(1):160-8.

Thatoi H, Behera BC, Mishra RR, Dutta SK. Biodiversity and biotechnological potential of microorganisms from mangrove ecosystems: A review. Annals of Microbiology 2012;63(1): 1-19.

Tuttle T, Kraka E, Cremer D. Docking , triggering , and biological activity of dynemicin a in DNA: A computational study. Journal of American Chemical Society 2005;127:9469-84.

World Health Organization (WHO). Critically Important Antimicrobials for Human Medicine. Switzerland: WHO publications; 2018. p. 1-45.

Widdick DA, Dodd HM, Barraille P, White J, Stein TH, Chater KF, et al. Cloning and engineering of the cinnamycin biosynthetic gene cluster from Streptomyces cinnamoneus cinnamoneus DSM 40005. Procedings of the National Academy of Sciences of the United States of America 2003;100(7):4316-21.

Yu X, Price NPJ, Evans BS, Metcalfa WW. Purification and characterization of phosphonoglycans from. Journal of Bacteriology 2014;196(9):1768-79.

Zaccai G, Bagyan I, Combet J, Cuello GJ, Demé B, Fichou Y, et al. Neutrons describe ectoine effects on water H-bonding and hydration around a soluble protein and a cell membrane. Scientific Reports 2016;6:1-12.

How does the Green Industry Policy Impact a Developing Country? A Case Study of the Electronic Products and Electrical Equipment Manufacturing Sector in Thailand

Phurita Noranarttakun[1] and Chanathip Pharino[2*]

[1]*Interdisciplinary Program in Environmental Science, Graduate School, Chulalongkorn University, Bangkok 10330, Thailand*
[2]*Department of Environmental Engineering, Faculty of Engineering, Chulalongkorn University, Bangkok 10330, Thailand*

ARTICLE INFO

Received: 2 Mar 2021
Received in revised: 15 Jun 2021
Accepted: 15 Jun 2021
Published online: 26 Jul 2021
DOI: 10.32526/ennrj/19/2021028

Keywords:
Green Industry (GI)/ Small and medium enterprises/ Electronic products/ Sustainable production/ Environmental practice/ Thailand

*** Corresponding author:**
E-mail: chanathip.p@chula.ac.th

ABSTRACT

Implementation of Green Industry (GI) strategy has long been recommended for industrial sectors to achieve sustainable production. Among various approaches, GI certification as a voluntary scheme has been implemented widely to promote the adoption of environmental-friendly practices for Thai industrial entrepreneurs. This research examined the progress and lessons learnt from existing schemes and identified the challenges of GI implementation and future improvement. The study particularly focused on small and medium-sized enterprises (SMEs) in the electronic products and electrical equipment manufacturing sector. A questionnaire-based survey was used to collect data, and the Mann-Whitney U Test was used to verify significant barriers and drivers among the samples. The results indicated that major common practices of SMEs are widely approved for fulfilling GI criteria, i.e., waste segregation and minimization, and energy saving, so as to comply with environmental law. While other environmental practices, such as greenhouse gas accounting, green labelling, and green supply chain management were limited in adoption. SMEs, both certified with GI and non-certified with GI, expressed the same opinion that all factors including financial, legal, social, personnel, technological and policies were barriers to GI adoption but significantly different from the economic factor. SMEs in both groups revealed the same opinion that incentive, expertise and technology were drivers of GI adoption but differ significantly from the financial support. Incentive-based instruments such as subsidies and voluntary schemes for green product certification are proposed as appropriate measures to encourage SMEs to adopt GI.

1. INTRODUCTION

The industry sectors are relevant to all Strategic Development Goals (SDG), specifically SDG 12 which strives to ensure sustainable consumption and production patterns. The industrial sector is the fundamental source of production which not only consumes resources to produce output, but also has a negative impact on the environment. However, industry does not require an ever-growing use of natural resources and can minimize the pollution by adopting green industry (UNIDO, 2018; Pedersen, 2018; Jones et al., 2018). The green industry concept is an important mechanism that will drive sustainable industrialisation, as the objective of green industry is sustainable production by considering the social and environmental aspects of business operations through the more efficient use of energy and raw materials, innovative practices, and applications of new green technologies (UNIDO, 2011; UNIDO, 2018). In the past decade, green initiatives, such as environmental management systems, eco-labelling, greening the supply chain, and corporate social responsibility (CSR) have been continuously promoted, which can contribute to the implementation of green industry (UNIDO, 2011; Lee, 2009; Potros and Enquist, 2007; Luan et al., 2016; Schoenherr and Talluri, 2013; Roy et al., 2013; Frey et al., 2013).

Citation: Noranarttakun P, Pharino C. How does the green industry policy impact a developing country? A case study of the electronic products and electrical equipment manufacturing sector in Thailand. Environ. Nat. Resour. J. 2021;19(5):402-412. (https://doi.org/10.32526/ennrj/19/2021028)

Many European countries applied green industry strategy to rebalance their economy after the economic crisis in late 2005, and presently, advanced green strategy and circular economy have been adopted (Zamfir et al., 2017; Katz-Gerro and López Sintas, 2019). South Korea, Japan and China are exemplary Asian countries that have adopted green industry strategy into their national policy framework. South Korea transformed the traditional industries to green industries under the green growth policy framework in 2009 (Mathews, 2012; OECD, 2017). Environment and green innovation were identified as the key drivers for Japan's future growth (OECD, 2010). China has focused on resource efficiency and recirculation, green technology, and renewable energy in its 12th five-year plan (Peng and Sun, 2015). Environmental performance was under the influence of internal and external context. Internal context in terms of firms' capabilities, such as turnover (Zamfir et al., 2017), and cost saving (Triguero et al., 2013), has correlation with green process adoption. Ghazilla et al. (2015) revealed that innovation, technology, environmental knowledge, and finances are key drivers and also barriers for SMEs to adopt green manufacture practices. High cost, lack of awareness, lack of resources, and outdated machines are the barriers to sustainable production (Ghadge et al., 2017), whereas external factors from stakeholder involvement in government policy, regulation, and market need correlates with sustainable production (Ghadge et al., 2017). Not only customer and social requirements affected the decision-making of European SMEs to adopt eco-innovation (Kesidou and Demirel, 2012), but law also affected the adoption of eco-product or eco-organization (Triguero et al., 2013). Regulations, incentives, subsidies, market needs, and stakeholder involvement are the drivers of green manufacture practices (Ghazilla et al., 2015).

The Thai green industry strategy has been implemented over a decade in parallel with the international context (Figure 1). It was initially promoted in the industrial sector under the Green Industry project of the Ministry of Industry. The project is a certification awarded to entrepreneurs who operate businesses while complying with five levels of green development criteria (Table 1) (Ministry of Industry, 2017). The certification is a national voluntary scheme consisting of the process of application, audit, decision, and surveillance. The GI certificate is issued to the entrepreneurs with a three-year certification period. The total number of GI certified entrepreneurs from 2011 to 2018 was 31,290 (Ministry of Industry, 2018), which was approximately 23% of 138,038 registered factories (Ministry of Industry, 2016). The government has aimed to award the GI certificate to 2,000 entrepreneurs in 2021, which might increase up to 70,000 entrepreneurs in 2025 (Department of Industry Works, 2021).

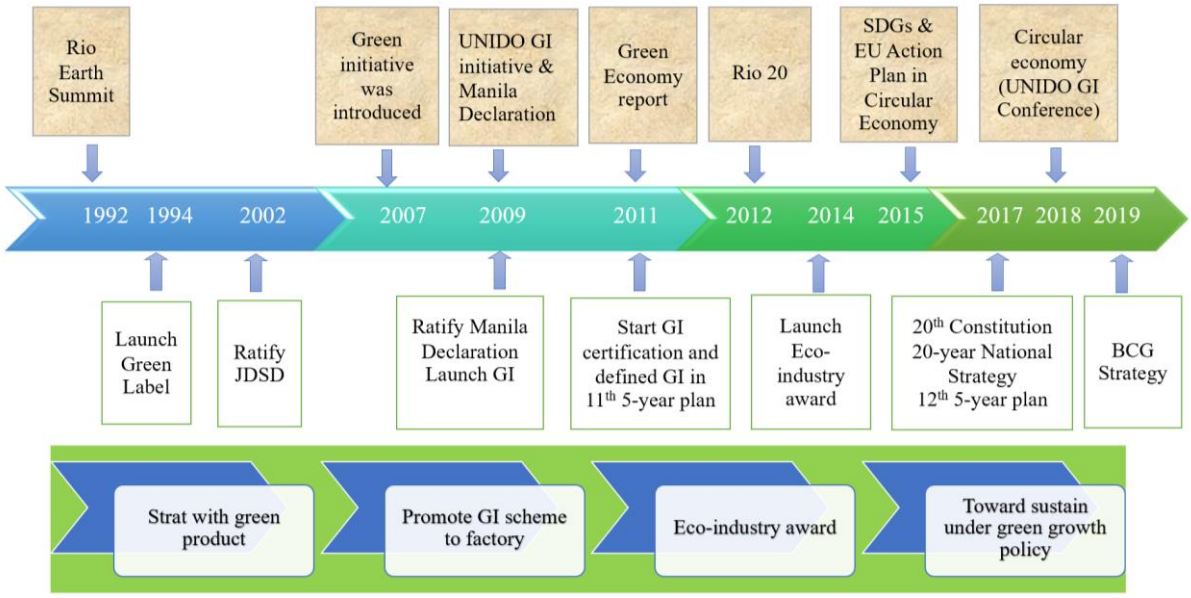

Figure 1. Green industry development in Thailand parallel with the international context (Remark: JDSD=Johannesburg declaration on sustainable development; BCG=Biology circular and green strategy)

Table 1. Five levels of Thai green industry criteria (Ministry of Industry, 2017)

Thai green industry	Criteria
Level 1: Green commitment	1. Organization must define environmental policy with the commitment related to environmental impact reduction or pollution prevention or sustainable resource use or climate change mitigation and adaptation or protection and restoration of natural environment. 2. Organization must communicate the environmental policy to all persons for acknowledgement.
Level 2: Green activity	1. Organization must define and communicate the environmental policy as defined in level 1. 2. Organization must prepare and implement environmental plan to comply with defined environmental policy, the environmental plan must consist of objective, target, procedure, responsible persons and completed time frames.
Level 3: Green system	Organization must establish, implement, maintain, continuous improvement the environmental management system which equal to ISO 14001.
Level 4: Green culture	1. Organization must have environmental management system as mentioned in level 3. 2. Organization must create organization culture in environment and implement it effectively by covering the criteria of standard of corporate social responsibility as ISO 26000. 3. Organization must prepare the environmental implementing report and communicate to the public.
Level 5: Green network	1. Organization must implement environmental management system and create organization culture with respect to green industry criteria of level 4 in all aspect. 2. Organization must implement promotion, creation, and interrelation of environmental activity with stakeholder throughout supply chain, community, and consumer by promote green industry implement to supply chain, encourage awareness and understanding in sustainable consumption to community and consumer. 3. Organization must prepare and distribute the report of promotion, creation and interrelation of environmental activity with stakeholders.

The level of GI achievement under the GI certification scheme could be reflected by the many number of certifications. However, factors supporting and hindering the success of the GI implementation in various industrial sectors have not yet been assessed, including the characteristics of the GI certified organization and its environmental policy and activities. In-depth analysis on this aspect should be carried out to clearly understand how to execute effective GI implementation policy. This information is a crucial input to develop the strategy to achieve sustainable production for industrial sectors. This paper investigates the status and outlook of GI development in Thailand focusing on SMEs in the electronic products and electrical equipment manufacturing sector. The main research questions were:

(1) What is the performance of SMEs in different GI levels?

(2) What are the barriers and drivers which impact SMEs capability to implement and improve according to GI criteria?

2. METHODOLOGY

SMEs have a vital role to play in the economy, employment, environmental protection and resource flows, as, globally, SMEs represent 90% of businesses and more than 50% of employment (World Bank, 2020). As of December 2020, Thai SMEs contribute to 9.05% of the total GDP (Office of Small and Medium Enterprises Promotion, 2020). Subsequently, Thai SMEs were the focus of this investigation to identify the lessons learned from GI implementation via the GI certified scheme. The electronic products and electrical equipment manufacturing sector (EE) was selected as a case study since this sector is one of the most promoted industrial sectors according to the National Industrial Development Plan 2012-2031. Moreover, it is also one of the top-rank exporters of Thailand. In February 2021, EE sector was known to have an export value of 317,877.2 million Baht and an import value of 134,265.3 million Baht (Ministry of Commerce, 2021). These export and import values accounts for 2.02% and 0.86% of the total GDP, respectively. There are more SMEs in EE sector, so they contribute significantly across the supply chain of this sector.

2.1 Questionnaire design

The questionnaire was developed based on the three pillars of sustainable concept and literature review relevant to green industry. The questions were designed in the context of social, economic and environmental factors (Annex A). The questionnaire for this study was divided into four main sections. The first section consisted of questions used to elicit demographic information concerning the SMEs, such as product category, employees, capital, and operation period. The second section consisted of statements

used to measure the GI performance such as certification status, environmental policies and activities. The third section consisted of questions used to measure the barrier of green industry implementation. The last sector included the items used to measure the factors that encourage the decision making to shift to GI. The questionnaire in the first and the second section was close-ended, while the questionnaire in the third and the last section was seven-point scale and five-point scale.

To confirm the validity of questions to acquire desirable data, the questionnaire was verified by a panel of experts comprised of seven professional representatives from academic, government and industrial backgrounds. The experts had more than five years of experience in green industry and environmental management system (EMS). The experts came from the Department of Industrial Works, the Office of Thai Industrial Standard Institute, the Office of National Standardization Council, the Office of the Permanent Secretary of the Ministry of Industry, The Federation of Thai Industries, EE SMEs and academia. The questionnaire was also tested in the preliminary piloting stage of the study, and its reliability was analyzed by Cronbach's Alpha analysis (Tavakol and Dennick, 2011; Yusup et al., 2015). The result is shown in the Table 2.

Table 2. Cronbach's Alpha of the validity of the questionnaire

Questionnaire	Number of items	Cronbach's Alpha	Remark
How important is each of factors for GI implementation in your organization?	7	0.894	Acceptable
What is the degree of these factors that encourages your organization to implement GI?	4	0.941	Acceptable

2.2 Sample

A list of prospective informants was obtained from the directory of registered SMEs database from the Office of Small and Medium Enterprises Promotion (OSMEP). SMEs in this study mean an enterprise with less than 200 employees according to the ministerial regulations of number of employments, and the fix asset value of small and medium enterprise, B.C. 2545 (Office of Small and Medium Enterprises Promotion, 2002). According to the OSMEP directory, 3,688 SMEs were registered in EE sector at the end of 2016 (Office of Small and Medium Enterprises Promotion, 2016). Yamane formula (Yamane, 1967) was then used to calculate the required sample size in this study:

$$n = \frac{N}{1+N(e)2}$$

Where; n is the sample size, N is the population size, and e is the level of precision. When this formula was applied to the 3,688 EE SMEs population, a sample size of 97 with an acceptable error of 10% was determined. From November 2017 to April 2018, a total of 1,300 questionnaires were mailed together with a cover letter to the EE SMEs. Responses of 179 valid questionnaires were obtained from sampling SMEs established in all regions of Thailand, a response rate of around 14%.

2.3 Statistical analysis method

The IBM SPSS software version 22 was applied for statistical analysis. The Mann-Whitney U test (Mann and Whitney, 1947) was used to verify the difference in key barriers and drivers between the two sampling groups, where one group of SMEs received a GI certificate, while the other group of SMEs did not receive a GI certificate (Yusup et al., 2015). This test is one of the most commonly used non-parametric statistical tests (Nachar, 2008). The assumptions of the test are:

(1) The two investigated groups must be randomly drawn from the target population.

(2) There is independence within groups and mutual independence between groups.

(3) The observations values are then of ordinal, relative or absolute scale type.

The Mann-Whitney U test initially implies the calculation of a U statistic for each group. The mathematical equations (Mann and Whitney, 1947) are defined by the following:

$$u_x = n_x n_y + ((n_x(n_x + 1))/2)) - R_x$$

$$u_y = n_x n_y + ((n_y(n_y + 1))/2)) - R_y$$

Where; n_x is the number of observations in the first group, n_y is the number of observations in the second group, R_x is the sum of the ranks assigned to

the first group and R_y is the sum of the ranks assigned to the second group.

Computing the Mann-Whithney U test using SPSS, the test results show the values of the ranks, the mean rank, the sum of ranks and the number of observations in the first table. In addition, SPSS automatically provides the tests results in the second table, i.e., the Mann-Whitney U, the Wilcoxon W and the Z results.

3. RESULTS AND DISCUSSION

3.1 The respondents' demographic profile

Most of the respondents in the survey were employed in management department, with 18% in the top management and 58% in environment and safety, quality control and production section (Figure 2). The remaining 24% were managers and staff from support departments, such as administration, human resources, and purchasing. Therefore, the data obtained from the questionnaire was reliable because more than 50% of respondents were the decision makers and part of the management personnel, who were well familiar with the organization's environmental performance.

Eighty five percent of the firms which responded to the questionnaire had been operating for more than ten years. The remaining 15% of firms had been operating for less than ten years. Fifty two percent of the firms that responded to the questionnaire had a capital less than 50 million Baht, while the rest had a capital of 51-200 million Baht (Figure 3).

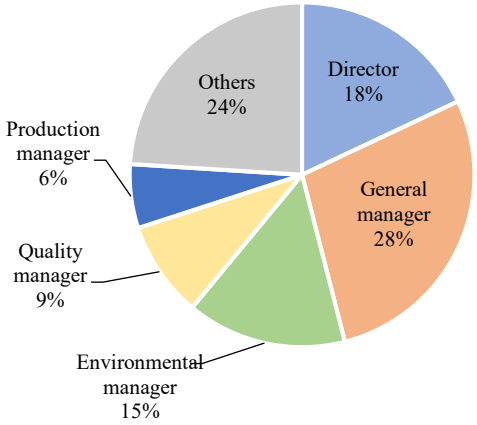

Figure 2. Profile of the respondents' position

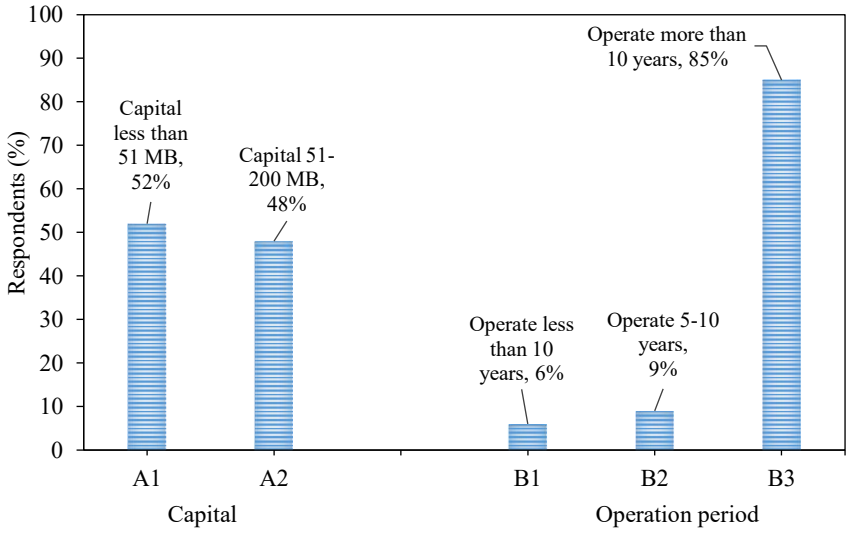

Figure 3. Profile of the capital and firm age of the respondents

3.2 GI Performance

GI performance is reflected by environmental policies and environmental practices adopted by SMEs. If environmental policies and practices contributed with international commitment and/or international standards, including required knowledge for implementation, it showed the performance rate of GI adoption by SMEs. Moreover, the level of GI certification can verify the GI performance.

3.2.1 GI certification

The survey results showed that majority of the SMEs in EE sector (68%) did not receive the GI certification, while 32% received the GI certification. The levels of these certifications were level 1: Green Commitment, level 2: Green Activity, level 3: Green System and level 4: Green Culture, as shown in Figure 4. The number of certified entrepreneurs was level 1 (12.50%), level 2 (15.62%), level 3 (65.63%) and level 4 (6.25%),

while none of the respondents received certification with GI level 5. It might be speculated that some importers of electronic products and electrical equipment have green procurement policy, then SMEs that had GI level 3 certification may have been impacted from their customers. Moreover, the GI level 3 certified by the Ministry of Industry is free of charge when compared to ISO 14001, which is certified by the certification body (CB). Thus, SMEs in the EE sector should rather adopt GI level 3 than ISO 14001 in order to manage environmental problems. This finding is different from SMEs in foreign countries that adopted a variety of advanced international standard, such as life cycle assessment (LCA), carbon footprint, eco-labelling, circular economy for environmentally friendly manner and sustainability (Jove- Llopis and Segarra- Blasco, 2018; Zamfir et al., 2017; Lefebvre et al., 2001; Jung, 2015; Wang and Chui, 2014).

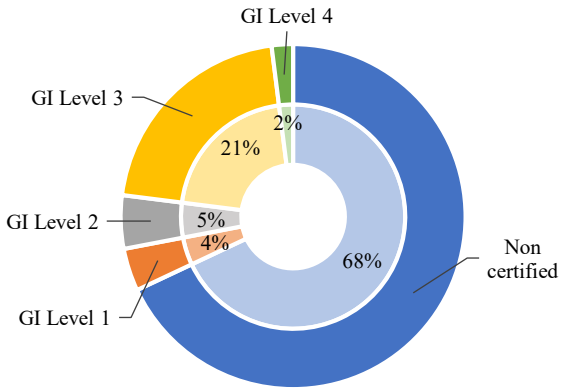

Figure 4. Profile of the green industry certification of the respondents

3.2.2 Environmental practices adoption

The environmental policy and practices for greening SMEs are presented in Figures 5 and 6. More than half of the respondents (52.5%) set environmental policies on the topic of environmental impact reduction or pollution prevention. Environmental policies on sustainable use of resources were set by 24.02% of the respondents. Furthermore, 9.5% and 8.9% of respondents set environmental policies on mitigation of climate change and the protection and restoration of natural resources, respectively, which was a very small number compared to the total sample size (Figure 5). It indicated that EE SMEs establish policy and target in order to comply with Thai environmental regulation, whose goal is to control the emissions at the end of pipe.

Figure 6 presented the data of environmental practices adopted by EE SMEs. The majority of SMEs implemented activities of energy saving (117), waste segregation (112), and minimization (110), while the environmental practices as green label certification, green supply chain management, and greenhouse gas quantification, were minority adoptions with 23, 23, and 22, respectively. It indicated that the majority of the environmental activities, such as energy saving, waste separation, and minimization are deployed with the policy of environmental impact reduction or pollution prevention, which is defined by a major part of SMEs. Whereas environmental practices, such as greenhouse gas quantification, eco labelling, green supply chain management, and product lifecycle assessment still

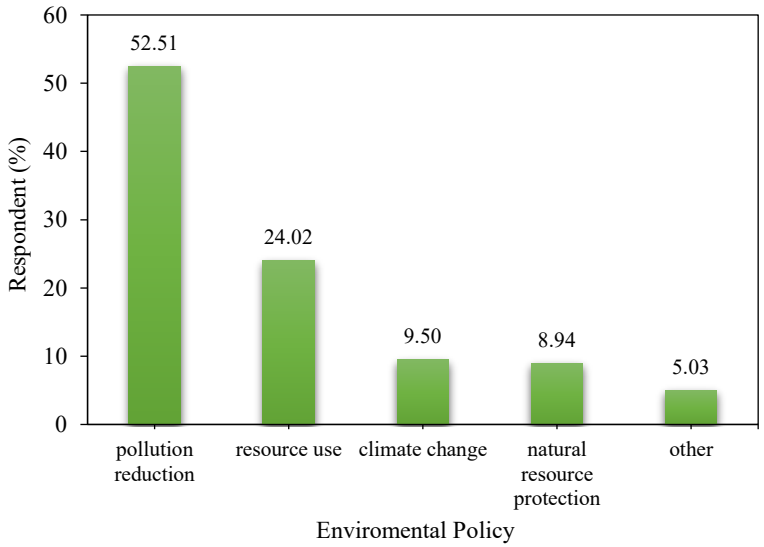

Figure 5. Issues of environmental policies on which SMEs focus

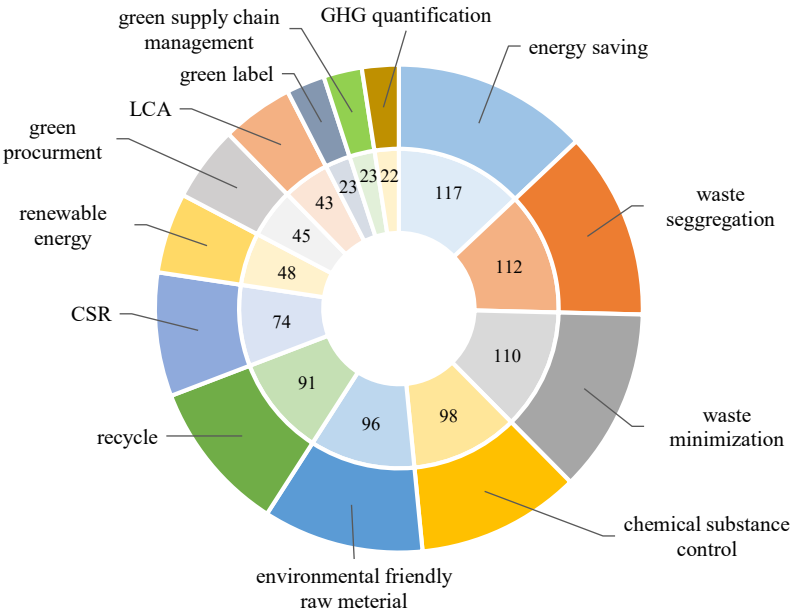

Figure 6. Environmental practices adopted by SMEs

only have minor application in SMEs. It seems that advanced GI development and implementation in SMEs has not been achieved yet. Even though Thailand announced Biology, Circular and Green strategy for a new business model to enhance circular economy and green industry in 2019, SMEs are still implementing environmental activities to comply with environmental regulations. It is in contradiction with other countries which have implemented a variety of advanced environmental practices for more than ten years. A comparative analysis in developed and developing economies indicated that the countries in Europe hold international leadership in sustainable consumption and production practices (Wang et al., 2019). SMEs in Belgium, Spain, France, Ireland, the Netherlands, Austria, Sweden, and Romania used renewable energy, redesigned product, and service to increase their environmental performances. SMEs in Italy and Poland minimized waste by recycling or circulating it (Zamfir et al., 2017). Spanish industrial SMEs have carried eco-innovation to reduce the environmental impact of unsustainable consumption and production (Kiefer et al., 2019) and implement circular economy as biodegradable material, environmentally efficient process, sustainable energy, eco innovation design product, industrial symbiosis, and environmental certifications (Prieto-Sandoval et al., 2018). In Asian countries, China transformed the traditional industry to green industry by adopting resource efficiency and recirculation, green technology and renewable energy (Chen et al., 2017). The new industry established in South Korea is the green industry which applies the climate technology, such as rechargeable battery, carbon capture and storage (CCS), smart-grid and sewage technology (Jung, 2015). Taiwan semiconductor manufacturers were promoted to adopt carbon footprint quantification, environmental management system and green labelling to transform to green supply chain (Wang and Chui, 2014). Malaysian government introduced green practice to construction entrepreneurs and SMEs. Malaysian green practice is similar to Thai GI criteria such as ISO/EMS, green technology, green procurement, green labelling, waste management (Bohari et al., 2015) recycling waste, complying with regulations and CSR (Ghazilla et al., 2015). SMEs in many other countries, especially across Europe, have applied environmental practices beyond their environmental pollution control. However, SMEs in Thailand have not made a big jump in applying environmental management tools to conduct business in an environmentally friendly manner.

3.3 Challenges of GI adoption in SMEs

Figure 7 showed the obstacles of GI adoption. SMEs were asked to score a number of different barriers on a scale of 1 (most important) to 7 (least important) to understand scale of impact. The result showed the rank scores of seven factors that could hinder SMEs to transition to green industry. Sixty SMEs agreed that financial (GI enhance cost reduction and competitivness) was the first priority issue. Moreover, 40 and 47 SMEs agreed that the second and third major obstacles were economic (Government

provide incentive to SMEs) and personnel (SMEs have competency personnel in environmental), respectively. The fourth major barrier was social (Interested parties require SMEs implement GI), which 33 SMEs agreed with. Whereas 63 SMEs agreed that the least important obstacle was the policy (SMEs completely establish environmentally friendly policy).

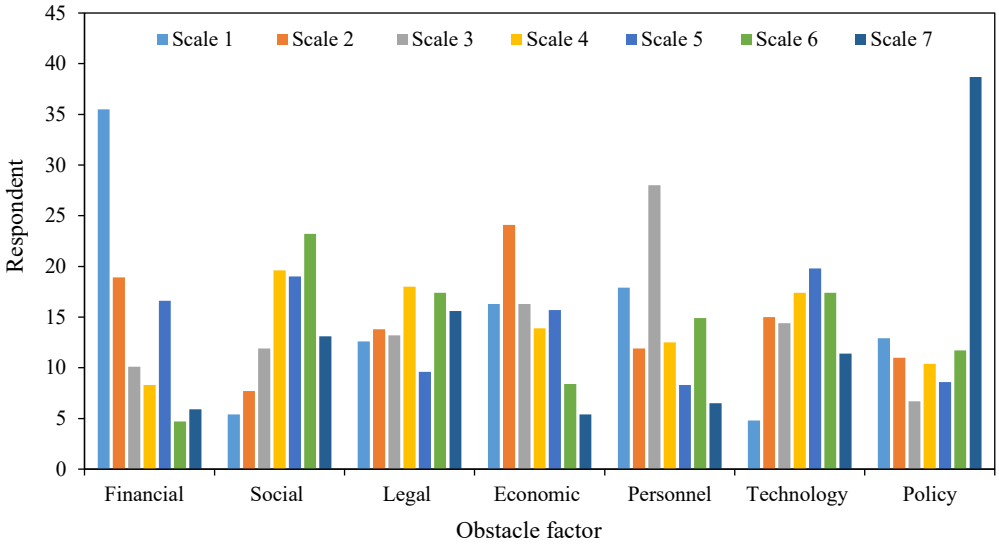

Figure 7. Important of perceived barriers to GI according to EE SMEs, on seven-point scale

The results of descriptive statistical analysis showed that SMEs with less capital than 50 million Baht received the GI certification less than SMEs with capital more than 50 million Baht. Approximately, one-third of SMEs that have the capital of less than 50 million Baht are certified GI, with GI 1 more common than other levels. While half of SMEs that have the capital higher than 50 million Baht are certified GI with GI 3 more common than other levels. Moreover, the majority (one-third) of SMEs having the capital of less than 50 million Baht expressed their opinion on the most important influence of finances to GI adoption, followed by personnel and technology (SMEs have capability of green technology).

It suggests that financial factor was the strongest challenges to SMEs adopting GI, which is a concept similar to the one found by Zamfir et al. (2017), Ormazabal et al. (2018), Stucki (2019), Caldera et al. (2019), and Woodard (2021). Moreover, this finding is consistent with the reports of UNIDO (2011), and the Office of Small and Medium Enterprises Promotion (2015), which stated that the economic problems such as financial and personnel force SMEs to focus more on business interests than environmentally friendly practices. The limit of human resources and budget could impact SMEs developing GI at a low level by setting and implementing environmental policies than creating green culture and green supply chains.

The Mann-Whitney U test was used to show the difference in the medians of the perception on the obstacles and drivers to GI adoption between two respective SMEs. The results are shown in Table 3 and Table 4.

Table 3 presented the results of the investigation of factors that impeded SMEs in being a GI. The ordinal data from the questionnaire (section 3) was analyzed by Mann-Whitney U test. The result showed that SMEs, both certified with GI and non-certified with GI, expressed the same opinion that all factors including financial, legal, economic, social, personnel, technological and policies were barriers to GI adoption. This finding is similar to Caldera et al. (2019), who revealed that the success of sustainable business practice was affected by SMEs' financial capability, expertise, regulation, and policy.

The economic factor was the obstacle that both groups of SMEs expressed their opinions significantly different. The mean sum of rank of economic factors in non-certified SMEs was more than certified SMEs. This implies that economic factor challenges non-certified SMEs in GI adoption more than certified SMEs. It may be caused by SMEs receiving GI certification to get more benefits and incentives from

the government. This finding is similar to Shrivastava and Tamvada (2019), who indicated that green products/services have a positive impact on firm performance. Therefore, it is highly recommended that the benefits of being GI should be recognized by SMEs' decision makers.

Table 3. The Mann-Whitney U test of the obstacles of greening SMEs

Obstacle	Mann-Whitney U (p-value) at level of significance (α=0.05)		Mean sum of rank order
	SMEs certified with GI	Non-certified	
Financial	Certified	0.495	Non-certified > Certified
	Non-certified	-	-
Social	Certified	0.3975	Non-certified > Certified
	Non-certified	-	-
Regulation	Certified	0.288	Non-certified > Certified
	Non-certified	-	-
Economic	Certified	0.0015*	Non-certified > Certified
	Non-certified	-	-
Personnel	Certified	0.437	Non-certified > Certified
	Non-certified	-	-
Technology	Certified	0.122	Non-certified > Certified
	Non-certified	-	-
Technology	Certified	0.248	Non-certified > Certified
	Non-certified	-	-

Remark: The definition of the obstacle - Financial, Social, Regulation, Economic, Personnel, Technology, Technology - referred to the questionnaire in the third section.

Table 4. The Mann-Whitney U test of the drivers to greening SMEs

Driver	Mann-Whitney U (p-value) at level of significance (α=0.05)		Mean sum of rank order
	SMEs certified with GI	Non-certified	
Financial	Certified	0.018*	Non-certified > Certified
	Non-certified	-	-
Incentive	Certified	0.0725	Non-certified > Certified
	Non-certified	-	-
Expertise	Certified	0.182	Non-certified > Certified
	Non-certified	-	-
Technology	Certified	0.161	Non-certified > Certified
	Non-certified	-	-

Remark: the definition of the driver - Financial, Incentive, Expertise, Technology - referred to the questionnaire in the fourth section.

Table 4 shows the result of Mann-Whitney U test on the drivers of GI (questionnaire section 4) comparing GI certified SMEs and non-certified SMEs. SMEs in both groups revealed the same opinion on the mechanism as incentivized, expert and technological. However, they expressed a different opinion with the finances ($p<0.05$) in which the mean sum of rank of non-certified SMEs was higher than certified SMEs. This implies that both groups of SMEs required finances, incentives, expertise and technology to improve their environmental practice toward advanced GI. This finding is similar to Kiefer et al. (2019), who indicated that internal financing resources and technology-push represent drivers to eco-innovation. Moreover, Shrivastava and Tamvada (2019) suggested that external financial support and green products/services adoption have significantly positive effects. Subsequently, subsidy mechanisms such as grants, funds, low-interest loans, moratoriums, tax exemptions, and fee exemptions should be provided to SMEs to enhance advanced GI adoption.

4. CONCLUSION

This study validated the GI performance in Thai EE SMEs which were successfully certified in GI level 1-level 3 more than GI Level 4 and Level 5. They mainly developed their organization to become a GI by implementing environmental policies and practices

in order to minimize environmental impact. EE SMEs currently implement rather simple environmental practices compared to those in large enterprises. The findings from Mann-Whitney U test on the importance of barriers and drivers to GI adopted by SMEs indicated that the median of opinion on economic factor and financial factor are significantly different between SMEs who are certified and non-certified with GI. However, Thai SMEs have significantly high potentials to contribute to sustainable production because they have commitment to transform to GI. Therefore, the incentive-based instruments as subsidies to SMEs is the first priority strategy by establishing a green industry fund for grant or loan to SMEs. Moreover, the regulation mechanism via product law and product tax in accordance with the voluntary agreement approach to green product certification is the second priority. Since the eligibility of the green product certification scheme requires that the manufacturers have to be a certified GI before they can manufacture certified green products, it can be supported by the enforcement of green product law and product tax.

This study focused on the EE sector in Thai SMEs, so further studies can focus on other industries, particularly S-curve industries of the national industrial plan, and form a comparison with this study. This study verified hypotheses with a questionnaire-based survey of only 179 responded questionnaires at the acceptable error of 10%, so this study is limited with sample size. Therefore, future studies should set an acceptable error of sampling with 5%. Furthermore, the statistical analysis of obstacles and drivers are to be refined and validated. The structural equation model (SEM) will be used in order to determine the level of importance for all barriers and drivers to shape a better framework to establish a more suitable strategy for enhancing SMEs adoption of the advance GI. Finally, this study hopes that the research results are beneficial to the policy maker in establishing the proper strategies to enhance the adoption of GI by Thai SMEs with an advance level of GI 4 and GI 5.

ACKNOWLEDGEMENTS

The authors gratefully acknowledge the financial aid provided by Graduate school, Chulalongkorn University through the 90th Anniversary of Chulalongkorn University Fund (Ratchadaphiseksomphot Endowment Fund).

REFERENCES

Bohari AAM, Skitmore M, Xia B, Teo M, Zhang X, Adham KN. The path towards greening the Malaysian construction industry. Renewable and Sustainable Energy Reviews 2015;52:1742-8.

Caldera HTS, Desha C, Dawes L. Evaluating the enablers and barriers for successful implementation of sustainable business practice in ‘ lean’ SMEs. Journal of Cleaner Production 2019;218:575-90.

Chen W, Chen J, Xu D, Liu J, Niu N. Assessment of the practices and contributions of China's green industry to the socio-economic development. Journal of Cleaner Production 2017;153:648-56.

Department of Industry Works. Plan 2564 [Internet]. 2021 [cited 2021 Apr 22]. Available from: http://www.diw.go.th/hawk/manual/policy/plan2564.pdf.

Frey M, Iraldo F, Testa F. The determinants of innovation in green supply chains: Evidence from an Italian sectoral study. R&D Management 2013;43(4):352-64.

Ghadge A, Kaklamanou M, Choudhary S, Bourlakis M. Implementing environmental practices within the Greek dairy supply chain. Industrial Management and Data Systems 2017;117(9):1995-14.

Ghazilla RAR, Sakundarini N, Abdul- Rashid SH, Ayub NS, Olugu EU, Musa SN. Drivers and barriers analysis for green manufacturing practices in Malaysian SMEs: A preliminary findings. Procedia CIRP 2015;26:658-63.

Jones P, Comfort D, Hillier D. Common ground: The sustainable development goals and the marketing and advertising industry. Journal of Public Affairs 2018;18:1-7.

Jove- Llopis E, Segarra- Blasco A. Eco- Efficiency Actions and Firm Growth in European SMEs. Sustainability 2018;10:281.

Jung TY. Climate technology promotion in the Republic of Korea. Advances in Climate Change Research 2015;6(3-4):229-33.

Katz- Gerro T, López Sintas J. Mapping circular economy activities in the European Union: Patterns of implementation and their correlates in small and medium- sized enterprises. Business Strategy and the Environment 2019;28:485-96.

Kesidou E, Demirel P. On the drivers of eco-innovations: Empirical evidence from the UK. Research Policy 2012; 41(5):862-70.

Kiefer CP, Del Río González P, Carrillo-Hermosilla J. Drivers and barriers of eco- innovation types for sustainable transitions: A quantitative perspective. Business Strategy and the Environment 2019;28(1):155-72.

Lee K-H. Why and how to adopt green management into business organizations? The case study of Korean SMEs in manufacturing industry. Management Decision 2009;47: 1101-21.

Lefebvre E, Lefebvre LA, Talbot S. Life cycle design approach in SMEs. The International Journal of Life Cycle Assessment 2001;6(5):273-80.

Luan CJ, Tien C, Chen WL. Which "green" is better? An empirical study of the impact of green activities on firm performance. Asia Pacific Management Review 2016;21(2):102-10.

Mann HB, Whitney DR. On a test of whether one of two random variables is stochastically larger than the other. Annals of Mathematical Statistics 1947;18(1):50-60.

Mathews JA. Green growth strategies-Korean initiatives. Futures 2012;44(8):761-9.

Ministry of Commerce. Trade report 2021 [Internet]. 2021 [cited 2021 Apr 22]. Available from: http://tradereport.moc.go.th/TradeThai.aspx.

Ministry of Industry. Green industry [Internet]. 2018 [cited 2019 Jul 26]. Available from: http://greenindustry.diw.go.th/greenindustry/searchfactory/.

Ministry of Industry. Green Industry. 8th ed. Bangkok, Thailand: Department of Industry Works; 2017.

Ministry of Industry. Summary of licensed factory 2016 [Internet]. 2016 [cited 2017 Apr 2]. Available from: http://www.diw.go.th/informationservice/factoryinformation/summary of licensed factory.

Nachar N. The Mann-Whitney U: A test for assessing whether two independent samples come from the same distribution. Tutorials in Quantitative Methods for Psychology 2008;4(1):13-20.

Organisation for Economic Cooperation and Development (OECD). OECD Environmental performance reviews: Japan 2010 [Internet]. 2010 [cited 2018 Jan 20]. Available from: http://www.oecdilibrary.org/environment/oecd-environmental-performance-reviews-japan-2010_9789264087873-en.

Organisation for Economic Cooperation and Development (OECD). OECD Environmental performance reviews: Korea 2017 [Internet]. 2017 [cited 2018 Jan 20]. Available from: http://www.oecdilibrary.org/environment/oecd-environmental-performance-reviews-korea-2017_9789264268265-en.

Office of Small and Medium Enterprises Promotion. Ministerial regulations of number of employment and the fix asset value of small and medium enterprise B.C. 2545 [Internet]. 2002 [cited 2017 Jun 26]. Available from: http://www.sme.go.th.

Office of Small and Medium Enterprises Promotion. SME Promotion Plan No.3 [Internet]. 2015 [cited 2017 Jun 26]. Available from: http://www.sme.go.th.

Office of Small and Medium Enterprises Promotion. SME situation report 2016 [Internet]. 2016 [cited 2017 Jun 26]. Available from: https://sme.go.th/th/page.php?modulekey=348.

Office of Small and Medium Enterprises Promotion. SME situation report 2020 [Internet]. 2020 [cited 2021 Apr 22]. Available from: https://sme.go.th/th/page.php?modulekey=348.

Ormazabal M, Prieto-Sandoval V, Puga-Leal R, Jaca C. Circular Economy in Spanish SMEs: Challenges and opportunities. Journal of Cleaner Production 2018;185:157-67.

Pedersen CS. The UN Sustainable Development Goals (SDGs) are a great gift to business. Procedia CIRP 2018;69:21-4.

Peng S, Sun X. Research on challenges and strategies for China's green economy development. Chinese Journal of Population Resources and Environment 2015;13(2):127-31.

Potros S, Enquist SB. ISO 14001 as a driving force for sustainable development and value creation. The TQM Magazine 2007;19(5):468-82.

Prieto-Sandoval V, Ormazabal M, Jaca C, Viles E. Key elements in assessing circular economy implementation in small and medium-sized enterprises. Business Strategy and the Environment 2018;27:1525-34.

Roy M-J, Boiral Q, Paillé P. Pursuing quality and environmental performance initiatives and supporting processes. Business Process Management Journal 2013;19(1):30-5.

Schoenherr T, Talluri S. Environmental sustainability initiatives: A comparative analysis of plant efficiencies in Europe and the U.S. IEEE Transactions on Engineering Management 2013;60(2):353-65.

Shrivastava M, Tamvada JP. Which green matters for whom? Greening and firm performance across age and size distribution of firms. Small Business Economics 2019;52: 951-68.

Stucki T. Which firms benefit from investments in green energy technologies? The effect of energy costs. Research Policy 2019;48(3):546-55.

Yamane T. Statistics: An Introductory Analysis. 2nd ed. New York, USA: Harper and Row; 1967.

Tavakol M, Dennick R. Making sense of Cronbach's alpha. International Journal of Medical Education 2011;2:53-5.

Triguero A, Moreno-Mondéjar L, Davia MA. Drivers of different types of eco-innovation in European SMEs. Ecological Economics 2013;92:25-33.

United Nations Industrial Development Organization (UNIDO). The 2030 Agenda for Sustainable Development: Achieving the Industry- related Goals and Targets. Vienna, Austria: UNIDO; 2018.

United Nations Industrial Development Organization (UNIDO). UNIDO Green Industry Initiative for Sustainable Industrial Development. Vienna, Austria: UNIDO; 2011.

Wang C, Ghadimi P, Lim MK, Tseng M-L. A literature review of sustainable consumption and production: A comparative analysis in developed and developing economies. Journal of Cleaner Production 2019;206:741-54.

Wang C-T, Chiu C-S. Competitive strategies for Taiwan's semiconductor industry in a new world economy. Technology in Society 2014;36:60-73.

Woodard R. Waste management in small and medium enterprises (SMEs): Compliance with duty of care and implications for the circular economy. Journal of Cleaner Production 2021;278:123770.

World Bank. Small and medium enterprises (SMEs) finance [Internet]. 2020 [cited 2020 May 22]. Available from: https://www. worldbank.org/en/topic/smefinance.

Yusup MZ, Mahmood WH, Salleh MR, Ab Rahman MN. The implementation of cleaner production practices from Malaysian manufacturers' perspectives. Journal of Cleaner Production 2015;108:659-72.

Zamfir A-M, Mocanu C, Grigorescu A. Circular economy and decision models among European SMEs. Sustainability 2017;9(9):1507.

Assessment and Prediction of Land Use/Land Cover Change in the National Capital of Burundi Using Multi-temporary Landsat Data and Cellular Automata-Markov Chain Model

Audace Ntakirutimana and Chaiwiwat Vansarochana*

Faculty of Agriculture, Natural Resource and Environment, Naresuan University, Phitsanulok 65000, Thailand

ARTICLE INFO

Received: 24 Feb 2021
Received in revised: 14 Jun 2021
Accepted: 28 Jun 2021
Published online: 20 Jul 2021
DOI: 10.32526/ennrj/19/202100023

Keywords:
Gitega District/ Land degradation/ Kappa statistics/ Simulation/ Land Change Modeler/ Geoinformatics

*** Corresponding author:**
E-mail: chaiwiwatv@gmail.com

ABSTRACT

Gitega District has experienced significant land use and land cover changes due to human activity. This has increased land degradation and environmental issues. However, there is no data on LULC change to guide land-use planning. This study assessed the rate and magnitude of LULC change over the last 35 years and also simulated future scenarios using Geoinformatics. In the first step, five LULC classes were extracted from satellite images from 1984, 2002, and 2019 using the supervised classification method. Overall accuracy and Kappa statistics of more than 85% and 82% respectively were achieved with 30 reference samples. Change analysis highlighted by Land Change Modeler (1984-2019) indicated a significant increase in Agriculture of 94 km^2, a slight increase in Shrub Land and Built-up Area of 5.5 km^2 and 2 km^2, respectively; and a steep decrease in Trees Cover and Grass Land of 62.5 km^2 and 39 km^2, respectively. Markov Chain and CA-Markov models were further calibrated to simulate LULC changes in 2038 and 2057 using the 2019 base map. Evaluation and analysis of 2019-2057 simulation results showed a moderate agreement of 75% for Kappa and the same trends of LULC change: Trees Cover, Grass Land, and Shrub Land will decrease by 11.5 km^2, 13 km^2, 11.5 km^2 respectively, whereas Agriculture and Built-up Area will increase by 30 km^2 and 6 km^2 respectively in 2057. These study outcomes can support decision-making towards restoration measures of land degradation and long-term environmental conservation in the region.

1. INTRODUCTION

Land cover change denotes alteration in physical land types such as forests, vegetation, and so on, whereas land-use change refers to changes in a specific area of land used or managed by humans for their provisions (Liu and Shi, 2019; Patel et al., 2019). Land use and land cover (LULC) change is a result of the human activities and subsequent development taking place across the world (Bai et al., 2008). Land use pattern is triggered by population dynamics which is directly responsible for the changes in land cover (IPBES, 2018; Serneels and Lambin, 2001; Verma and Raghubanshi, 2019).

The impact of LULC change on the Earth's environment has increased as a result of rapid growth in human population which leads in turn to deforestation, intensive agricultural activities, urbanization, and other unplanned human settlement (Boissière et al., 2009; Lambin et al., 2000; Meyer et al., 1994). According to a global report published by FAO, 24% of the world's land is degraded due to anthropogenic influences, primarily in Africa, Asia, Australia, and North America (Bai et al., 2008). In recent years, assessing and modelling LULC change has become an essential aspect since the LULC change has influences on socioeconomic, and environmental structure (Halmy et al., 2015; Twisa and Buchroithner, 2019).

The study of assessing and modelling LULC change is an expensive and time-consuming process. However, through Remote Sensing (RS) and Geographic Information System (GIS) techniques, it is possible to examine LULC change on large spatial

Citation: Ntakirutimana A, Vansarochana C. Assessment and prediction of land use/land cover change in the National Capital of Burundi using multi-temporary Landsat data and Cellular Automata-Markov Chain Model. Environ. Nat. Resour. J. 2021;19(5):413-426. (https://doi.org/10.32526/ennrj/19/202100023)

and temporal scales (Dewan and Yamaguchi, 2009; Nijimbere et al., 2019). R.S advancements allow us to obtain synoptic information about LULC at a specific time and location (Anderson, 1976; Patil et al., 2012). Multi-temporary satellite images have been widely used for LULC change detection (Kumar et al., 2010; Vila and Barbosa, 2010). The GIS approach, namely Geoinformatics, through its ability to analyze, update and backdate LULC information with object-oriented or pixel-based image classification, has been shown to produce accurate results for LULC monitoring (Mishra et al., 2014; Shen, 2019). Such classification accuracy is performed by both the spatial and spectral resolution of satellite image data (Poursanidis et al., 2015).

Moreover, the future LULC change prediction requires the integration of past trends and current landscape, and plausible assumptions. Therefore, the literature describes various forecasting models based on research purposes, i.e., landscape dynamics, ecological modelling, disaster and deforestation assessment, agriculture projects and urban sprawl planning, etc., (Baker, 1989). Verburg (2006) argues that no single land-use model can be superior to another. But, some other researchers have expressed their confidence in the significant results obtained when integration of Cellular Automata and Markov Chain models is used in the LULC modelling process (Mondal et al., 2016; Nadoushan et al., 2015). Several national land cover mapping programs have been developed to continuously monitor LULC changes and produce national and regional land cover maps (Gómez et al., 2016). This has contributed to a better understanding of natural-human interactions and advanced monitoring and modelling of landscape dynamics (Ghosh et al., 2017; Turner et al., 2007).

Burundi is a small landlocked country with an area of 27,834 km^2, and the most densely populated country in Africa with 480 people/km^2 (UNdata, 2020). Due to an increasing number of householders who rely on agriculture to meet their needs (Moore, 2007), the country is vulnerable to major landscape dynamics and environmental problems (Kamungi et al., 2005; Nzabakenga et al., 2013). It is currently agreed that access to arable land is a top priority for any household. With 90% of the 12 million as workforces in farming land, land resources are being much more depleted and scarcer than in the past (Nzabakenga et al., 2013).

Gitega District, one of the most densely populated regions in Burundi with 476 people/km^2 (Niyuhire, 2018), is prone to land degradation and environmental vulnerabilities as a result of long-term major landscape dynamics. This region has attracted a large number of immigrants due to its geographic location in the center of the country, which is an important aspect of being a National Capital (Guichaoua, 1982). Significant LULC change started occurring in 2007, when the government of Burundi began the process of restoring that district's former status as National Capital (Patel et al., 2019). Thus, the rapid population increase in that area results in agricultural expansion along with built-up area and reduction of forest and grassland in the Gitega's landscape (Guichaoua, 1982; Niyuhire, 2018). As per El-Hassanin et al. (1993) and Marathianou et al. (2000), LULC changes reduce normalized difference vegetation index (NDVI) of land. This provokes other extreme impacts on the environment such as climate change, extreme radiative forcing, pollution and quality reduction of natural ecosystems, changes in hydrological regimes, runoff, soil loss and depletion of soil fertility (IPBES, 2018; Verma and Raghubanshi, 2019). Certain recent studies have only addressed agricultural issues confronting farmers at the national and district levels. Kamungi et al. (2005), land access, Nzabakenga et al. (2013), agriculture and farmers' livelihoods, Nijimbere et al. (2019), soil erosion, Niyuhire (2018), soil depletion and integrated soil fertility. Though, they did not study land degradation with LULC change patterns.

However, Burundi has neither national nor regional mapping platforms for generating basic information about the LULC change and environmental dynamics that could aid in land use planning (Burrell et al., 2018; Ndzabandzaba, 2015). Therefore, the main objective of this study was to assess LULC changes that occurred in the Gitega District over the last 35 year by calculating the rate and magnitude of change for the LULC category. This study also aimed to simulate the future scenario of LULC changes under an assumption of the continuation of past and current trends using the combination of RS, GIS, and Cellular Automata and Markov Chain approach.

2. METHODOLOGY

The Figure 1 shows the overall methodology used for this study in three main parts: data source, data processing, and results analysis.

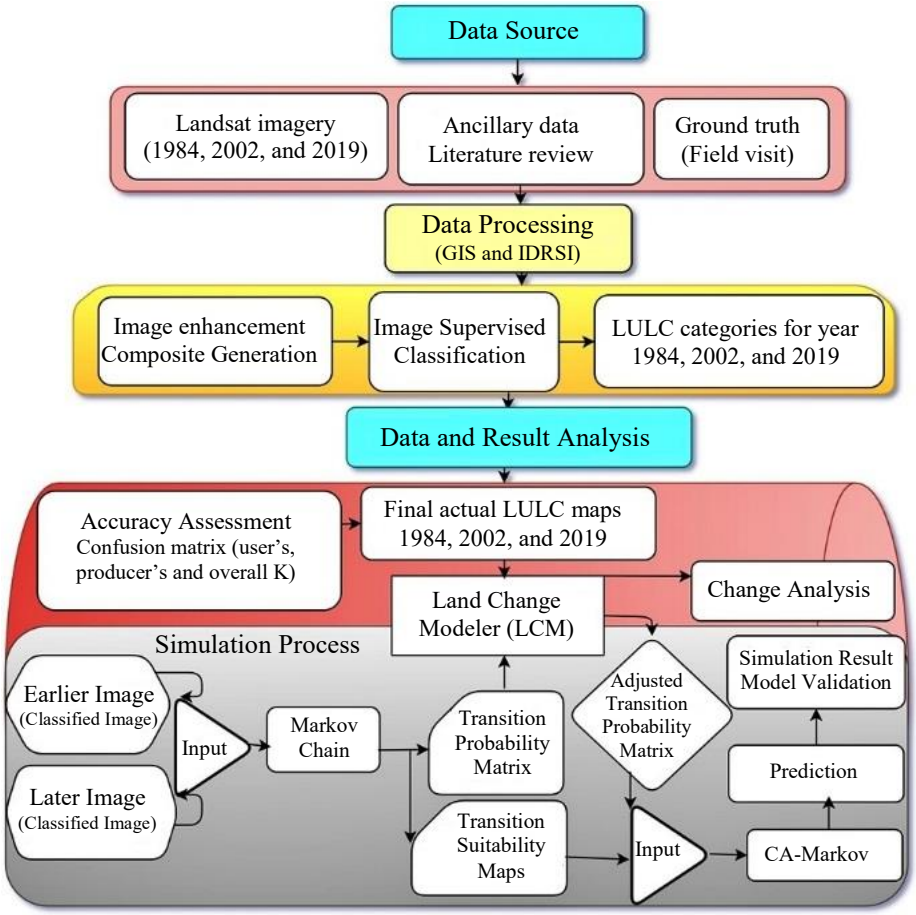

Figure 1. General methodology of the research

2.1 Study area

Gitega District is located in the center of Burundi at a specific geographic grid reference of "03° 25' 35" South Latitude and 29° 50' 37" East Longitude (Figure 2). It has an area of 315 km^2, 150,151 people, and a density of 476 inhabitants/km^2 (Niyuhire, 2018). Its topography dominated by plateau dispersed by hills, valleys, and moderate plains rises between 1,600-2,000 m. Climate is subtropical highland and tropical savanna climate depicting summer and winter (Vassolo et al., 2019). The average annual temperature is 20°C with lower and higher temperatures of 10°C and 26°C respectively, while the average annual rainfall is 1,130 mm with lower and higher rainfall in July and April respectively (Vassolo et al., 2019). Due to those mild climate and plentiful rainfall, the area is ideal for forests, vegetation, and plantations. However, high population pressure on land and poor farming practices are unsuitable for environmental preservation (El-Hassanin et al., 1993; Kamungi et al., 2005). With two harvests per year, cultivation of subsistence foods such as bananas, corn, manioc, sweet potatoes, Irish potatoes, beans, peas, wheat, peanuts, vegetables, etc., is intensified even on steep slopes and hilltops (Kamungi et al., 2005; Nijimbere et al., 2019). This study area, which includes both urban and rural land use characteristics, is likely to experience the most change in its landscape. Since the project to restore its former status as the national capital was launched in 2007, several buildings and road patterns have been constructed to meet the county's second city functions.

2.2 Data acquisition and processing

Three Landsat Images with 30 m resolution were downloaded from the United States Geological Survey (http://earthexpolorer.usgs.gov/) and important information is shown in Table 1. All these images were taken on satellite track path/row:173/062 and projected in UTM with WGS-84 datum 36 N.

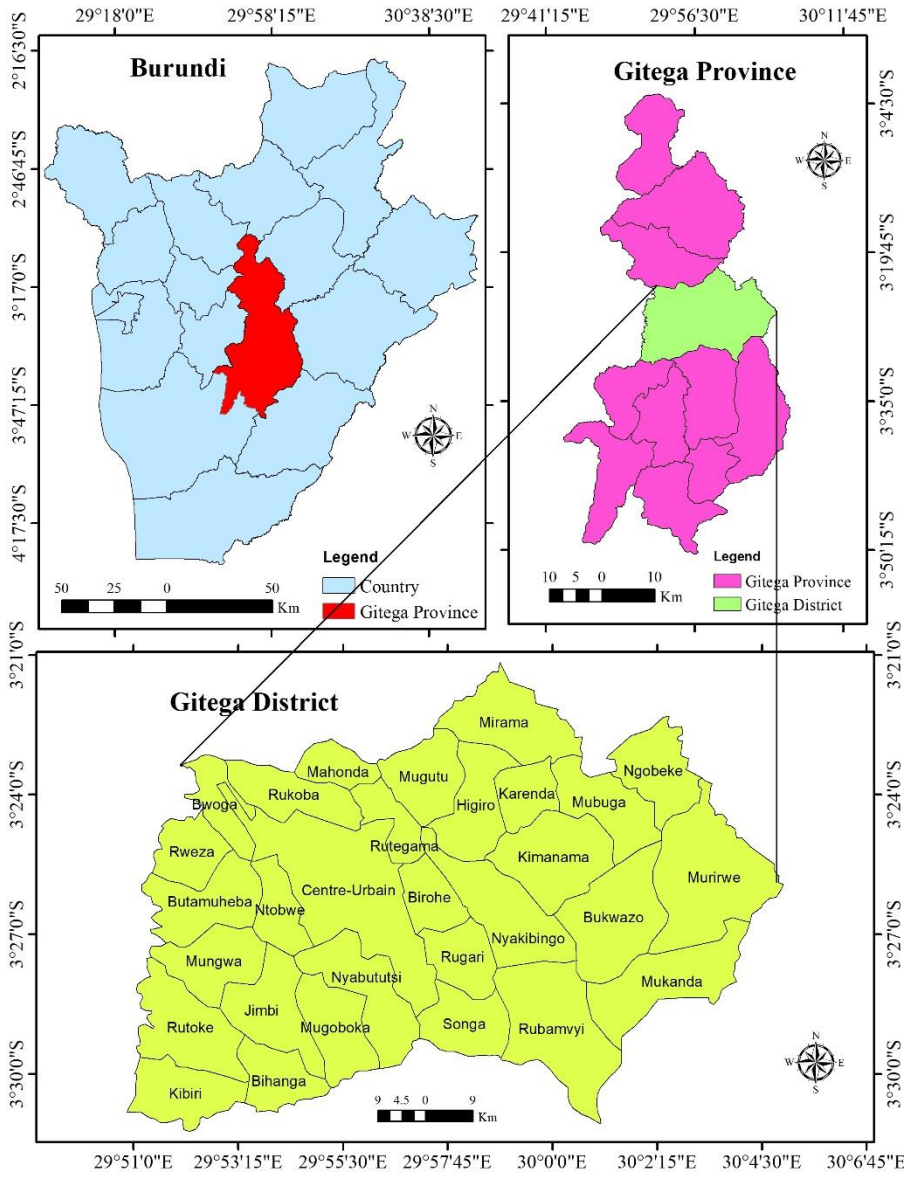

Figure 2. Location map of the study area

Table 1. Details of Landsat data

Satellite sensor	Path/row	Acquisition date	Bands	Resolution
Landsat 5 TM	172/062	20 June 1984	2, 3, 4	30 m
Landsat 7 ETM	172/062	17 August 2002	2, 3, 4	30 m
Landsat 8 OLI	172/062	23 July 2019	3, 4, 5	30 m

Prior to classifying the above satellite images from different dates, an image-based atmospheric correction was performed by subtracting a common minimum digital number (DN) value from the image using Idrisi software. Aside from noise removal, another image preprocessing based on image optical properties, such as sun elevation, angle, and spectral was applied using image metadata file. False-color composite and contrast stretching techniques were further applied to improve brightness and tonal differentiation between various features (Song et al., 2001).

2.2.1 Image classification and mapping

Several classification methods were developed to extract useful information from imagery. Two of the most popular land cover classification machines were also used in this research (Pulighe et al., 2016; Tilahun and Islam, 2015):

Supervised classification, which involves manually defining land cover classes and forcing signatures based on field identification and local knowledge of land cover types (Eastman, 2009; Patil et al., 2012). In this process, the common classification scheme in the LULC system (Anderson, 1976) and field survey data were used to form five LULC categories, for what training sits" samples were created.

Maximum Likelihood classifier was then used, whose function is to assign the pixel to the class with the highest probability. The training site samples generated during the supervised process were fully distributed on the entire image in terms of spectral information for each LULC class. The signature file containing spectral information was thereby generated (Eastman, 2009; Patil et al., 2012). Finally, ArcGIS software was used to map the five LULC categories: Agriculture, Built Area, Grass Land, Shrub Land, and Tree Cover. Figure 3 shows LULC maps for 1984, 2002, and 2019, respectively, and results of image classification and the area distribution is given in Table 2.

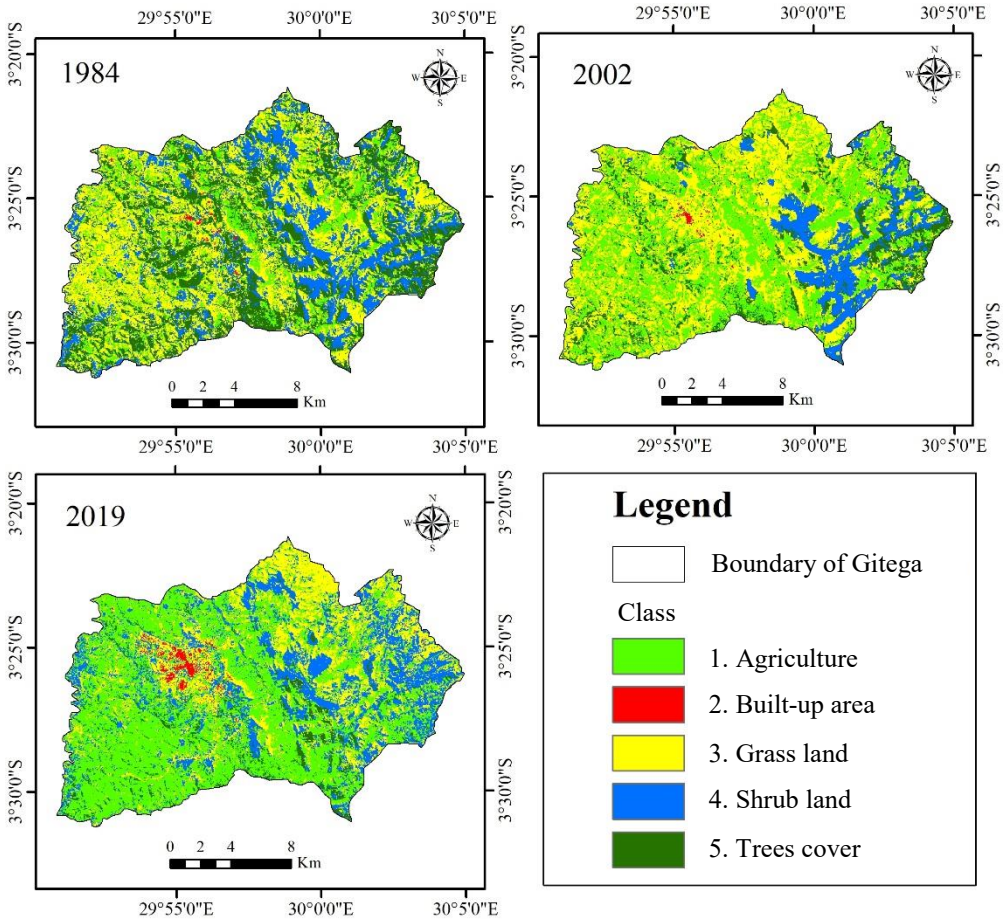

Figure 3. LULC maps from image classification for the year 1984, 2002, and 2019

Table 2. Area distribution for LULC in km^2

LULC class	1984	2002	2019
Agriculture	48	111.5	142
Built-up area	1	1.5	3
Grass land	112	121	73
Shrub land	61	31	66.5
Trees cover	81	38	18.5

2.2.2 Classification evaluation process

The high-resolution contemporary satellite imagery available on Google Earth pro was used to collect the ground truth data for 1984, 2002, and 2019 maps. Thirty pixels were selected using a stratified sample random method with ArcGIS to examine image classification accuracy (Pulighe et al., 2016; Tilahun and Islam, 2015). The confusion matrix

method reporting overall accuracy (OA) user's accuracy (UA), producer's accuracy (PA) and Kappa statistics (K) were generated (Dewan and Yamaguchi, 2009; Rwanga and Ndambuki, 2017). OA measures the percentage of total classified pixels that were truly labeled into the specific land cover and is computed by dividing the total correctly classified pixels (TCS or the sum of the diagonals) by the number of reference pixels (TS) in the error matrix using equations (1), (2), and (3):

$$OA = \frac{\Sigma TCS_{ij}}{TS} \quad (1)$$

$$PA = \frac{\Sigma TCS_{ij}}{TSc_i} \quad (2)$$

$$UA = \frac{\Sigma TCS_{ij}}{TSr_i} \quad (3)$$

Where; TCS_{ij} is the total number of the correctly classified pixels in row i and column j, TS is the total reference sample, TSc_j is the total number of pixels in column j and TSr_i is the total number of pixels in the row i. The quantitative measure of the level of agreement was done with utilization of kappa statistic (K) assumed that a K of 1 indicates ideal agreement, whereas a kappa of 0 indicates agreement equivalent to chance to truly classify the pixels as computed in the equation (4):

$$k = \frac{(TS \times TCS) - \Sigma\, TSc_j\, TSr_i}{TS^2 - \Sigma(TSc_j - TSr_i)} \quad (4)$$

Where; TCS_{ij} is the total number of the correctly classified pixels in row i and column j, TS is the total reference sample, TSc_j is the total number of pixels in column j and TSr_i is the total number of pixels in the row i. Moderate agreement of more than 85% and 82% for overall accuracy and Kappa statistics respectively was obtained as presented in Table 3.

Table 3. Results from classification accuracy assessment

Year	1984		2002		2019	
LULC	Producer	User	Producer	User	Producer	User
Agriculture	71	100	87	87	100	100
Built-up area	100	100	100	100	100	80
Grass land	100	62	82	62	100	88
Shrub land	71	83	66	100	66	100
Trees cover	100	100	100	100	100	100
Overall accuracy	86		86		93	
Kappa statistics	0.83		0.83		0.91	

2.3 Cellular Automata and Markov Chain for simulation the future LULC Change

The combination of Cellular Automata and Markov Chain models have been the most popular integrated model used for modelling spatial and temporal changes (Borana and Yadav, 2017; Sang et al., 2011). Markov Chain is a dynamic process that calculates the probability of changes from a particular object (e.g., vegetation) to another object (e.g., agriculture) in the next state depending on the former state. It has been used equally in LULC studies due to its ability to quantify conversion rates between two categories (Ghosh et al., 2017). Cellular Automata (CA) is a discrete dynamic system consisting of a normal finite cell network that can change in various directions in neighboring (Singh, 2003; Torrens, 2000). CA is also widely used in simulating LULC change because it is fairly close to GIS raster data (Pijanowski et al., 2002; Surabuddin et al., 2013). Therefore, the combination of the two above models was also applied in this study to simulate the LULC in 2019, 2038, and 2057 using the following equations (5) and (6) (Mondal et al., 2016; Nadoushan et al., 2015):

$$S(t, t+1) = Pij \times S(t) \quad (5)$$

Where; S (t) is the system status at time t; S (t+1) is the system status at a time of t+1, and Pij is the transition probability obtained in equation (6) below:

$$P = |P_{ij}| = \begin{vmatrix} P_{1,1} P_{1,2} \dots P_{1,N} \\ P_{2,1} P_{2,2} \dots P_{2,N} \\ \dots\dots\dots \\ P_{N,1} P_{N,2} \dots P_{N,N} \end{vmatrix} \quad 0 \le P_{ij} \le 1 \quad (6)$$

Where; P=Transition probability; Pij=stands for probability of changing from particular state i to another state j; P_N=state probability of any time, and N=Land cover type (Eastman, 2009; Mishra et al., 2014).

In this study, 1984, 2002, 2019 LULC maps were used to run Markov Chain. Firstly, 1984 and 2002 LULC maps were used as earlier and later images to project the 2019 LULC map (Figure 7), along with transition probability matrix shown in Table 4. This method produced a suitability map matching the current rate and quantity of 2019 LULC which will be further used to simulate future scenarios (Sang et al., 2011). The 1984 LULC map was used in CA-Markov as base map and Cellular automata iterations were set to 35 as the time interval between 1984 and 2019 to predict the 2019 LUC map. This simulation outcome was compared with the existing LULC to evaluate the model performance (Figure 4) (Gupta and Sharma, 2020). The 2019 LULC simulation was achieved using 1984-2002 transition probability area matrix, transition suitability map, and a set window technique 5*5 kernels called standard contiguous filter for influencing each cell center. After successful validation of 2019 simulation result, predictions of 2038 and 2057 LULC maps were done (Figure 7). At this stage, we used the 2019 real LULC map as the simulation's input, along with the relevant transition probability area matrices, and transitional suitability maps generated from Markov Chain (Nadoushan et al., 2015; Singh, 2003). Based on the modelling theory, we kept a default set of 5*5 kernel size contiguity filter, while the cellular automata iteration was set to 19 to simulate the 2038 LULC map, and the same method was used to simulate 2057 LULC map.

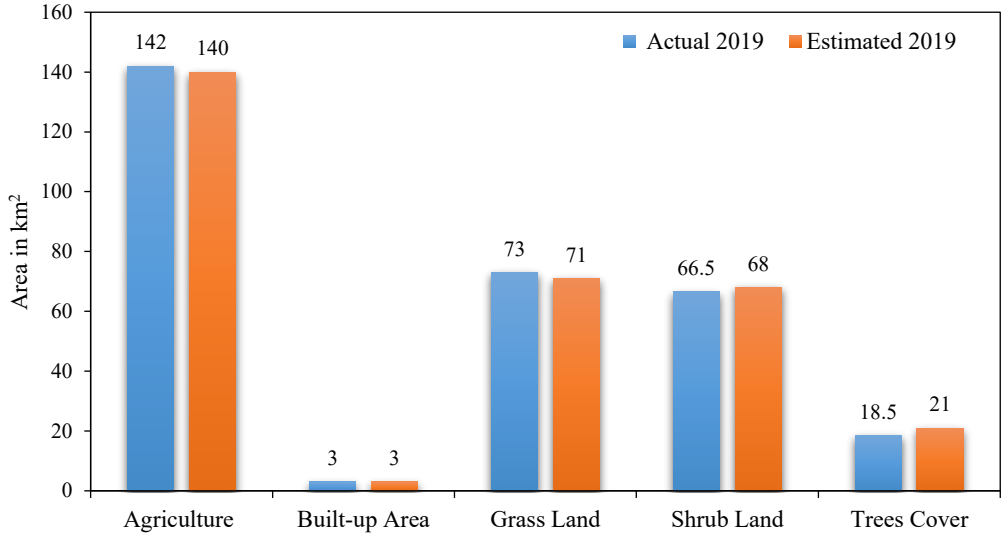

Figure 4. Area (in km^2) of LULC category in actual and simulated maps (2019)

2.4 Simulation accuracy and model evaluation

Simulation accuracy and model validation were determined by comparing the predicted LULC maps for 2019, 2038, and 2057 to the actual LULC map for 2019. The Kappa statistics is the most widespread method agreed to quantify the power and suitability of the simulation model (Maingi et al., 2002). This study utilized the submodule in Idrisi namely, GIS Analysis, to generate the Kappa index of Agreement shown in Table 5. The validation was done based on the assumption that the higher the kappa values, the better the model (Borana and Yadav, 2017). All kappa index values surpass the minimum acceptable standard and they range from 65% to 89%. This indicates a high degree of agreement between projected and actual LULC maps, thus a successful validation of the CA-Markov Chain model (Kundel and Polansky, 2003; van Vliet et al., 2011).

3. RESULTS AND DISCUSSION

3.1 LULC Change Analysis

The LULC changes analysis enables an understanding of physical modification or loss of features in the natural landscape such as vegetation and forests clearing, agricultural land, waterbody as worthwhile information useful for planning land use and environmental conservation (Wang et al., 2021). We applied the comparative method to analyze five LULC classes from image classifications based on remote sensing techniques (Dewan and Yamaguchi, 2009). The land use and land cover change analysis were accomplished by using land cover data with an interval of 35 years, from 1984 to 2019 which depicts

two sub-time intervals: 18 years (from 1984 to 2002), and 17 years (from 2002 to 2019).

Based on Figure 5, it is revealed that the landscape of Gitega in 1984 was extensively covered by Grass Land and Trees Cover: 112 km^2 (36.97%) and 81 km^2 (26.73%), respectively. Shrub Land is the third most dominant class, accounting for 61 km^2 (20.13%), while Agriculture and Built-up Area account for 48 km^2 (15.84%) and 1 km^2 (0.33%), respectively. In the year 2002, the study area was largely covered with Grass Land and Agriculture:121 km^2 (39.84%) and 111.5 km^2(36.92%), respectively. However, Trees Cover and Shrub Land decreased to 38 km^2 (12.24%) and 31 km^2 (10.21%), respectively, and Built-up Area had slightly increased. In 2019, the largest land cover was Agriculture with 142 km^2, an increase of 10% from 2002 to 2019. Grass Land took a second areal position with 73 km^2 due to a decrease of nearly 5%. Shrub Land rose to the third position due to an increase by 11.74% with an area of 66,5 km^2, while Trees Cover steeply decreased by 6.44% and occupied 18.5 km^2. Built-up Area has a steady increase of 1.5 km^2 from 2002-2019.

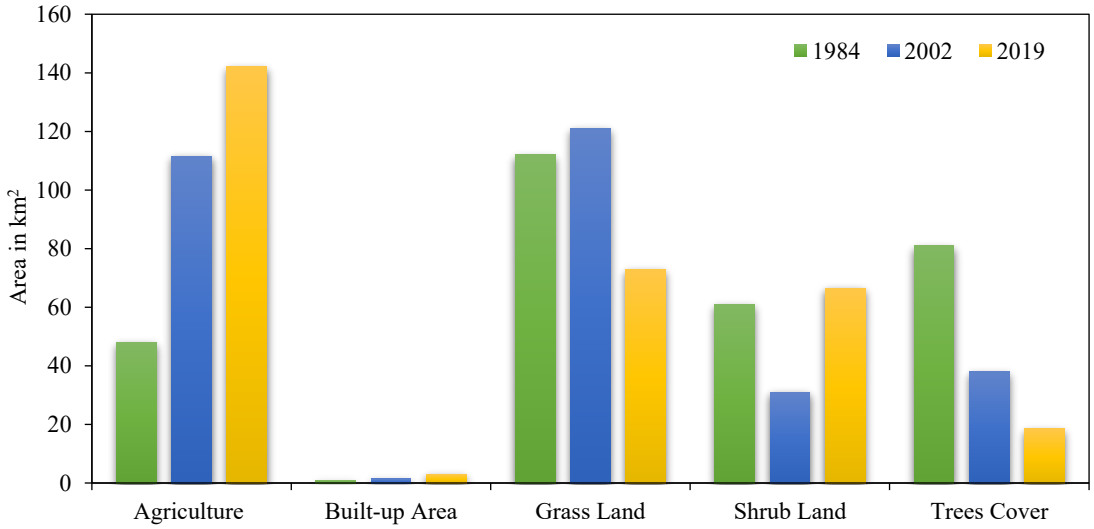

Figure 5. Comparison of existing LULC category by statistical area in km^2

Over past 35 years, the dynamic in LULC change patterns is intensely high. Trees Covers and Grass Land were continuously reduced by 62.5 km^2 at an annual rate of 1.79 km^2 and 39 km^2 at the rate of 1.12 km^2 per year, respectively. In contrast, a net change indicates a large extension in Agriculture of 94 km^2 at the rate of 2.68 km^2 per year. A slight increase is also detected in both Shrub Land and Built Area, which is 5.5 km^2 with a rate of 0.15, and 2 km^2 with a rate of 0.8 km^2 per year, respectively. For getting a better understanding, LULC change detection was investigated using Land Change Modeler (LCM), and the model outputs shown in Figure 6 are consistent with certain results of land cover change detection obtained using the same model. For instance, Gupta and Sharma (2020) have acknowledged interesting results of LULC change monitoring by LCM model in LULC dynamics study (over past 50 years) conducted in India. These decreasing areas in Trees Cover and Grass Land (by about 101.5 km^2 in total with an annual rate of 2.9 km^2) have been converted mostly into Agriculture (94 km^2), and little to Shrub Land and Built-up Area (7.5 km^2 together) from 1984 to 2019.

Similar trends of LULC change, especially deforestation and agricultural expansion, were globally addressed (FAO, 2016), and in many other developing countries (Alawamy et al., 2020; Berakhi, 2013; Henry et al., 2011; Islam et al., 2018). Interesting LULC change issues in terms of urban sprawl were recently dealt with by Patel et al. (2019) in India. Thereby, a general perception is that forest and vegetation reductions lead to dramatic degradation of productive ecosystems and loss of biodiversity (Wang et al., 2021). Primarily, the land degradation will radiate outwards within the global environment (IPCC, 2019; Marathianou et al., 2000; Niyogi et al., 2009). Deforestation alters hydrological processes and affects water conductivity like surface runoff (El-Hassanin et al., 1993) and, therefore, the occurrence of soil erosions and soil losses as observed in the study area (Henry et al., 2011; Nijimbere et al., 2019; Niyuhire, 2018; Nzabakenga et al., 2013).

A review of the trends in population growth and density (476 people/km^2) in the Gitega District can reveal that the most LULC changes are likely the shortcomings of human encroachment on natural land resources and ecosystems (Kamungi et al., 2005). In this study, the results of the LULC change analysis for the last thirty-five years were used to make predictions for the next thirty-eight years.

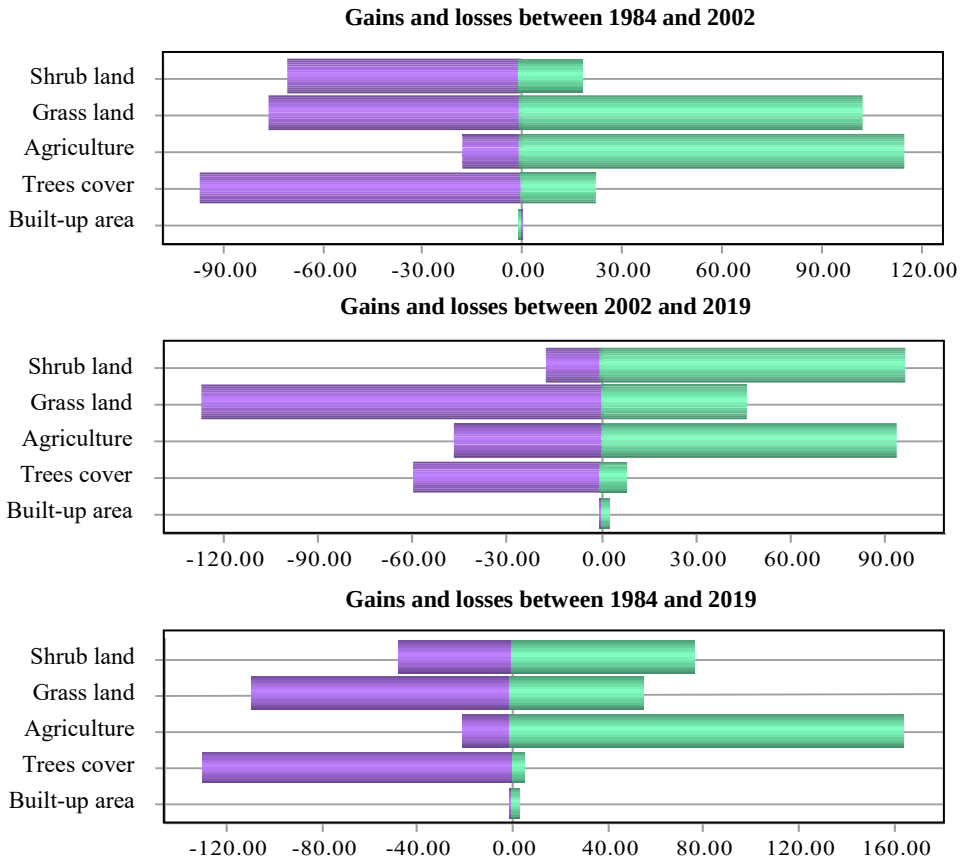

Figure 6. Gains (Green) and losses (Purple) in km^2 by category of LULC in different periods

3.2 Simulation result analysis

CA-Markov Chain simulation model requires earlier and later LULC maps to predict the future scenario (Sang et al., 2011). Future LULC simulations were projected for 2057 with a time interval of 38 years, from 2019 to 2057, which also depict two sub-time intervals: 19 years (from 2019 to 2038) and 19 years (from 2019 to 2057). According to the Markov Chain concept, changes that occurred in the previous period can be used to predict changes in the next period (Ghosh et al., 2017; Wang et al., 2021). In this study, the simulation inputs were the real and projected LULC maps for 2019 and the probability matrix for the transition to land-use change in 2019-2038 and 2019-2057.

Based on the theory of transition probability, the Markov model performs the likelihood of a change from one land cover category to another within a dimensioned matrix of LULC classes (Nadoushan et al., 2015). For example, the analysis of the results from Markov Chain application in this study given in the cross-tabulation showed revealed that from 2019 to 2038, the probability of change for Agriculture to Agriculture is 68.24%, while the probability of future change of Agriculture to Grass Land is 20.76%. Trees Cover has a probability as low as 5.9% to remain as they are but has a probability of 37.06% to change to Agriculture and the same process for other LULC classes. In the second prediction scenario, from 2019 to 2057, Agriculture has the highest probability of 71.09% to remain the same in 2057, whereas Trees Cover indicates the most declining probability of 3% to remain same in 2057. Built-up Area, Grass Land, and Shrub Land have the probability of 49.01%, 30.84%, and 26.24%, respectively, to remain as they are in 2019. Table 4 records the transition probability matrix of Gitega District LULC conversions that could occur from 2019 to 2038 and 2019 to 2057, with dimensions of 5×5.

Table 4. Transition probability matrices used during simulation process

a. Probability of changing from … by 2019 to:

1984	Agriculture	Built-up Area	Grass Land	Shrub Land	Trees Cover	Total	Omission
Agriculture	0.629	0.0072	0.1051	0.2336	0.0251	1	0.371
Built-up Area	0.1401	0.4638	0.198	0.1903	0.0078	1	0.802
Grass Land	0.3922	0.0186	0.4532	0.1131	0.0229	1	0.9814
Shrub Land	0.2925	0.0166	0.3138	0.3534	0.0237	1	0.6466
Trees Cover	0.4634	0.0071	0.1968	0.294	0.0387	1	0.9613
Total	1.9172	0.5133	1.2669	1.1844	0.1182	5	
Commission	1.2882	0.0495	0.8137	0.831	0.0795		

b. Probability of changing from … by 2038 to:

2019	Agriculture	Built-up Area	Grass Land	Shrub Land	Trees Cover	Total	Omission
Agriculture	0.6824	0.0045	0.2076	0.0839	0.0216	1	0.3176
Built-up Area	0.1681	0.4321	0.1959	0.1987	0.0052	1	0.8041
Grass Land	0.5423	0.0021	0.3811	0.0601	0.0144	1	0.9979
Shrub Land	0.368	0.0175	0.3905	0.2139	0.0101	1	0.7861
Trees Cover	0.3706	0.0039	0.2147	0.3518	0.059	1	0.941
Total	2.1314	0.4601	1.3898	0.9084	0.1103	5	
Commission	1.449	0.028	1.0087	0.6945	0.0513		

c. Probability of changing from…by 2057 to:

2019	Agriculture	Built-up Area	Grass Land	Shrub Land	Trees Cover	Total	Omission
Agriculture	0.7109	0.0027	0.1733	0.0901	0.023	1	0.2891
Built-up Area	0.1248	0.4901	0.2536	0.1256	0.0059	1	0.7464
Grass Land	0.4026	0.0034	0.3084	0.2591	0.0265	1	0.9966
Shrub Land	0.4801	0.0083	0.2102	0.2648	0.0366	1	0.7352
Trees Cover	0.6446	0.004	0.1124	0.2032	0.0358	1	0.9642
Total	2.363	0.5085	1.0579	0.9428	0.1278	5	
Commission	1.6521	0.0184	0.7495	0.678	0.092		

Cellular Automata and Markov Chain models were spatially integrated to predict change location (Verburg, 2006). This simulation process for 2019-2057, which combines Cellular Automata and the Markov model, is similar to the simulation process for 1984-2019. The difference was in the time interval of input data used as the basis for simulation, which was due to the need for high-quality image data to successfully detect and model Gitega District LULC changes. The transition probability and changing area prediction from the Markov Chain process served as the input basis for Cellular Automata to determine the change location represented in pixel (Nadoushan et al., 2015; Singh, 2003). The simulation results are presented as predicted LULC maps. Table 5 displays the index values that indicate reasonable agreement for the model validation and the prediction results accuracy.

Table 5. Simulation accuracy assessment result by kappa index

k indicators	2019	2038	2057
K_{no}	0.7205	0.8330	0.7870
$K_{location}$	0.7569	0.8785	0.8324
$K_{location\ Strata}$	0.7569	0.8785	0.8324
$K_{standard}$	0.6565	0.7978	0.7528

The Figure 7 depicts maps of LULC prediction results in the Gitega District for 2038 and 2057 respectively simulated using estimated LULC map for 2019.

Based on Table 6, it is projected that Agriculture will continuously expand with the increase of 14 km^2 and 30 km^2 in 2038 and 2057, respectively. Built-up Area will increase by 6 km^2 in 2057. However, trees cover, grass land, and shrub land will be decreasing by 11.5 km^2, 13 km^2 and 11.5 km^2,

respectively, in 2057. These predicted trends of LULC change showing such continuous agricultural expansion at expenses of forest and vegetation are also similar to those reported by other LULC modelling studies (Henry et al., 2011; Mondal et al., 2016; Nadoushan et al., 2015; Wang et al., 2021). Eventually, a better decision is needed to avoid these projected major LULC changes in Gitega District. Table 6 displays the results of change analysis of predicted LULC maps.

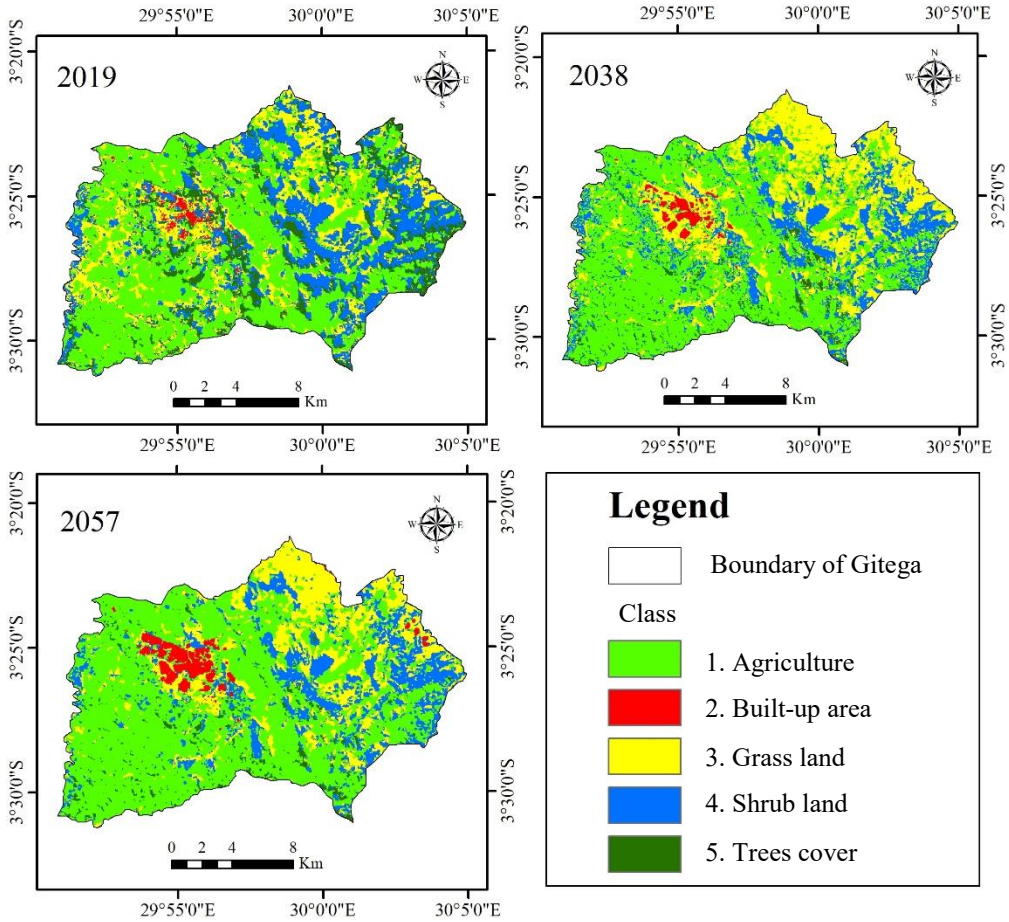

Figure 7. Predicted LULC maps for 2019, 2038, and 2057

Table 6. Change analysis of future projected LULC

LULC category	Simulated area (in km^2)		Change detection (in km^2)	
	2038	2057	2038-2019	2057-2019
Agriculture	156	172	14	30
Built-up area	5	9	2	6
Grass land	78	60	5	-13
Shrub land	54	55	-12.5	-11.5
Trees cover	10	7	-8.5	-11.5

4. CONCLUSION

This paper assessed the rate and trends of change in LULC patterns quantified and predicted using Geoinformatics in Gitega District. The Change analysis was performed using 5 LULC classes obtained from images classification of years 1984, 2002, and 2019 and was highlighted with Land Change Modeler. Markov Chain and CA-Markov models were applied to project future trends of LULC changes in 2038 and 2057. Satisfactory accuracy with good agreements of more than 85% and 82%, respectively, for overall accuracy and Kappa statistics was achieved. RS, GIS, and Cellular Automata and Markov Chain models were therefore proven to be

effective tools for LULC change monitoring and generating multi-temporary land cover dataset to assist decision-makers towards land use planning and environmental protection.

Overall findings reveal dramatic decreasing area in Trees Cover and Grass Land of 101.5 km^2 together, and which was likely converted mostly to Agriculture (which increased by 94 km^2 at a rate of 2.68 km^2 per year), and to Shrub Land and Built-up Area (7.5 km^2 together) over the past 35 years. These results are reflective of the current rate, trends, and magnitude of LULC changes and local policies in the study area. If Gitega attempts to avoid further irreversible land degradation and associated environmental problems, the government and policymakers should urgently apply agroecological approaches and reforestation.

Similar trends in LULC change patterns are revealed by predictive result analysis. Agriculture has 71.09% probability of remaining as Agriculture in 2057, with an expected area of 172 km^2 (56.76%). On the other hand, Trees Cover have the lowest probability of 3% to remain as Trees in 2057, with an area of 7 km^2. These study outcomes are the potential to support decision-making to undertake restoration measures of land degradation and future sustainable land use management and environmental presser-vation . However, future studies should consider the correlation of Gross Domestic Products (GDP) and Population Growth with these LULC changes analysis results.

ACKNOWLEDGEMENTS

I would like to thank Thailand International Cooperation Agency and Naresuan University for their financial and material support of this research. I am also grateful to the Burundian government and the local community for supplying useful data for this study. Anonymous reviewers and editors are also acknowledged for constructive comments.

REFERENCES

Alawamy JS, Balasundram SK, Hanif AHM, Sung CTB. Detecting and analyzing land use and land cover changes in the region of Al-Jabal Al-Akhdar, Libya using time-series landsat data from 1985 to 2017. Sustainability 2020;12(11):4490.

Anderson JR. A Land Use and Land Cover Classification System for Use with Remote Sensor Data. US Government Printing Office; 1976.

Bai ZG, Dent DL, Olsson L, Schaepman ME. Proxy global assessment of land degradation. Soil Use and Management 2008;24(3):223-34.

Baker WL. A review of models of landscape change. Landscape Ecology 1989;2(2):111-33.

Berakhi RO. Implication of Human Activities on Land Use Land Cover Dynamics in Kagera Catchment, East Africa [dissertation]. Southern Illinois University Carbondale; 2013.

Boissière M, Sheil D, Basuki I, Wan M, Le H. Can engaging local people's interests reduce forest degradation in Central Vietnam? Biodiversity and Conservation 2009;18(10): 2743-57.

Borana S, Yadav S. Comparison of model validation techniques for land cover dynamics in Jodhpur City. International Journal of Emerging Trends and Technology in Computer Science. 2017;6(5):215-9.

Burrell AL, Evans JP, Liu Y. The impact of dataset selection on land degradation assessment. Journal of Photogrammetry and Remote Sensing 2018;146:22-37.

Dewan AM, Yamaguchi Y. Using remote sensing and GIS to detect and monitor land use and land cover change in Dhaka Metropolitan of Bangladesh during 1960-2005. Environmental Monitoring and Assessment 2009;150(1-4):237.

Eastman JR. Idrisi Taiga guide to GIS and image processing [Internet]. 2009 [cited 2020 Oct 15]. Available from: http://web.pdx.edu/~nauna/resources/TaigaManual.pdf.

El-Hassanin A, Labib T, Gaber E. Effect of vegetation cover and land slope on runoff and soil losses from the watersheds of Burundi. Agriculture, Ecosystems and Environment 1993;43(3-4):301-8.

Food and Agriculture Organization (FAO). State of the world's forests, 2016: Forests and agriculture: Land use challenges and opportunities [Internet]. 2016 [cited 2021 Mar 7]. Available from: http://www.fao.org/3/a-i5588e.pdf.

Ghosh P, Mukhopadhyay A, Chanda A, Mondal P, Akhand A, Mukherjee S, et al. Application of cellular automata and markov-chain model in geospatial environmental modeling: A review. Remote Sensing Applications: Society and Environment 2017;5:64-77.

Gómez C, White JC, Wulder MA. Optical remotely sensed time series data for land cover classification: A review. ISPRS Journal of Photogrammetry and Remote Sensing. 2016; 116:55-72.

Guichaoua A. Population migrante et types de mobilité au Burundi. Les Cahiers d'Outre-Mer 1982;35(138):141-59 (in French).

Gupta R, Sharma LK. Efficacy of spatial land change modeler as a forecasting indicator for anthropogenic change dynamics over five decades: A case study of Shoolpaneshwar Wildlife Sanctuary, Gujarat, India. Ecological Indicators 2020;112:106171.

Halmy MWA, Gessler PE, Hicke JA, Salem BB. Land use/land cover change detection and prediction in the north-western coastal desert of Egypt using markov-CA. Applied Geography 2015;63:101-12.

Henry M, Maniatis D, Gitz V, Huberman D, Valentini R. Implementation of REDD+ in sub-Saharan Africa: State of knowledge, challenges and opportunities. Environment and Development Economics 2011;16(4):381-404.

Intergovernmental Science-Policy Platform on Biodiversity and Ecosystem Services (IPBES). Summary for policymakers of the assessment report on land degradation and restoration [Internet]. 2018 [cited 2021 Mar 10]. Available from: https://www.ipbes.net/system/tdf/spm_3bi_ldr_digital.pdf?file=1&type=node&id=28335.

Intergovernmental Panel on Climate Change (IPCC). Climate Change and Land: An IPCC Special Report on Climate Change, Desertification, Land Degradation, Sustainable Land Management, Food Security, and Greenhouse Gas Fluxes in Terrestrial Ecosystems. IPCC; 2019.

Islam K, Jashimuddin M, Nath B, Nath TK. Land use classification and change detection by using multi-temporal remotely sensed imagery: The case of Chunati wildlife sanctuary, Bangladesh. The Egyptian Journal of Remote Sensing and Space Science 2018;21(1):37-47.

Kamungi PM, Oketch JS, Huggins C. Land access and the return and resettlement of IDPs and refugees in Burundi: From the Ground Up. Project Relationships between Land Rights, Conflict and Peace in Sub-Sahara Africa. Pretoria: Institute for Security Studies; 2005 p. 195-267.

Kumar M, Mukherjee N, Sharma GP, Raghubanshi A. Land use patterns and urbanization in the holy city of Varanasi, India: A scenario. Environmental Monitoring and Assessment 2010;167(1):417-22.

Kundel HL, Polansky M. Measurement of observer agreement. Radiology 2003;228(2):303-8.

Lambin EF, Rounsevell MD, Geist HJ. Are agricultural land-use models able to predict changes in land-use intensity? Agriculture, Ecosystems and Environment 2000;82(1-3): 321-31.

Liu Q, Shi T. Spatiotemporal differentiation and the factors of ecological vulnerability in the Toutun River Basin based on remote sensing data. Sustainability 2019;11(15):4160.

Maingi J, Kepner S, Edmonds W. Accuracy assessment of 1992 landsat-MSS derived land cover for the Upper San Pedro Watershed (US/Mexico). Las Vegas: Environmental Protection Agency; 2002.

Marathianou M, Kosmas C, Gerontidis S, Detsis V. Land-use evolution and degradation in Lesvos (Greece): A historical approach. Land Degradation and Development 2000; 11(1):63-73.

Meyer WB, Turner BL. Changes in Land Use and Land Cover: A Global Perspective. United Kingdom: Cambridge University Press; 1994.

Mishra VN, Rai PK, Mohan K. Prediction of land use changes based on land change modeler (LCM) using remote sensing: A case study of Muzaffarpur (Bihar), India. Journal of the Geographical Institute Jovan Cvijic SASA 2014;64(1):111-27.

Mondal MS, Sharma N, Garg P, Kappas M. Statistical independence test and validation of CA markov land use land cover (LULC) prediction results. The Egyptian Journal of Remote Sensing and Space Science 2016;19(2):259-72.

Moore ML. An Examination of Contributing Factors to Land Use/Land Cover Change in Southern Belize and the Use of Satellite Image Analysis to Track Changes [dissertation]. Ames, Iowa State University; 2007.

Nadoushan MA, Soffianian A, Alebrahim A. Modeling land use/cover changes by the combination of markov chain and cellular automata markov (CA-Markov) models. Journal of Earth, Environment and Health Sciences 2015;1(1):16.

Ndzabandzaba C. Data Sharing for Sustainable Development in Less Developed and Developing Countries. Global Sustainable Development Report; 2015.

Nijimbere G, Lizana CR, Riveros PJIK. Assessment of soil erosion of Burundi using remote sensing and GIS by RUSLE model. RUDN Journal of Ecology and Life Safety 2019;27(1):17-28.

Niyogi D, Mahmood R, Adegoke JO. Land-use/land-cover change and its impacts on weather and climate. Boundary Layer Meteorology 2009;133(3):297.

Niyuhire MC. Integrated Soil Fertility Management for Bean-Maize Based Farming Systems in Gitega Province, Burundi: Understanding and Enhancing the Agronomic and Economic Benefits of Organic and Mineral Inputs [dissertation]. Belgium, KU Leuven; 2018.

Nzabakenga A, Feng LX, Yaqin H. Agricultural income determinants among smallholder farmers: Case of northern part of Burundi. Asian Journal of Agriculture and Rural Development 2013;3(11):780-7.

Patel SK, Verma P, Singh GS. Agricultural growth and land use land cover change in peri-urban India. Environmental Monitoring and Assessment 2019;191(9):1-17.

Patil MB, Desai CG, Umrikar BN. Image classification tool for land use/land cover analysis: A comparative study of maximum likelihood and minimum distance method. International Journal of Geology, Earth and Environmental Sciences 2012;2(3):189-96.

Pijanowski BC, Brown DG, Shellito BA, Manik GA. Using neural networks and GIS to forecast land use changes: A land transformation model. Computers, Environment and Urban Systems 2002;26(6):553-75.

Poursanidis D, Chrysoulakis N, Mitraka Z. Landsat 8 vs. Landsat 5: A comparison based on urban and peri-urban land cover mapping. International Journal of Applied Earth Observation and Geoinformation 2015;35:259-69.

Pulighe G, Baiocchi V, Lupia F. Horizontal accuracy assessment of very high resolution google earth images in the city of Rome, Italy. International Journal of Digital Earth 2016;9(4):342-62.

Rwanga SS, Ndambuki JM. Accuracy assessment of land use/land cover classification using remote sensing and GIS. International Journal of Geosciences 2017;8(04):611.

Sang L, Zhang C, Yang J, Zhu D, Yun W. Simulation of land use spatial pattern of towns and villages based on CA-markov model. Mathematical and Computer Modelling 2011;54(3-4):938-43.

Serneels S, Lambin EF. Proximate causes of land-use change in Narok District, Kenya: A spatial statistical model. Agriculture, Ecosystems an Environment 2001;85(1-3):65-81.

Shen L. Multi-Layer Perceptron-Markov Chain Based Geospatial Analysis of Land Use and Land Cover Change: A Case Study of Stoney Creek Watershed, BC, Canada [dissertation]. China, North China Electric Power University; 2019.

Singh AK. Modelling Land Use Land Cover Changes Using Cellular Automata in a Geo-Spatial Environment [dissertation]. Netherlands, ITC; 2003.

Song C, Woodcock CE, Seto KC, Lenney MP, Macomber SA. Classification and change detection using Landsat TM data: When and how to correct atmospheric effects? Remote Sensing of Environment 2001;75(2):230-44.

Surabuddin M, Sharma N, Kappas M, Garg P. Modeling of spatio-temporal dynamics of land use and land cover in a part of Brahmaputra River basin using Geoinformatic techniques. Geocarto International 2013;28(7):632-56.

Tilahun A, Islam Z. Google earth for land use land cover change detection in the case of Gish Abbay Sekela, West Gojjam, Amhara state, Ethiopia. International Journal of Society and Humanities 2015;3:80-7.

Torrens PM. How Cellular Models of Urban Systems Work (1. Theory). Centre for Advanced Spatial Analysis, UK: University College London; 2000.

Turner BL, Lambin EF, Reenberg A. The emergence of land change science for global environmental change and sustainability. Proceedings of the National Academy of Sciences 2007;104(52):20666-71.

Twisa S, Buchroithner MF. Land use and land cover change detection in Wami River Basin, Tanzania. Land 2019; 8(9):136.

United Nations Data Retrieval System (UNdata). A world of information [Internet]. 2020 [cited 2021 Mar 5]. Available from: https://data.un.org/en/iso/bi.html.

van Vliet J, Bregt AK, Hagen-Zanker A. Revisiting kappa to account for change in the accuracy assessment of land use change models. Ecological Modelling 2011;222(8):1367-75.

Vassolo S, Neukum C, Tiberghien C, Heckmann M, Hahne K, Baranyikwa D. Hydrogeology of a weathered fractured aquifer system near Gitega, Burundi. Hydrogeology Journal 2019;27(2):625-37.

Verburg PH. Simulating feedbacks in land use and land cover change models. Landscape Ecology 2006;21(8):1171-83.

Verma P, Raghubanshi A. Rural development and land use land cover change in a rapidly developing agrarian South Asian landscape. Remote Sensing Applications: Society and Environment 2019;14:138-47.

Vila JPS, Barbosa P. Post-fire vegetation regrowth detection in the Deiva Marina region (Liguria-Italy) using landsat TM and ETM+ data. Ecological Modelling. 2010;221(1):75-84.

Wang SW, Munkhnasan L, Lee WK. Land use and land cover change detection and prediction in Bhutan's high altitude city of Thimphu, using cellular automata and markov chain. Environmental Challenges 2021;2:100017.

INSTRUCTION FOR AUTHORS

Publication and Peer-reviewing processes of Environment and Natural Resources Journal

Environment and Natural Resources Journal is a peer reviewed and open access journal that is published twice a year (January-June and July-December). Manuscripts should be submitted online at https://ph02.tci-thaijo.org/index.php/ennrj/about/submissions by registering and logging into this website. Submitted manuscripts should not have been published previously, nor be under consideration for publication elsewhere (except conference proceedings papers). A guide for authors and relevant information for the submission of manuscripts are provided in this section and also online at: https://ph02.tci-thaijo.org/index.php/ennrj/author. All manuscripts are refereed through a **double-blind peer-review** process.

Submitted manuscripts are reviewed by outside experts or editorial board members of **Environment and Natural Resources Journal**. This journal uses double-blind review, which means that both the reviewer and author identities are concealed from the reviewers, and vice versa, throughout the review process. Steps in the process are as follows:

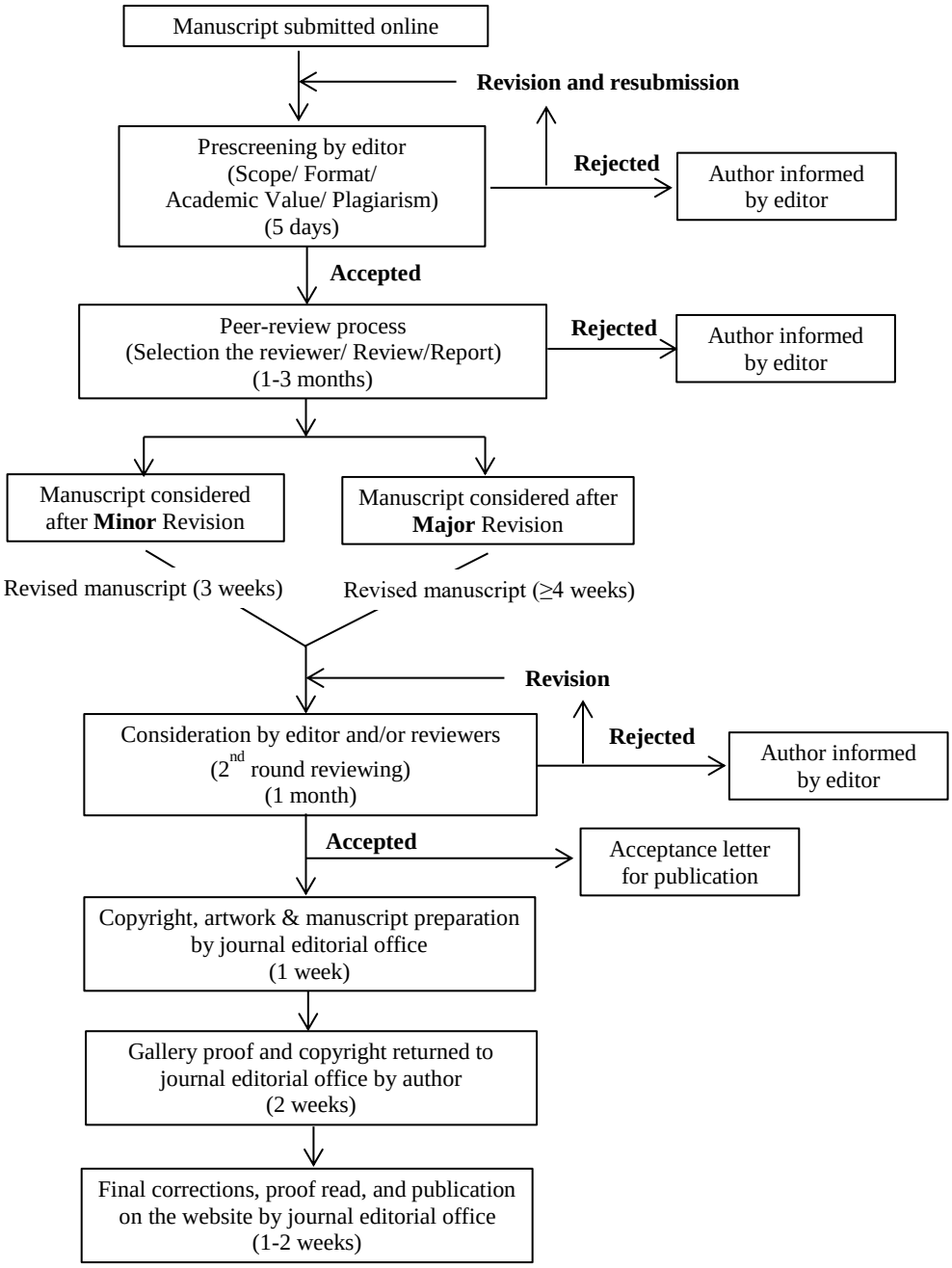

The Environment and Natural Resources Journal (EnNRJ) accepts 2 types of articles for consideration of publication as follows:

- *Original Research Article:* Manuscripts should not exceed 3,500 words (excluding references).
- *Review Article (by invitation):* This type of article focuses on the in-depth critical review of a special aspect in the environment and also provides a synthesis and critical evaluation of the state of the knowledge of the subject. Manuscripts should not exceed 6,000 words (excluding references).

Submission of Manuscript

Cover letter: Key points to include:

- Statement that your paper has not been previously published and is not currently under consideration by another journal
- Brief description of the research you are reporting in your paper, why it is important, and why you think the readers of the journal would be interested in it
- Contact information for you and any co-authors
- Confirmation that you have no competing interests to disclose

Manuscript-full: Manuscript (A4) must be submitted in Microsoft Word Files (.doc or .docx). Please make any identifying information of name(s) of the author(s), affiliation(s) of the author(s). Each affiliation should be indicated with superscripted Arabic numerals immediately after an author's name and before the appropriate address. Specify the Department/School/Faculty, University, Province/State, and Country of each affiliation.

Manuscript-anonymized: Manuscript (A4) must be submitted in Microsoft Word Files (.doc or .docx). Please remove any identifying information, such as authors' names or affiliations, from your manuscript before submission and give all information about authors at title page section.

Reviewers suggestion *(mandatory)*: Please provide the names of 3 potential reviewers with the information about their affiliations and email addresses. *The recommended reviewers should not have any conflict of interest with the authors. Each of the reviewers must come from a different affiliation and must not have the same nationality as the authors.* Please note that the editorial board retains the sole right to decide whether or not the recommended potential reviewers will be selected.

Preparation of Manuscript

Manuscript should be prepared strictly as per guidelines given below. The manuscript (A4 size page) must be submitted in Microsoft Word (.doc or .docx) with Times New Roman 12 point font and a line spacing of 1.5. *The manuscript that is not in the correct format will be returned and the corresponding author may have to resubmit*. The submitted manuscript must have the following parts:

Title should be concise and no longer than necessary. Capitalize first letters of all important words, in Times New Roman 12 point bold.

Author(s) name and affiliation must be given, especially the first and last names of all authors, in Times New Roman 11 point bold.

Affiliation of all author(s) must be given in Times New Roman 11 point italic.

Abstract should indicate the significant findings with data. A good abstract should have only one paragraph and be limited to 250 words. Do not include a table, figure or reference.

Keywords should adequately index the subject matter and up to six keywords are allowed.

Text body normally includes the following sections: 1. Introduction 2. Methodology 3. Results and Discussion 4. Conclusions 5. Acknowledgements 6. References

Reference style must be given in Vancouver style. Please follow the format of the sample references and citations as shown in this Guide below.

Unit: The use of abbreviation must be in accordance with the SI Unit.

Format and Style

Paper Margins must be 2.54 cm on the left and the right. The bottom and the top margin of each page must be 1.9 cm.

Introduction is critically important. It should include precisely the aims of the study. It should be as concise as possible with no sub headings. The significance of problem and the essential background should be given.

Methodology should be sufficiently detailed to enable the experiments to be reproduced. The techniques and methodology adopted should be supported with standard references.

Headings in Methodology section and Results and Discussion section, no more than three levels of headings should be used. Main headings should be typed (in bold letters) and secondary headings (in bold and italic letters). Third level headings should be typed in normal and no bold, for example;

2. Methodology
2.1 Sub-heading
2.1.1 Sub-sub-heading

Results and Discussion can be either combined or separated. This section is simply to present the key points of your findings in figures and tables, and explain additional findings in the text; no interpretation of findings is required. The results section is purely descriptive.
Tables Tables look best if all the cells are not bordered; place horizontal borders only under the legend, the column headings and the bottom.
Figures should be submitted in color; make sure that they are clear and understandable. Please adjust the font size to 9-10, no bold letters needed, and the border width of the graphs must be 0.75 pt. *(Do not directly cut and paste them from MS Excel.)* Regardless of the application used, when your electronic artwork is finalized, please 'save as' or convert the images to TIFF (or JPG) and separately send them to EnNRJ. The images require a resolution of at least 300 dpi (dots per inch). If a label needed in a figure, its font must be "Times New Roman" and its size needs to be adjusted to fit the figure without borderlines.

All Figure(s) and Table(s) should be embedded in the text file.

Conclusions should include the summary of the key findings, and key take-home message. This should not be too long or repetitive, but is worth having so that your argument is not left unfinished. Importantly, don't start any new thoughts in your conclusion.

Acknowledgements should include the names of those who contributed substantially to the work described in the manuscript but do not fulfill the requirements for authorship. It should also include any sponsor or funding agency that supported the work.

References should be cited in the text by the surname of the author(s), and the year. This journal uses the author-date method of citation: the last name of the author and date of publication are inserted in the text in the appropriate place. If there are more than two authors, "et al." after the first author' name must be added. Examples: (Frits, 1976; Pandey and Shukla, 2003; Kungsuwas et al., 1996). If the author's name is part of the sentence, only the date is placed in parentheses: "Frits (1976) argued that . . ."

Please be ensured that every reference cited in the text is also present in the reference list (and vice versa).

In the list of references at the end of the manuscript, full and complete references must be given in the following style and punctuation, arranged alphabetically by first author's surname. Examples of references as listed in the References section are given below.

Book
Tyree MT, Zimmermann MH. Xylem Structure and the Ascent of Sap. Heidelberg, Germany: Springer; 2002.

Chapter in a book
Kungsuwan A, Ittipong B, Chandrkrachang S. Preservative effect of chitosan on fish products. In: Steven WF, Rao MS, Chandrkachang S, editors. Chitin and Chitosan: Environmental and Friendly and Versatile Biomaterials. Bangkok: Asian Institute of Technology; 1996. p. 193-9.

Journal article
Muenmee S, Chiemchaisri W, Chiemchaisri C. Microbial consortium involving biological methane oxidation in relation to the biodegradation of waste plastics in a solid waste disposal open dump site. International Biodeterioration and Biodegradation 2015;102:172-81.

Published in conference proceedings
Wiwattanakantang P, To-im J. Tourist satisfaction on sustainable tourism development, amphawa floating marketSamut songkhram, Thailand. Proceedings of the 1st Environment and Natural Resources International Conference; 2014 Nov 6-7; The Sukosol hotel, Bangkok: Thailand; 2014.

Ph.D./Master thesis

Shrestha MK. Relative Ungulate Abundance in a Fragmented Landscape: Implications for Tiger Conservation [dissertation]. Saint Paul, University of Minnesota; 2004.

Website

Orzel C. Wind and temperature: why doesn't windy equal hot? [Internet]. 2010 [cited 2016 Jun 20]. Available from: http://scienceblogs.com/principles/2010/08/17/wind-and-temperature-why-doesn/.

Report organization:

Intergovernmental Panel on Climate Change (IPCC). IPCC Guidelines for National Greenhouse Gas Inventories: Volume 1-5. Hayama, Japan: Institute for Global Environmental Strategies; 2006.

Remark

** Please be note that manuscripts should usually contain at least 15 references and some of them must be up-to-date research articles.*

** Please strictly check all references cited in text, they should be added in the list of references. Our Journal does not publish papers with incomplete citations.*

Copyright transfer

The copyright to the published article is transferred to Environment and Natural Resources Journal (EnNRJ) which is organized by Faculty of Environment and Resource Studies, Mahidol University. The accepted article cannot be published until the Journal Editorial Officer has received the appropriate signed copyright transfer.

Online First Articles

The article will be published online after receipt of the corrected proofs. This is the official first publication citable with the Digital Object Identifier (DOI). After release of the printed version, the paper can also be cited by issue and page numbers. DOI may be used to cite and link to electronic documents. The DOI consists of a unique alpha-numeric character string which is assigned to a document by the publisher upon the initial electronic publication. The assigned DOI never changes.

Mahidol University

Wisdom of the Land

Research and Academic Service Section, Faculty of Environment and Resource Studies, Mahidol University
999 Phutthamonthon 4 Rd, Salaya, Nakhon Pathom 73170, Phone +662 441-5000 ext. 2108 Fax. +662 441 9509-10
E-mail: ennrjournal@gmail.com Website: https://www.tci-thaijo.org/index.php/ennrj